Extreme winds and waves for offshore turbines: Coupling atmosphere and wave modeling for design and operation in coastal zones

Larsén, Xiaoli Guo; Bolanos, Rodolfo; Du, Jianting; Kelly, Mark C.; Kofoed-Hansen, Henrik; Larsen, Søren Ejling; Karagali, Ioanna; Badger, Merete; Hahmann, Andrea N.; Imberger, Marc

Total number of authors:
16

Publication date:
2017

Document Version
Publisher's PDF, also known as Version of record

Extreme winds and waves for offshore turbines

Coupling atmosphere and wave modeling for design and operation in coastal zones

© Bent Medvind

Final report for ForskEL project PSO-12020 X-WiWa

Xiaoli Guo Larsén; Rodolfo Bolaños; Jianting Du; Mark Kelly; Henrik Kofoed-Hansen; Søren Larsen; Ioanna Karagali; Merete Badger; Andrea Hahmann; Marc Imberger; Jacob T. Sørensen; Sara Jackson; Patrick Volker; Ole Svenstrup Petersen; Alastair Jenkins; Angus Graham

October 2017

DTU Wind Energy E-0154
ISBN: 978-87-93549-22-7

Extreme winds and waves for offshore turbines
Coupling atmosphere and wave modeling for design and operation in coastal zones

Report DTU Wind Energy E-0154
2017

By
Xiaoli Guo Larsén; Rodolfo Bolaños; Jianting Du; Mark Kelly; Henrik Kofoed-Hansen; Søren Larsen; Ioanna Karagali; Merete Badger; Andrea Hahmann; Marc Imberger; Jacob T. Sørensen; Sara Jackson; Patrick Volker; Ole Svenstrup Petersen; Alastair Jenkins; Angus Graham

Published by: Department of Wind Energy, Frederiksborgvej 399
Request report from: www.dtu.dk

ISBN: 978-87-93549-22-7 (electronic version)

ISSN: [0000-0000] (printed version)
ISBN: [000-00-0000-000-0] (printed version)

Final Report for Project PSO-12020: X-WiWa
Extreme winds and waves for offshore turbines

–Coupling atmosphere and wave modeling for design and operation in coastal zones

Xiaoli Guo Larsén[1]
Rodolfo Bolaños[2]
Jianting Du[1]
Mark Kelly[1]
Henrik Kofoed-Hansen[2]
Søren Larsen[1]
Ioanna Karagali[1]
Merete Badger[1]
Andrea Hahmann[1]
Marc Imberger[1]
Jacob T. Sørensen[2]
Sara Jackson[2]
Patrick Volker[1]
Ole Svenstrup Petersen[2]
Alastair Jenkins[3]
Angus Graham[3]
1.Department of Wind Energy, Risø campus, DTU
2.DHI
3.Uni.Research Bergen

October 31, 2017

Contents

Abstract

The X-WiWa project was motivated by Denmark's long term vision for offshore wind energy and the many technical and scientific challenges in existing methodologies for assessing the design parameters, for both winds and waves.

X-WiWa succeeded in developing a most up-to-date modeling system for wind modeling for offshore wind farms. This modeling system consists of the atmospheric Weather Research and Forecasting (WRF) model, the wave model SWAN and an interface the Wave Boundary Layer Model WBLM, within the framework of coupled-ocean-atmosphere-wave-sediment transport modeling system COAWST (Hereinafter the WRF-WBLM-SWAN model). WBLM is implemented in SWAN, and it calculates stress and kinetic energy budgets in the lowest atmospheric layer where the wave-induced stress is introduced to the atmospheric modeling. WBLM ensures consistent calculation of stress for both the atmospheric and wave modeling, which was considered a major improvement to previous attempts in the literature. This methodology thus provides an option to avoid the parametrization of an often used interface parameter, the roughness length. Many parametrization schemes for the roughness length have brought diverse estimates and associated uncertainties to the modelled wind speed. Data validation using measurements from the Baltic Sea and North Sea around Denmark suggests that the coupled modeling system WRF-WBLM-SWAN outperforms the non-coupled, no-wave, WRF modeling of wind; an improvement by 10% or more is present at strong winds, which can affect the choice of the offshore wind turbine type.

X-WiWa examined various methodologies for wave modeling. The offline coupling system using atmospheric data such as WRF or global reanalysis wind field to the MIKE 21 SW model has been improved with considerations of stability, air density, currents and new wind drag relations. X-WiWa suggests that, implementation of an online coupling technology does not necessarily provide better estimation of the waves, if the physics have not been properly described. This is supported by the comparisons of the modeled wave data between offline MIKE 21 SW modeling and the WRF-WBLM-SWAN modeling. The two provide comparably good wave calculations for coastal areas but the latter underestimates the wave height for far offshore areas, which is speculated to be related to the dissipation description in the wave source functions, where further improvement is seen necessary.

X-WiWa puts modeling efforts on storms that are defined to be contributors to the extreme wind and extreme significant wave height through the annual maximum method. Thus for 23 years from 1994 to 2016, 429 storm days are simulated for the extreme wind, and for 1994 to 2014, 932 storm days are simulated for the extreme significant wave height. The 50-year winds at 10 m, 50 m and 100 m over the waters around Denmark are calculated and validated and agreement is satisfactory. The 50-year significant wave height for the Danish waters and surrounding North Sea and Baltic Sea are presented from the online and offline systems.

The modeling systems, data, analysis, results and publications are introduced and provided on www.xwiwa.dk. These outputs are expected to be useful for general offshore wind and wave applications such as Operation and Maintenance, Forecasting, and Design.

1 Preface

This is the final report of the project X-WiWa which was funded by PSO ForskEL.

The project aims at reducing cost related to offshore functions for wind energy, in line with the Danish government's long term vision to be free of fossil fuels. The government defined the goal of having half of the Danish electricity consumption covered by renewable energy in 2025, especially through wind energy. It is seen as an effective solution to reach this goal by building a large number of small wind farms offshore, especially in coastal zones (within 20 km from the coast) [1].

X-WiWa deals with a chain of issues related to the calculations for wind turbine design and wind power operations offshore, for which two conditions are particularly challenging: coastal zones and during storms. The challenges are both for the wind and wave calculations.

The estimates of extreme wind and extreme wave are essential for the offshore wind energy applications. Existing estimates for offshore conditions are mostly based on data from not-coupled modeling systems.

For the wind modeling, current calculation approaches are heavily based on parameterizations for the sea surface conditions through the roughness length z_0. There are a variety of parameterization-schemes for z_0, some simply as a function of wind speed and some involved with a number of derived wave parameters. These schemes have been derived and calibrated through a limited number of measurements and they can be significantly different from each other (see section 3.2.1). Most of the measurements are made over homogenous open sea surface, which makes the credibility of those empirical relations questionable in coastal areas. Most measurements are also made through light to moderate winds and the descriptions for stormy winds are mostly derived on wind measurements and it is often simplified as an extrapolation from moderate winds.

The wave modeling has been speculated to be challenged by the following situations: inaccurate wind input during storms, resolution of wind field is not sufficiently fine in coastal zones, missing effect from currents on wave growth and missing the stability effect. DHI created and maintains the MIKE model suit that is used for relevant applications in Denmark. Currently the coupling mode for MIKE is one-way offline, meaning that the wind field from an atmospheric model is used as input to MIKE, but the wave field is not fed back to the atmospheric modeling.

The misrepresentation of the sea surface conditions determined by the underlying waves results in inaccurate calculation of wind at hub height. Prediction of high waves suffers from inaccurate wind forcing. Roughly speaking, a 10% error in the wind speed results in 15% in the wave height and 30% error in the wave loads in the marine structures. Errors in the prediction of strong winds and waves bring considerable risks to the secure operation system and maintenance of offshore wind farms.

X-WiWa aims at improving the wind and wave modeling during storm conditions particularly for the applications in the Danish coastal zones. However the technology to be developed is of general use. The efforts target at solving a series

[1] Kystnære havmøller i Danmark. Screening af havmølleplaceringer inderfor 20 km fra kysten Juni 2012. http://www.ens.dk/da-dk/info/nyheder/nyhedsarkiv/2012/sider/20120627havmoelleudvalgetudpeger16kystnaereomraader.aspx

of scientific as well as technical issues, specifically: (1) the coupling technique for the atmospheric and wave modeling (2) the description of exchange variables at the air-sea interface (3) coastal impact on the setting up of the wave modeling (4) impact of stability on the wave modeling

The main outcome of the project includes: (1) a new and improved modeling system for coupling wind and wave models that are suitable for coastal areas and storm conditions (2) extreme wind atlas (3) extreme wave atlas (4) data sets for storms over the North Sea that can be used for deriving other relevant wind and wave parameters for particular applications.

At the end of the project, we reached the following milestones, which have been prepared in separate reports that can be found in the attachments of this report:

- Database of simulated storms affecting the Danish extreme winds
- Atlas of the 50-year wind at 100 m for the Danish coastal zone
- Strong wind statistics from the storms
- A coupler and coupling tools for the atmospheric and wave modeling - the wave boundary layer model
- Atlas of the 50-year H_{m0} for the Danish coastal zone

The work has been presented at quite a number of conferences and workshops, in the format of scientific and technical proceedings, oral and poster presentations. Five journal papers are published and three more are under preparation. The complete list of the dissemination is given in section 12.

Particularly, the new coupling approach through the wave boundary layer model for Weather Research and Forecasting (WRF) and the spectral wave model for near shore (SWAN) has become a useful contribution to the community and interests have been shown by several institutes in Europe and Canada. It made contributions to the EU INNWIND project [2], IRPWIND project [3] and IEAWIND project[4]. The EU project CEASELESS [5] will use it to examine the current methodologies for coastal applications. It has also been introduced to an ongoing ForskEL project OffshoreWake [6] to add in calculations of sea conditions to the wind-to-power calculation system. The new modeling system has been implemented at DTU Wind Energy Department and it is made ready with guidance for everyone to use.

Improvements to MIKE 21 SW have also been used for research projects (e.g. CEASLESS where the model will be used to assess satellite products) and commercial projects related to offshore wind farms (OWF) (e.g. Holland Kurst Zuid and Noord (HKZN), Seastar and Mermaid OWF's).

In the following, section 2 introduces X-WiWa structure in three phases and the development of the project. Section 3 introduces the background of X-WiWa regarding scientific knowledge, technology and data and highlights the challenges and opportunities X-WiWa faced at the beginning. Here we also summarize the objectives of X-WiWa. X-WiWa values measurements for modeling calibration, validation and verification. The project collected various types of measurements

[2]http://www.innwind.eu/
[3]http://www.irpwind.eu/
[4]https://www.ieawind.org/
[5]*https* : *//ceaseless.barcelonatech* − *upc.eu/en/ceaseless_project*
[6]www.offshorewake.dk

that we could get hold of and the details of the measurements and use of them are given in section 4. From section 5 on, the major outputs and contributions from X-WiWa are presented.

2 Project structure

The project is structured in three phases, combining research, development and application. The project initiates with the development phase for the core of the development of technology. This first phase served as project basis to establish planning of the activities and work flow. During this phase, the project came to a decision to expand our original plan of using WRF to be coupled with MIKE, by introducing the use of WRF coupled with SWAN. Since MIKE is owned by DHI and SWAN is open source and the basic physics are consistent between the two, introducing the open source model SWAN, together with the open source atmospheric model WRF, gives us much more freedom in how we would explore the numerical reactions in mathematical interpretations of physics, as well as in implementing new ideas.

In the second phase, the focus was to develop the new modeling system. A large number of experiments were made to understand the technical impacts from the following factors: (1) how the model components are linked, including the information exchange rate, where in the work flow to calculate the common parameters for wind and wave, namely in the atmospheric or wave model (2) the traffic of information flow: one-way (from WRF to SWAN (or MIKE) only) or two-way (both from WRF to SWAN (or MIKE) and from SWAN (or MIKE) to WRF), online or offline, see section 5. The technical part needs to be secured to ensure the scientific part be correctly described in the modeling system. There have also been numerous experiments done in this project to find out the reasonable ways to set up the model in order to capture the storm peak (since it is most relevant for extreme value estimate) in the model domain, including storm track detection and validation, storm resolution, size and location. This part is necessary in order to put our focus on the effect related to air-sea coupling (section 5.7). Finally the focus has been put on how to best transfer the wave impact to the atmospheric modeling and vise versa. This leads to the core of the project. After a thorough examination of the impact of the existing approaches using parameterizations of roughness length or stress transfer, this project contributes with a physics-based interface model between the atmospheric modeling and wave modeling through momentum and turbulence kinetic energy conservation budget throughout the interface (section 5.1).

Parallel to the development of WRF-SWAN model, developments to the MIKE 21 SW model also occurred (see sections 5.4 and 5.5 for more details).

The model system has been tested both in ideal and real case modes. The outputs are verified with measurements (section 4). The satisfactory results encourage us to use the modeling system to simulate hundreds of storms that have contributed to the samples for extreme winds and waves over waters around Denmark. Accordingly, extreme wind and wave atlases (sections 6, 7.1 and 8) have been obtained from both online and offline models. This is the third phase of the project. Additionally, WRF and SWAN within the COAWST framework are already implemented in an online mode, facilitating the implementation of new physical processes.

3 Background and Objectives

3.1 Extreme winds and extreme waves

Extreme wind and significant wave height data are essential for design of offshore and coastal structures such as wind turbines and platforms and floating objects (e.g. floating lidar carriers), to avoid structures obtaining damage from severe wind or wave conditions.

Such an estimate requires reliable long term measurements, which are seldom available. In the absence of such measurements, long term, climatological outputs from atmospheric and wave models seem to be attractive are used as alternatives.

DTU is in an internationally leading position regarding extreme wind estimation. DTU Wind Energy Department owns and maintains the software Wind Engineering (WEng) [7], including the technical and scientific parts, in which a microscale model Linear Computational Model is implemented and it calculates the site-specific conditions. This software has become a standard industrial tool for assessing site conditions for turbine classification. Originally it calculates the siting conditions based on long term measurements from a site close to the farm site. As new farms are being planned rapidly over the globe, often there are no long term wind measurements. In the past several years DTU has developed two main methods relying on numerical modeling. The first is the Spectral Correction Method (SCM). It uses the long term extreme wind information from climate data, but adds in the missing wind variability for relatively high frequency over which the climate data usually suffer from spatial and temporal smoothing effect [1]. SCM uses the wind variability from measurements for the high frequencies through power spectrum, which does not require measurements longer than one year. In the absence of measurements, a spectral model can be used; this model has been derived from a large database of measurements. The correction is done through the frequency domain to a standard 10 min resolution, which serves as input to WEng [1, 2]. Note that the correction through the frequency domain only assumes a spatial homogeneity over an area of the equivalent scale of 10 min for a given wind speed. This method has been rather well validated with measurements from stations over non-complex land conditions for estimating the extreme wind [2]. However, this method is foreseen to be less reliable for coastal sites, where the spatial variability is large and should not be neglected (see detailed analysis in section 8.1.1).

The other method for extreme wind estimation from DTU is the selective dynamical downscaling method [3]. This method uses mesoscale weather model to downscale individual storm events that contributed as the annual maximum wind over a specific area (see section 6). This method has been applied to create extreme wind atlas for Denmark, Gulf of Suez, part of Spain and South Africa and it has been better validated mostly for land conditions. The study [3] was published in 2013 and there were only very limited years of measurements offshore available for a decent validation. Also the database DTU created for public use [4] were based on mesoscale modeling of a spatial resolution of 5 km with a standard setup, which is seen with our new experience as not sufficient in resolving the frequent organized features over the North Sea in connection with extreme wind weather.

Extreme wave atlases have also been created from modeled data in many

[7] http://www.wasp.dk/weng

institutes [5, 6, 7, 8, 9, 10, 11]. Before X-WiWa, these atlases are of horizontal resolutions of 10 km to more than a hundred of kilometers. These modeled data are almost all from spectral modeling and they also face the challenge of smoothing effect related to the numerical modeling, reflected in the time series of the significant height as a flattened variability at relatively high frequencies, similar to the wind time series. In addition, in the coastal areas, the modeling is also challenged by descriptions of swell and dissipation. Larsén et al [12] applied SCM to two sites: one deep water and relatively open water FINO 1, and one shallow water coastal site Horns Rev I. The relatively short measurements are sufficient in providing the spectral information for the frequencies greater than 10^{-5} Hz, for which the long term data from WAM significantly underestimates the fluctuations (Figs. 3 and 8 in [12]). This seems to give consistent estimates in comparison with measurements and Altimeter data (Wimmer et al. 2006)[13]. However, this method does not work if we do not have access to in-situ measurements.

3.2 Methodologies

Before X-WiWa, here are several facts for offshore wind and wave modeling in Denmark :

- Winds were modeled using weather models, not coupled to any wave models at e.g. DMI, DTU Wind Energy and other companies such as Vestas and Vattenfall.
- Waves were modeled with wind input from global or mesoscale model; it was called one-way offline coupling, meaning the wind field is not affected by the wave field. This is performed at e.g. DHI, DMI and some companies (e.g. GeoStorm).
- There were initial efforts in coupling ocean model to wave model from DHI.

Before X-WiWa, around the world, the coupling efforts include:

- The coupled-ocean-atmosphere-wave-sediment transport modeling system (COAWST), where the atmospheric model is WRF and wave model is SWAN, has been developed to include a number of parameterization schemes for the roughness length (z_0) as the wind-wave modeling interfaces. z_0 was calculated in SWAN and transported to WRF, see Fig. 1.
- WRF and SWAN were running within COAWST mostly in non-nested mode. The nesting function was just starting to be implemented.
- Considerable effort in modeling tropical cyclones where the heat exchange is a research focus. There started to appear a few studies addressing mid-latitude storms.
- There missed in general an effort in tackling modeling challenges for coastal zones.

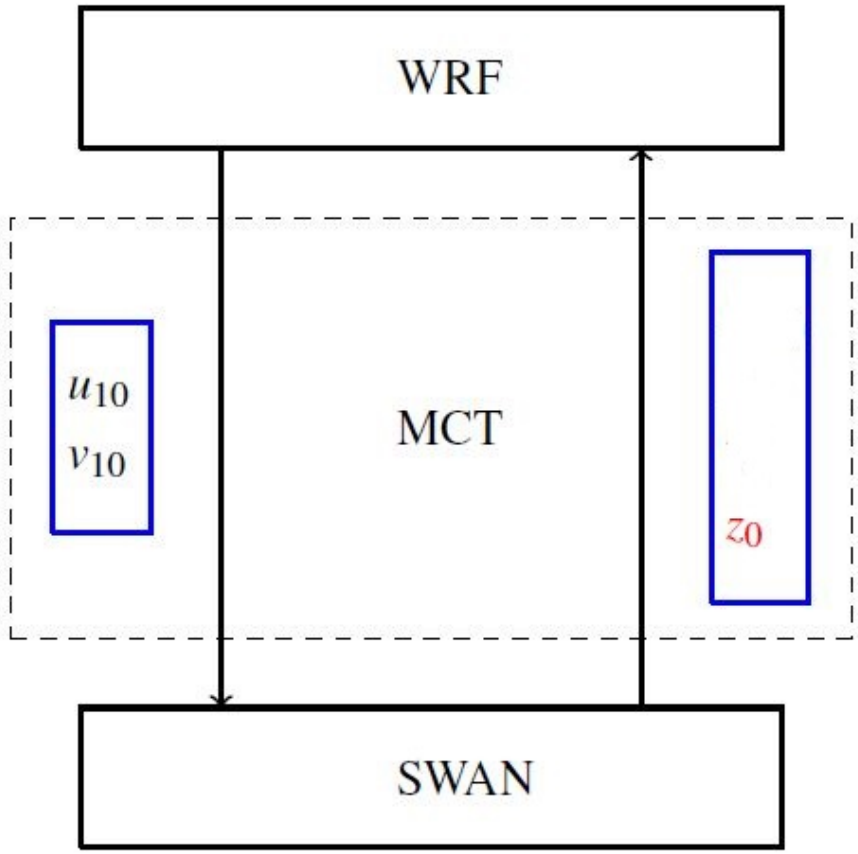

Figure 1: Diagram showing the two model components WRF and SWAN and the interface for information exchange through the Model Coupling Tool in the COAWST model system.

3.2.1 Challenge: diverse parametrization schemes for roughness length

To introduce the wave impact to the atmospheric modeling, it is most often through a description of the roughness length z_0 in terms of wave-related parameters, similar to what is illustrated in Fig. 1 where the arrow pointing from wave model to the atmospheric model through z_0. Mostly, z_0 is described through the Charnock relation [14]:

$$z_0 = \alpha u_*^2/g \tag{1}$$

where α is the Charnock constant, and u_* is the frictional velocity and g is the gravitational acceleration.

In the last decades, major efforts in the coupled modeling have been to obtain a good description of z_0, which are in principle empirical expressions derived from measurements. Among these measurements, in-situ mast and buoy or ship and wave tank experiment data provided light to moderate wind speeds, radio soundings data provided us certain information for hurricane force winds, see Table 1 for a brief overview. These measurements are mostly used to derive an empirical relation between the drag coefficient C_D and the wind speed at 10 m

Table 1: Details about the five parametrization schemes for the roughness length z_0.

scheme	validation measurements	U_{10} range (ms^{-1})	water depth (m)
Taylor-Yelland	HEXMAX,RASEX	$2-20$	≤ 18
	Lake Ontario		
Drennan	FETCH,WAVES	$2-20$	≤ 100
	AGILE,SWADE,HEXOS		
Oost	ASGAMAGE	$1-20$	~ 18
Fan	FETCH, SWADE	$2-50$	deep and shallow
	CBLAST,Powell		
Liu	SCOR, Powell	$2-50$	deep and shallow

U_{10}. Note that for neutral conditions C_D and z_0 are related through:

$$C_D = (\frac{\kappa}{\ln(z/z_0)})^2, \tag{2}$$

following the logarithmic wind law.

The distributions of C_D with U_{10} from the most known measurement campaigns are plotted together in Fig. 2. These measurements include mostly open sea areas but also some coastal sites (e.g. RASEX [15]). For light to moderate winds, the wave tank measurements from Donelan (2004) give systematically smaller drag at the same wind speed. For $20 < U_{10} < 40$ ms^{-1}, the different sources of measurements consistently suggest a level-off of C_D with U_{10}; here the scatter is larger compared to that for smaller wind speeds. The scatter and uncertainty become enormous when $U_{10} > 50$ ms^{-1}, and it does not support the simple extrapolation of the monotonic increasing relation between C_D and U_{10}.

While it is an attractive simple approach to derive a C_D and U_{10} relation for the wind and wave coupling as used in SWAN and [16], such a simple relation is not capable of describing the variation of C_D at a certain U_{10}. It is generally assumed that the variation of C_D at a certain U_{10} is to a large degree caused by the surface wave characteristics.

The Charnock relation Eq. (1) was derived for fully developed wind sea for open ocean conditions and the Charnock "constant" has been found to vary with sea state related parameters. Since it is shown not to be a "constant", hereinafter we call it Charnock parameter. In the past decades there have been considerable amount of work, both from atmospheric and wave modeling communities, addressing this interface parameter z_0 in terms of the Charnock constant. A number of schemes have been derived for z_0, and hence C_D, using wave parameters such as wave age c_p/u_*, wave length at peak frequency L_p, wave steepness H_s/L_p and wave height H_{m0}. The often cited and used schemes include those from Drennan et al. [17], Fan et al. [18], Liu et al. [19], Oost et al. [20], Taylor and Yelland [21] and Andreas et al. as in SWAN.

In the Drennan scheme, z_0 is parameterized through the significant wave height H_{m0} and the inverse wave age u_*/c_p, with c_p the wave phase velocity at the peak frequency of the wave spectrum:

$$z_0 = 3.35 H_{m0}(u_*/c_p)^{3.4} + 0.11\nu/u_* \tag{3}$$

where ν is the viscosity coefficient. The second term of the right hand side of Eq. (3) describes the contribution from smooth flow to the roughness length, which is important only at light winds e.g. the 10 m mean wind speed $U_{10} < 3$ ms^{-1}.

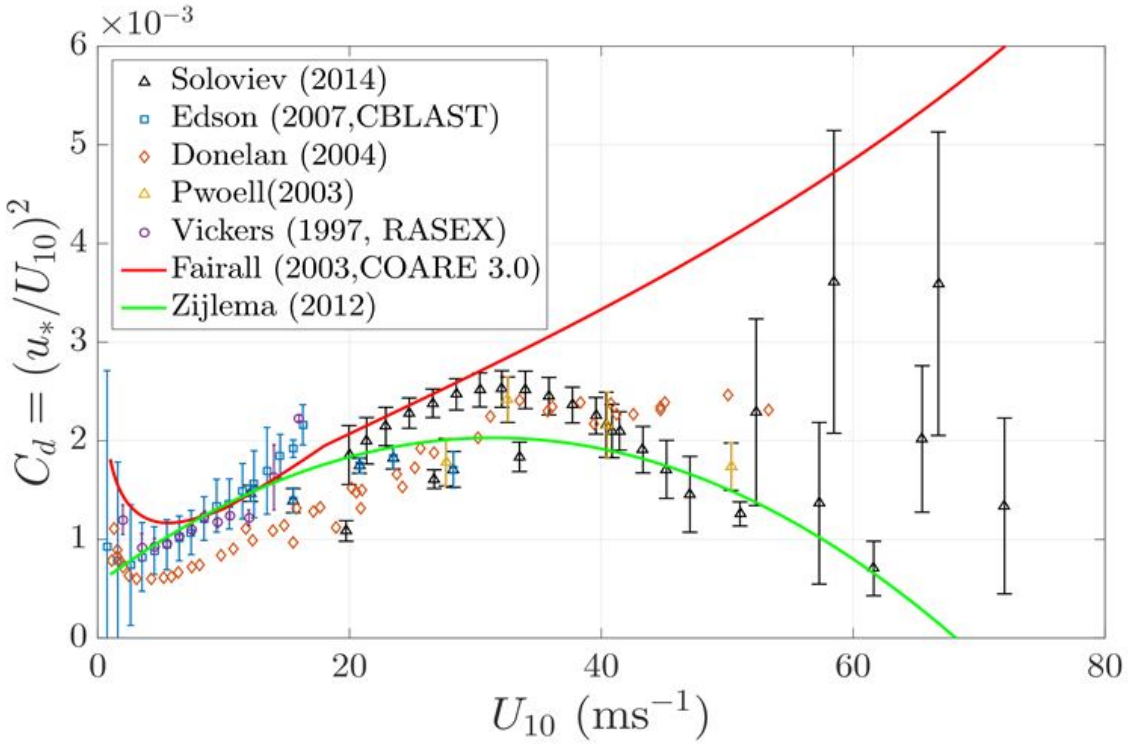

Figure 2: Drag coefficient as a function of wind speed, collection of measurements (symbols) and two most often used models (solid curves).

The Fan scheme [18] includes the smooth flow contribution and a Charnock formulation base:

$$z_0 = \alpha u_*^2/g + 0.11\nu/u_*. \tag{4}$$

Here the Charnock parameter α is parameterized with the wave age c_p/u_*:

$$\alpha = a(c_p/u_*)^{-b} \tag{5}$$

where

$$a = \frac{0.023}{1.0568^{U_{10}}}, \qquad b = 0.012U_{10}. \tag{6}$$

The Liu's scheme [19] has the same base format as Eq. (4); here α is also parameterized through the wave age c_p/u_*, but in a different form from the Fan formulation Eq. (5). For young waves, $0.35 < c_p/u_* < 35$:

$$\alpha = (0.085(c_p/u_*)^{3/2})^{1-1/\omega}(0.03c_p/u_* \exp(-0.14c_p/u_*))^{1/\omega} \tag{7}$$

and for old waves $c_p/u_* > 35$:

$$\alpha = 17.61^{1-1/\omega}0.008^{1/\omega}, \tag{8}$$

where $\omega = \min(1,\ a_{cr}/(\kappa u_*))$, with a_{cr} =0.64 ms^{-1}, and κ is the von Karman constant 0.4.

Oost et al. [20] parameterizes z_0 in terms of the wave length at the peak frequency, L_p, and the inverse wave age u_*/c_p:

$$z_0 = \frac{50}{2\pi} L_p (\frac{u_*}{c_p})^{4.5} + 0.11\nu/u_* \tag{9}$$

The Taylor and Yelland [21] formulation reads:

$$z_0 = 1200 H_{m0} (H_{m0}/L_p)^{4.5} \tag{10}$$

where H_{m0}/L_p represents the wave steepness.

By examining thousands of eddy-covariance measurements of the air-sea surface stress, [22] found the following simple description to be useful up to U_{10} of about 25 ms^{-1}:

$$z_0 = z \exp\left(-u_*/U_{10}\right) \tag{11}$$

with u_* and U_{10} being bounded by the following relationship:

$$u_* = 0.239 + 0.0433 \left((U_{10} - 8.271) + \sqrt{0.12(U_{10} - 8.271)^2 + 0.181} \right) \tag{12}$$

Here $z = 10$ m. The above derivations have been validated with measurements from various places, with most representing open water conditions, see Table 1 for details.

The behaviors of z_0 in the coastal zones could be different from the open water conditions, due to factors such as fetch, stability under the impact of upwind land, bathymetry, shoaling and wave breaking processes (e.g. [23, 15]). Figure 3 shows the relations of C_D and U_{10} from the RASEX experiment for offshore (short fetch) and onshore (long fetch) conditions [15]. For $U_{10} < 14$ ms^{-1}, the drag is larger when the flow is from land to sea than that when the flow is from sea to land. This adds yet another challenge since in most atmospheric modeling, simple parametrization schemes for z_0 are for the open sea conditions.

Measurements of turbulence fluxes and wave parameters, together with standard meteorological measurements from Horns Rev made it possible to demonstrate the variety of the many parametrization schemes for z_0, and this is shown in Fig. 4. The Horns Rev site is about 20 km from the shoreline of the Danish west coast. The water depth at this site varies from 6 m to 12 m. More details of this site are given in section 4. A 62-m tall mast (M2) was raised before the wind farm was built. On the mast there are standard meteorological measurements at several heights, including winds at 15, 30, 45 and 62 m and turbulence measurements at 50 m, and at the same time waves were measured with a nearby buoy. In our analysis, the measurements are divided into two groups, one with flow from land to sea (red dots in Fig. 4) and one with flow from sea to land (blue circles). The plot, Fig. 4, from the measurements from Horns Rev, is based on the wind speed bins of 0.5 ms^{-1}. Consistent with [15], the C_D and U_{10} relations are different for onshore and offshore flow. When winds are smaller than about 12 ms^{-1}, the drag is larger for short fetch than the long fetch conditions. For the offshore flow, the drag coefficient levels off at the 10 m wind of about 10 ms^{-1}. For the onshore flow, the dependence of C_D on U_{10} follows closely those that are based on open ocean observations, such as the COARE 3.0 and Zijlema [24]. Wave parameters were derived and applied to the five parameterization schemes for both the onshore (solid curves) and offshore (dashed curves) categories. Here one can see that these schemes do not distinguish the differences in the onshore

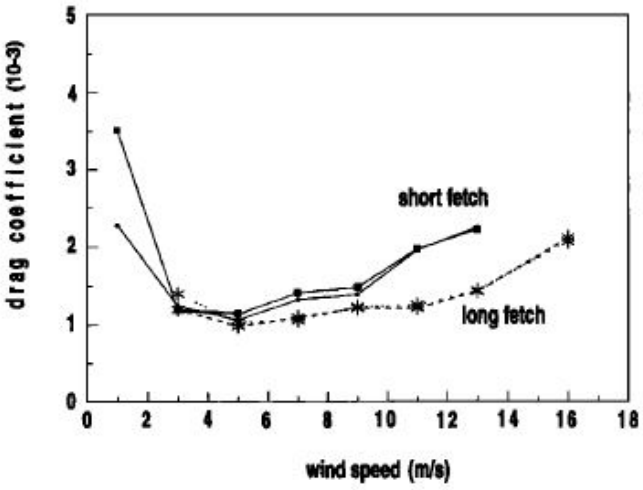

Figure 3: The drag coefficient for the short and long fetch records and the corresponding values reduced to neutral conditions. The data are from a coastal shallow water site Vindeby. A copy of Figure 9 from [15].

and offshore data categories, since they represent only the onshore flow. Another aspect that needs to be pointed out is that the difference in z_0 between the five schemes is rather small when wind speed is less than about 15 ms^{-1}, but the difference increases with increasing wind speed and we expect even larger difference when winds are stronger than the maximum wind of this data set.

One should be careful in interpreting these differences and their corresponding effect in modeling: Is it caused by the different values of z_0 from the many different ways or is it caused by coupling?

Figure 4 therefore outlines two major challenges in the conventional coupling approach through the parametrization of z_0: strong winds and coastal conditions.

For moderate to strong winds, the large difference in z_0 between the different schemes causes considerable difference in the surface wind in a coupled modeling system (section 8.1.2 and [25] Chapter 8).

3.2.2 Challenge: introducing wave-induced stress to atmospheric modeling

Apart from using parametrization of z_0 as the model interface parameter, some have been trying to couple the atmospheric and wave modeling through the stress conservation in the atmospheric layer close to the water surface. Janssen et al. (1989) introduced a method that describes the distribution of stress components in the interface between atmosphere and water surface. The interface is also called the wave boundary layer, where the impact of surface waves is important. The impact was in Janssen et al. (1989) and [26] described through the wave-induced stress τ_w. The wave-induced stress τ_w, the atmospheric turbulence stress $\vec{\tau}_t(z)$ and the viscous stress $\vec{\tau}_v(z)$ together give the total stress $\vec{\tau}_{tot}(z)$, which is constant throughout the wave boundary layer. The viscous stress contribution becomes negligible a few centimeters above the water surface, so that

$$\vec{\tau}_{tot}\left(z\right) = \vec{\tau}_t\left(z\right) + \vec{\tau}_w\left(z\right) = constant \tag{13}$$

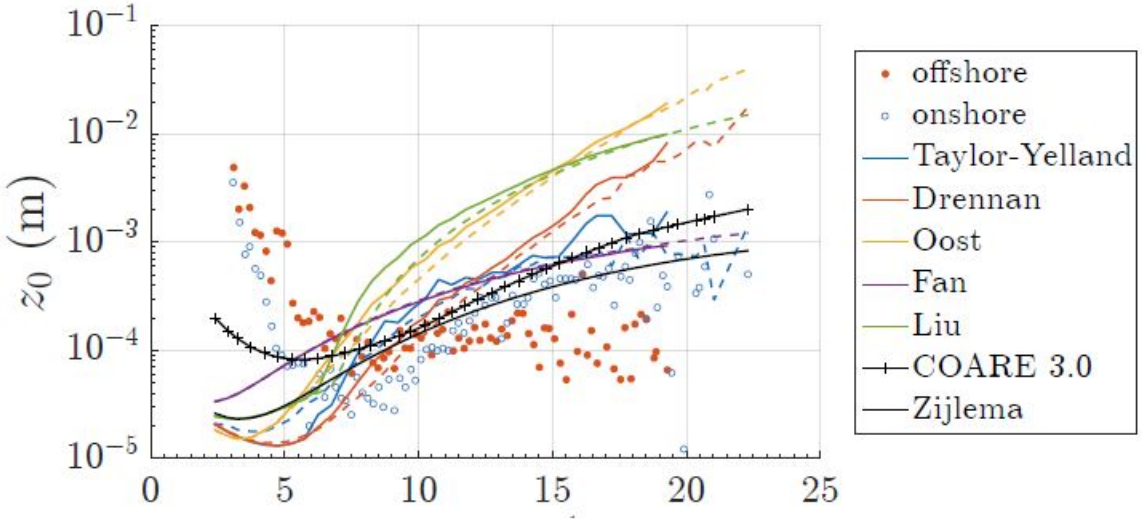

Figure 4: Roughness length z_0 as a function of wind speed at 10 m, the measurements from Horns Rev M2 are used and shown here as dots for offshore and onshore conditions. Also shown are 7 models applied to the corresponding parameters from the two groups of Horns Rev M2 data, with the solid for onshore flow and dashed curve for offshore flow. A copy of Figure 8.5 from [25]

Since Janssen et al. (1989) [27], this concept has been developed by [26], Chalikov and Markin (1991)[28], Makin (1995)[29], Hara and Belcher (2002, 2004) [30, 31] and Moon et al. (2004)[32]. Among them, Janssen (1991) successfully introduced this concept into coupling the wind and wave modeling through wind-input source functions, e.g. the WAve Model (WAM) [33], Simulating WAves Nearshore (SWAN) [34] and WAVEWATCH III Tolman and Chalikov (1996) and MIKE 21 SW [35].

However, it has been reported that the Janssen 1991 scheme overestimates the wind stress in strong wind conditions (e.g. Jensen and Cardone 2006 [36]) and later this was reported in connection with the use of WAVEWATCH III using other wind-input source terms (Moon et al. 2004, 2009[32, 37]). In a simple manner to limit the values of stress at strong winds, Jensen and Cardone (2006)[36] used a cap to limit u_*/u_{10} to be in the range of 0.05 and 0.06, Ardhuin et al. (2010)[38] used 0.0015 m as the upper limit for z_0 which is used in Janssen's wind-input source function. Alternatively, some used a spectral sheltering mechanism to reduce the wind-input at high frequencies (Chen and Belcher 2000 [39], Hara and Belcher 2002[30], Kudryavtsev et al. 1999[40], Makin et al. 2007[41], Banner 2010[42]). Introduction of the sheltering effect reduces growth rate, providing smaller stress at strong winds in connection with the use of Janssen's wind input source functions.

These joint efforts have however not been successfully implemented in a wind-wave coupled modeling system.

3.3 Objectives

X-WiWa aims at improving our modeling ability for two most challenging situations: offshore winds and waves under storm conditions and coastal areas, and aims at providing most up-to-date calculation of extreme wind and wave conditions for the waters around Denmark.

The specific efforts from X-WiWa were defined as:

- New coupling approach using stress rather than parameterized z_0 to transport the wave information to the atmospheric modeling (section 5).
- The thorough investigation of a collection of key parameters on their impact on storm modeling: resolution, domain position and size, data exchange rate, boundary and initial conditions and coupling. To setup the atmospheric model systematically to best contain the storm path and intensity in comparison with large scale forcing (section 5.7)
- The investigation of the impact of the key parameters for modeling for coastal zones (which was initially defined as a few tens of kilometers from the shoreline), such as resolution, fetch, input of different resolution of bathymetry data, water level data input and SST data
- To investigate the best way to couple: which models; which resolution; one-way or two-way; online or offline
- To go to high resolution using COAWST with nesting functions.
- To calculate the extreme wind atlas over the Danish waters
- To calculate the extreme wave atlas over the Danish waters

4 Measurement database

4.1 In-situ measurements

We classify the measurements into three groups, according to how they are used.

Group-I is over the North Sea but not included in the high resolution, innermost, domain of the X-WiWa model setup (domain III , Fig. 5). The setup of this innermost domain is targeted at including the waters around Denmark. The group-I data stations are listed in Table 2 and their locations are shown in Fig. 6 (from [43]). Most of these sites have data length more than 13 years, rather acceptable for assessing the 50-year wind and wave estimation. However, since the final evaluation is only for model domain III, these data are not used for the extreme wind and wave estimate for Denmark, but they have been used to calibrate and verify modeling [43, 25]. The nine stations are the Norwegian offshore platforms; the data are from www.eklima.met.no and they are 20-min values. It is speculated that flow distortion caused by the platform construction would considerably affect the data quality, especially close to the water surface. Unfortunately this project has limited access to the details of these measurement quality. Therefore the use of these data has been kept qualitative with references to the literatures including [44], [45] and [46].

Group-II consists of stations inside domain III but the measurements are rather short. They can not be used directly for validation for extreme wind and wave estimation but useful for validating individual storms. These sites are: RUNE, Anholt and Horns Rev II mast 8 (M8). Brief details of the wind measurements at these sites are given in Table 3. For the details of the RUNE site meteorological measurements, please refer to [47] and [48], and for the wave measurements, please refer to [49, 50].

Group-III includes Horns Rev I mast 2 (M2), FINO 1, 2 and 3, and Høvsøre where the wind measurements are longer than 6 years. Measurements shorter than 10 years are in principle too short for a proper estimation of extreme wind. However, if we disregard all sites where measurement record is shorter than 10 years, there are only two sites left. Therefore, we address the uncertainties in connection with the application of statistical approaches when the extreme value estimates are used to verify the modeled results. Measurements from Horns Rev I M2 can be found in [51] and [52], and wave measurements from the buoys close to Horns Rev I M2 can be found in e.g. [12]. Details about FINO 2 measurements can be found in [53], and FINO 3 measurements in [54]. The site and measurements about Høvsøre are well documented in [55].

Table 5 summarizes the sites where buoy data have been used for data validation, where the coordinates, data period and water depth are given for each site.

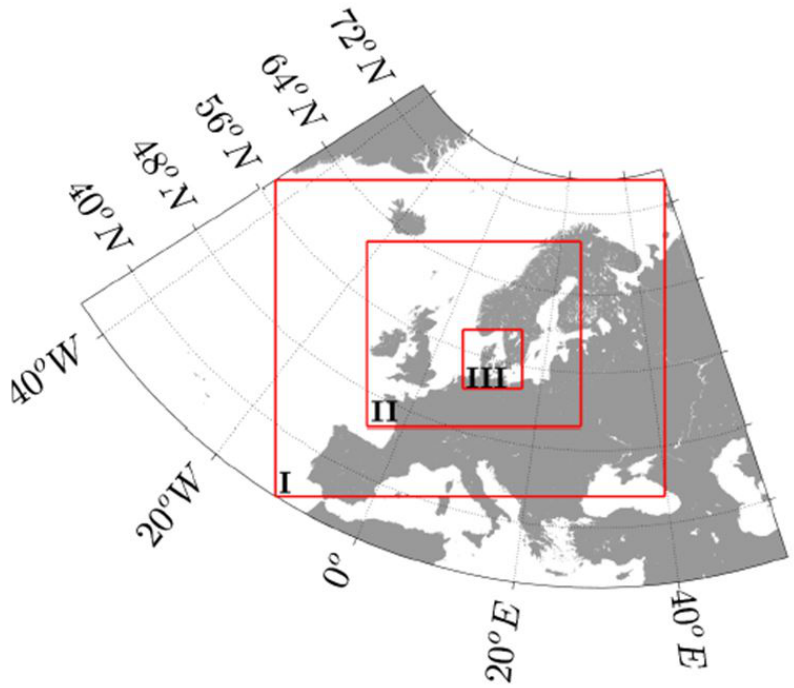

Figure 5: X-WiWa model domains I, II and III.

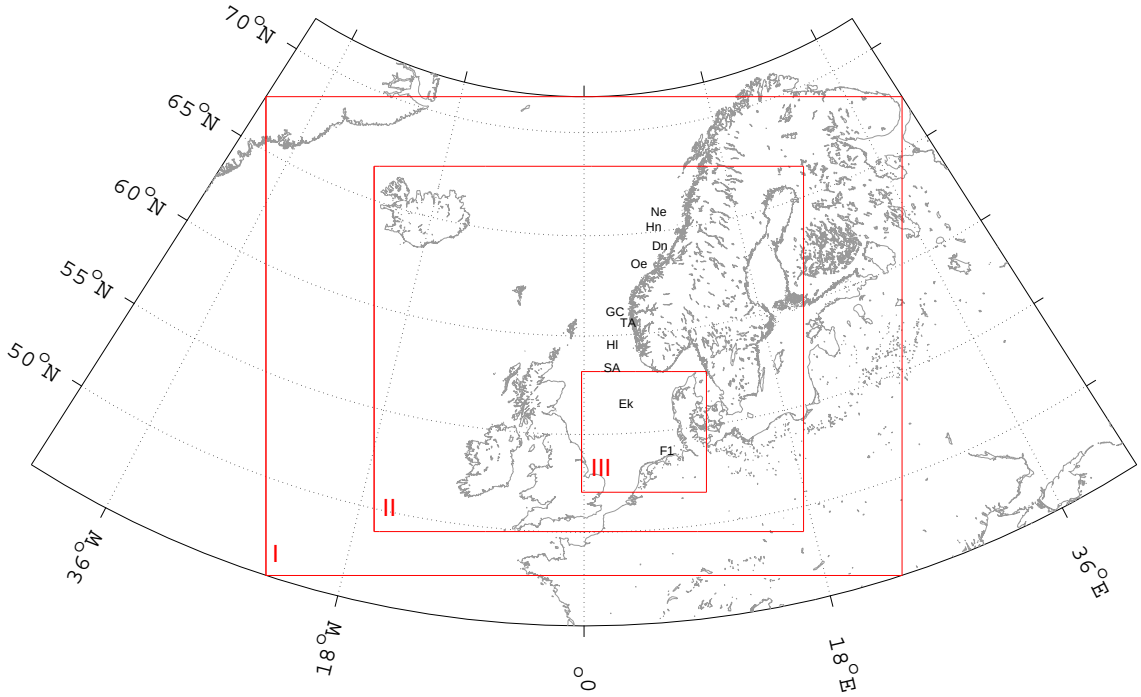

Figure 6: Locations of 9 group-I stations in the North Sea, see also Table 2. The sites are marked by the first and last letter of the site names. This is a modified copy of Figure 2a from [43] and it is not the X-WiWa storm model setup.

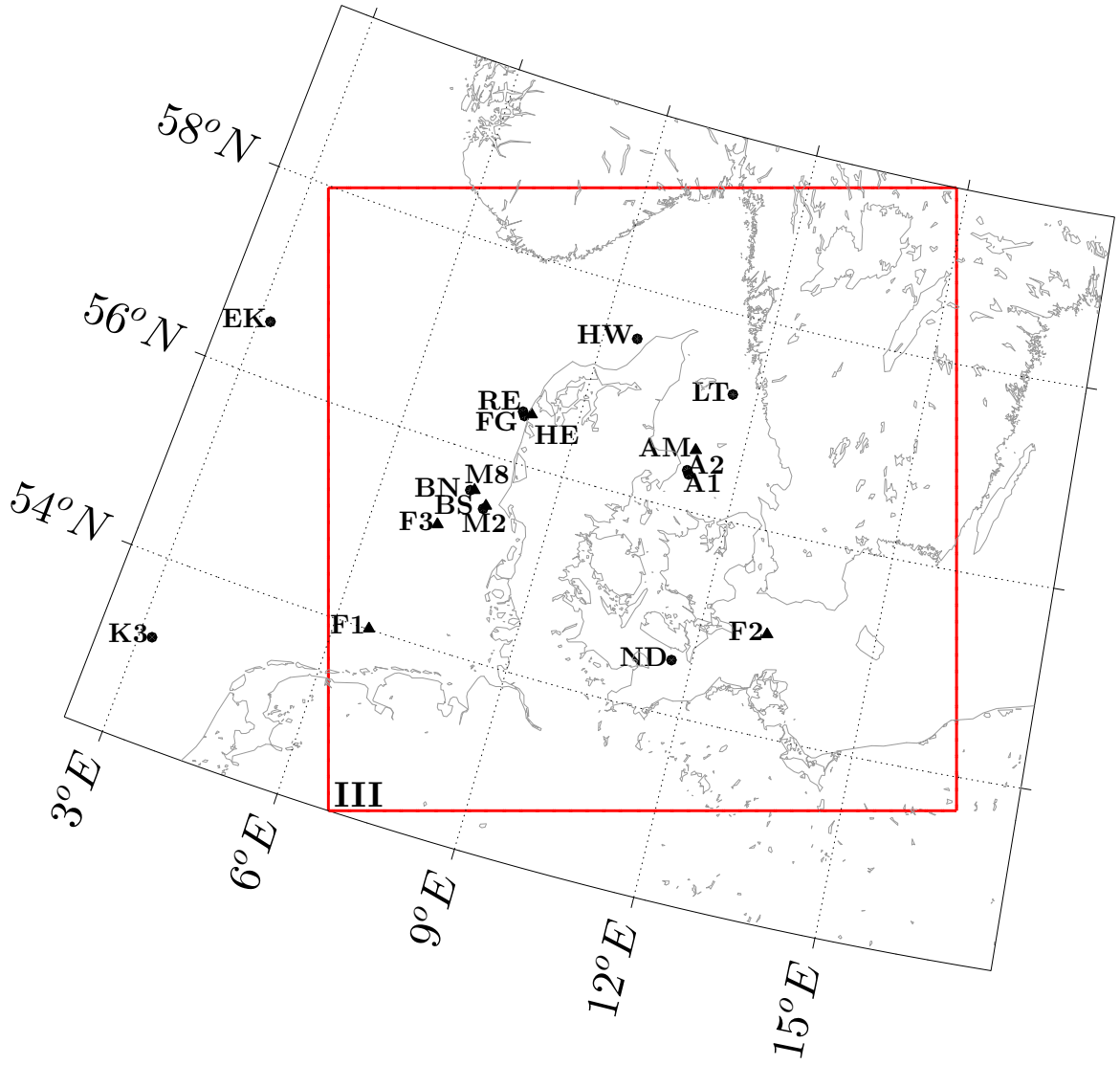

Figure 7: Locations of group-II and -III data stations inside model domain III, see also Table 3 and 4. Here RE - RUNE, HE - Høvsøre, M8 - Horns Rev II mast 8, M2 - Horns Rev I mast 2, F1 - FINO 1, F2 - FINO 2, F3 - FINO3, AM - Anholt lidar site, BN - the northern buoy close to M2, BS - the southern buoy close to M8, A1 and A2 - two buoys close to Anholt site, FG - Fjaltring, HW-Hirtshals West, LT - Läsö Ost, ND - Nysted.

Table 2: Measurements of Group-I: sites outside X-WiWa domain III, but in the North Sea (sorted from north to south) and their coordinates, measurement periods and variables. U_z is wind speed at height z, WD is the wind direction, H_{m0} is the significant wave height, H_{max} is the maximum wave height, PWD is the wave direction at the peak frequency, T_z is temperature at height $z = 40$, 70 and 100 m and SST is the sea surface temperature. From [43].

site	coordinates	Period	Variables
Norne	8.0850°E, 66.0256°N	2000 - 2012	U_z, WD, H_{m0}, H_{max}, PWD
Heidrun	7.3156°E, 65.3229°N	1996 - 2012	U_z, WD, H_{m0}, H_{max}, PWD
Draugen	7.7792°E, 64.3520°N	2000 - 2012	U_z, WD, H_{m0}, H_{max}, PWD
Ormen-Lange	5.2351°E, 63.5640°N	2008 - 2009, 2011 - 2012	U_z, WD, H_{m0}, H_{max}, PWD
Gullfaks-C	2.2687°E, 61.2042°N	1990 - 2001, 2007 - 2012	U_z, WD, H_{m0}, H_{max}, PWD
Troll-A	3.7193°E, 60.6435°N	2002 - 2012	U_z, WD, H_{m0}, H_{max}, PWD
Heimdal	2.2273°E, 59.5742°N	2003 - 2010, 2012	U_z, WD, H_{m0}, H_{max}, PWD
Sleipner-A	1.9091°E, 58.3711°N	2003 - 2012	U_z, WD, H_{m0}, H_{max}, PWD
Ekofisk	3.2149°E, 56.5453°N	1980 - 1983, 1986 - 2012	U_z, WD, H_{m0}, H_{max}, PWD

Table 3: Measurements of Group-II: sites inside X-WiWa domain III but measurements are short.

site	coordinates	Period	Variables
RUNE lidar	7.9967°E, 56.5°N	2015.11 - 2016.01	u_{100}
Anholt Lidar	11.1528°E, 56.5957°N	2013.01 - 2015.07	u_{100}
M8 mast	7.6227°E, 55.5996°N	2009 - 2014	u_{107}

Table 4: Measurements of Group-III: sites inside X-WiWa domain III and measurements are relatively long.

site	coordinates	Period	Variables
M2	7.875°E, 55.508°N	2000 - 2006	$u_{62}, u_{45}, u_{30}, u_{15}$
FINO1	6.588°E, 54.014°N	2004 - 2017	u_{100}
FINO2	13.1542°E, 55.007°N	2007 - 2017	u_{100}
FINO3	7.1583°E, 55.195°N	2009 - 2017	u_{100}
Høvsøre	8.15°E, 56.433°N	2005 - 2017	u_{100}

4.2 Satellite data

X-WiWa uses three types of satellite data: the cloud picture, the Quick Scatterometer (QSCAT) data and the Synthetic Aperture Radar (SAR) data.

The cloud pictures have been used to assist finding the storm centers ([25] Chapter 8), detecting the storm paths and identifying spatial features such as open cellular structures in the atmosphere [43]. These information is also used for model validation [25]. The cloud pictures are provided by the NERC Satellite Receiving Station, Dundee University, Scotland at http://www.sat.dundee.ac.uk.

Both QSCAT and SAR utilize the fact that radar backscatter from the sea surface depends on centimeter-scale, local wind generated, waves. The relationship of radar backscatter to the 10-m wind speed is described by an empirical model function [57].

The QSCAT data used here are gridded in a 0.25 degree latitude by 0.25 degree longitude. The data are thus approximately of 25 km spatial resolution. When the methodology for QSCAT wind retrieval was developed at Remote Sensing Systems, validation data containing high winds were extremely limited (http://www.remss.com/missions/qscat.html). Extrapolations and assumptions were made for winds greater than 20 ms^{-1}. During storm conditions, another challenge for QSCAT data is the rain contamination since it is difficult to separate the wind and rain signals in the retrieval. QSCAT data have been applied to describe wind characteristics over the North Sea and the Baltic Sea [58, 59]. They are used here in X-WiWa to validate the 10-m wind field from storm simulations over open waters ([25] Chapter 4, [60]). Fig. 9 shows such an example how the wind fields from QSCAT are used to validate the modeled wind field during one particular storm on 22nd December 2002.

SAR data are of much finer spatial resolution in comparison with QSCAT data. This strength makes it possible to examine the wind fields that are close to shore as well as the wind fields that contain special atmospheric structures.

DTU Wind Energy operates a system for routine wind retrieval from satellite

Table 5: Buoy sites.

site	coordinates	Period	water depth (m)
Anholt buoy 1	11.1374°E, 56.3524°N	2013.01 - 2014.11	16
Anholt buoy 2	11.1374°E, 56.3892°N	2013.01 - 2015.06	17
M2 buoy S	7.835°E, 55.4798°N	1999 - 2006	6-12
M2 buoy N	7.5298°E, 55.6118°N	2006 - 2015	6-12
Ekofisk	3.2149°E, 56.5453°N	1994.01 - 2012.08	70
Fjaltring	8.0568°E, 56.4742°N	1994.01 - 2013.05	30
Hirtshals west	9.6127°E, 57.5149°N	1999.08 - 2012.08	20
Läsö Øst	11.57°E, 57.22°N	2005.01 - 2009.02	70
Nysted	11.6627°E, 54.5348°N	2004.10 - 2007.02	9
RUNE	7.9967°E, 56.50°N	2015.11 - 2015.12	16
K13	3.2203°E, 53.2178°N	1989.04 - 2013.06	29
Väderöarna	10.93°E, 58.48°N	1999.11 - 2012.04	74
Trubaduren	11.63°E, 57.60°N	1999.11 - 2012.04	30
Nymindegab	7.9398°E, 55.809°N	1999.11 - 2012.04	20

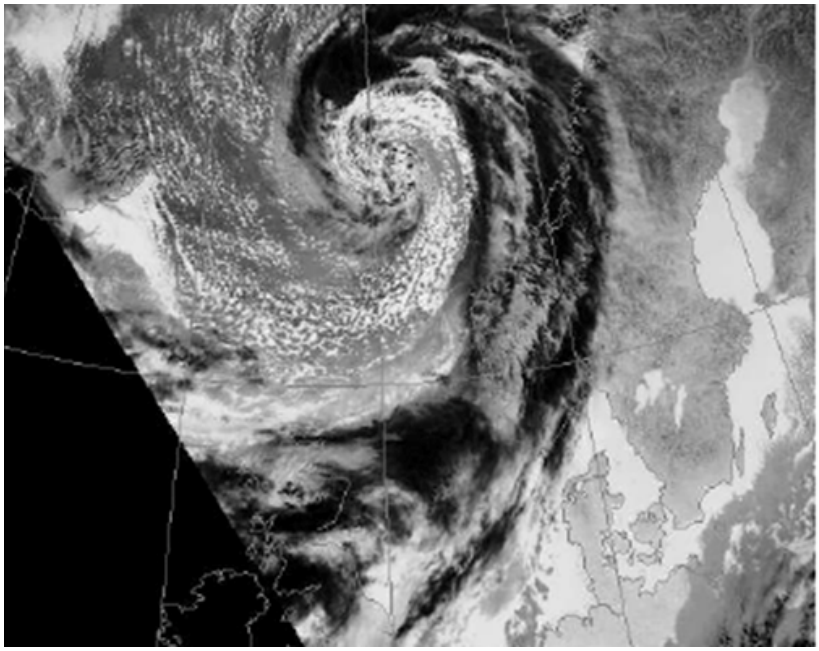

Figure 8: Cloud picture at 20:45, 2004-02-23. A copy from [56]

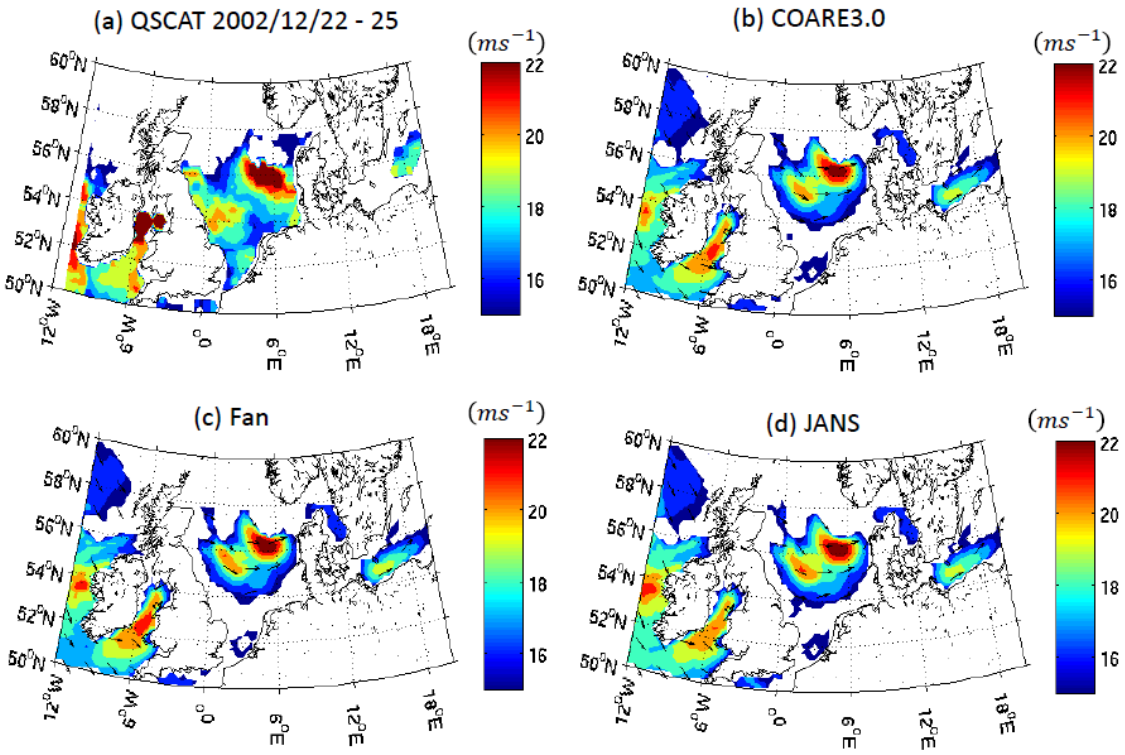

Figure 9: Footprint of 10-m wind speed during a storm in December 2003, using (a) QSCAT data to validate modeling from (b) not-coupled WRF (c) coupled using the Fan roughness length scheme and (d) coupled using Janssen stress scheme. A copy of Fig. 4.6 from [25]

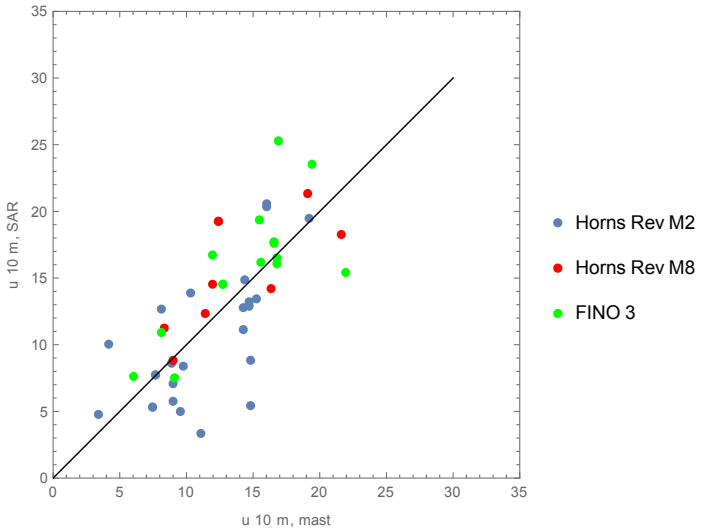

Figure 10: Comparison of wind speed at 10 m, from masts at M2, M8 and FINO3 corrected from other levels to 10 m, and all SAR data at the corresponding pixel cells

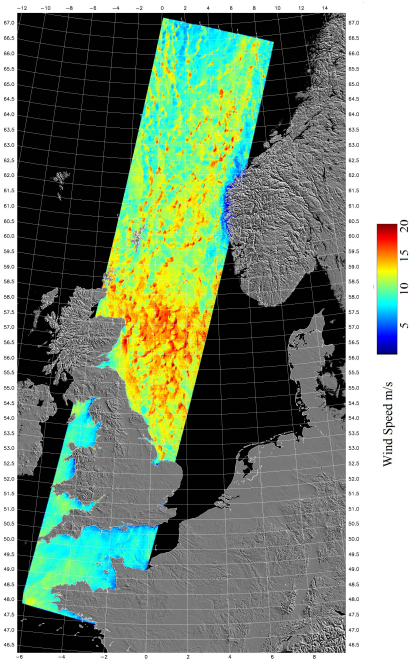

Figure 11: ENVISAT SAR 10 m wind speed on 2006-11-01 10:26:41 from [43]

SAR scenes. New SAR scenes are obtained from the European Space Agency on a daily basis and converted to maps of the wind speed at 10 m above the sea surface. The maps are available at *https* : *//satwinds.windenergy.dtu.dk/* together with further descriptions of the processing method.

The SAR data used for X-WiWa are from the Envisat satellite, which was in operation during 2002-2012. When operated in Wide Swath Mode, the Advanced SAR onboard Envisat would scan the Earth surface in 400-m wide swaths. The spatial resolution of the original satellite data is 150 m but during the wind retrieval processing, the scenes are reduced to 500-m pixels to eliminate effects of random image noise and inclination of the sea surface due to long-period ocean waves.

The spatial resolution of the SAR data that are used in X-WiWa is about 500 m. Through comparison with in-situ wind speed measurements, [53, 61, 48] show that the root-mean-square-error of the SAR 10-m wind speed is between about 1.3 and 1.5 ms^{-1}, although the bias depends on the model function chosen for SAR retrieval. Figure 10 shows the comparison of the 10-m wind speed between mast measured wind speed corrected to 10 m using a simple Charnock parameterization for z_0 and all available SAR data at the corresponding pixels to the masts for our simulated storms over model domain III. There is an overall good correlation between the two data sets, however the scatter is large, which reflects the uncertainty related to the absolute values of the SAR wind speed, although the bias at each of the three sites is different. In this project the SAR data and images are mostly used to identify special atmospheric features as used in [43], see Fig. 11 for an open cell case.

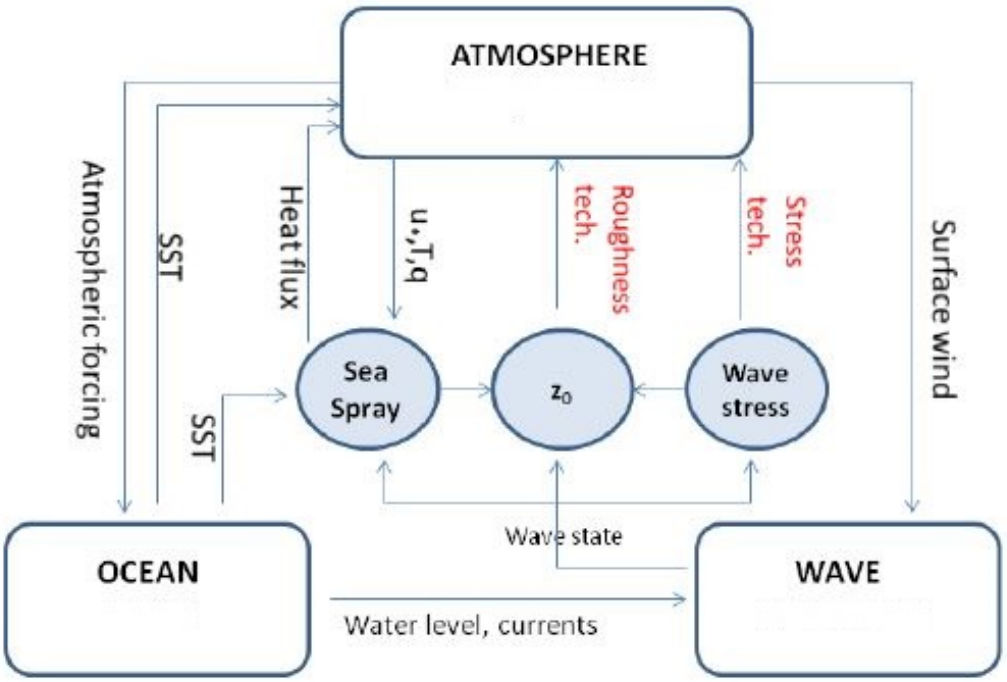

Figure 12: X-WiWa model structure. A copy from the X-WiWa proposal.

5 The X-WiWa modeling system and the development of it

Within X-WiWa, the development of the modeling system has gone through numerous experiments. The fundamental interest is to find the numerical expressions to best describe the physical processes of the air-sea interaction.

The complex air-sea exchange processes for momentum and heat have been simplified to the diagram presented in our original proposal, which is reproduced here in Fig 12. Most commonly, coupling system consists two stream lines as shown in the diagram of Fig. 12: $[atmosphere] \rightarrow (wind) \rightarrow [wave]$, and $[wave] \rightarrow (wave\ state) \rightarrow [z_0] \rightarrow (roughness\ tech.) \rightarrow [atmosphere]$. In this flow, the red text "roughness tech." is the method of parametrization of z_0. We here use "[ ]" to represent model as in the flow and "( )" to represent input parameter. Thus, $[atmosphere]$ and $[wave]$ means atmospheric and wave modeling, respectively, and $(wind)$ means the input parameter that leads the calculation flow, and so on and so forth. As explained in section 2, the atmospheric modeling is through WRF and wave modeling is through SWAN as well as MIKE.

X-WiWa obtained new findings and knowledge in the following flow as included in the project workflow shown in Fig. 12:

1. $[atmosphere] \rightarrow (atmospheric\ forcing) \rightarrow [ocean] \rightarrow (water\ level,\ currents) \rightarrow [wave]$ through CFSR data and MIKE model, (see deliverables D1.3, D1.15 in section 11, and descriptions in section 5.4).
2. $[sea\ spray] \rightarrow (heat\ flux) \rightarrow [atmosphere]$ through WRF and parameterizations, (see deliverables D1.16 and D1.7 in section 11).
3. $[wave] \rightarrow (wave\ state) \rightarrow [z_0] \rightarrow (roughness\ tech.) \rightarrow [atmosphere]$,

through WRF and SWAN, as well as WRF and MIKE [25].

4. $[wave] \rightarrow (wave\ state) \rightarrow [wave\ stress] \rightarrow (stress\ tech.) \rightarrow [atmosphere]$, through WRF and SWAN, [62, 25]. The last one is a unique contribution from X-WiWa.

The core structure of the current X-WiWa model systems are:

1. Two-way online: $[WRF] \leftrightarrow (WBLM) \leftrightarrow [SWAN]$;
2. One-way offline: $[WRF] \rightarrow (wind) \rightarrow [MIKE\ 21\ SW]$,

which are denoted as WRF-WBLM-SWAN and WRF-MIKE, respectively. WRF-WBLM-SWAN is used for modeling of both wind and waves. WRF-MIKE is used for modeling waves only. Here WBLM takes care of the part of "stress tech." as highlighted in Fig. 12.

In coupling WRF and SWAN, X-WiWa uses the framework of COAWST and its model coupling tool kit (MCT), see Fig. 1. X-WiWa improved COAWST during the project, including strengthening the numerical stability in two-way nested model setup, correction of the Janssen stress table by importing the table from WAM model, and implementation of several more parametrization schemes for z_0 such as the Fan and the Liu schemes. However, one of the most important contributions from X-WiWa to COAWST and the wind-wave modeling in general is the implementation of the wave boundary layer model WBLM in SWAN [62].

5.1 The Wave Boundary Layer Model

A key contribution from X-WiWa to the community of wind-wave coupled modeling is the implementation of the wave boundary layer model (WBLM) in the third-generation ocean wave model SWAN. This was first investigated under idealized, fetch-limited condition [62], and the model was later calibrated for real cases [25] (Chapter 8).

The details of WBLM can be found in [62]. Here we briefly describe the principles. The WBLM was initially developed by [31] and [32]. It is implemented here in SWAN to modify the Janssen wind-input source function. The WBLM is characterized by two conservation equations which provide the distribution of stress and kinetic energy (KE) with height and introduce the wave impact from the wave modeling to the atmospheric modeling. The two equations describe the momentum and KE conservations. The momentum conservation reads as Eq. (13), in which the wave-induced stress is calculated according to:

$$\vec{\tau}_w(z) = \rho_w \int_{\sigma_{min}}^{\sigma_z} \int_{-\pi}^{\pi} \beta_g(\sigma,\theta)\,\sigma^2 N(\sigma,\theta)\,\frac{\vec{k}}{k} d\theta d\sigma \tag{14}$$

where $\sigma_z = \sqrt{g\delta/z}$, $\delta = 0.01$ [32], σ_{min} is the minimum radian frequency of the wave spectrum. Eq. (14) means that the wave-induced stress at height z is equal to the integration of momentum flux to the waves within the range of $\sigma_{min} < \sigma < \sigma_z$. In developing the X-WIWa modeling system, we employ the sheltering mechanism which suggests that the growth of short waves is reduced by low frequency waves. Combining Eq. (13) and (14) gives:

$$\vec{\tau}_t(z) = \vec{\tau}_{tot} - \rho_w \int_{\sigma_{min}}^{\sigma_z} \int_{-\pi}^{\pi} \beta_g(\sigma,\theta)\,\sigma^2 N(\sigma,\theta)\,\frac{\vec{k}}{k} d\theta d\sigma. \tag{15}$$

Following the sheltering mechanism, it is the turbulent stress, rather than the total stress, that contributes to the wave growth. The Janssen source function is

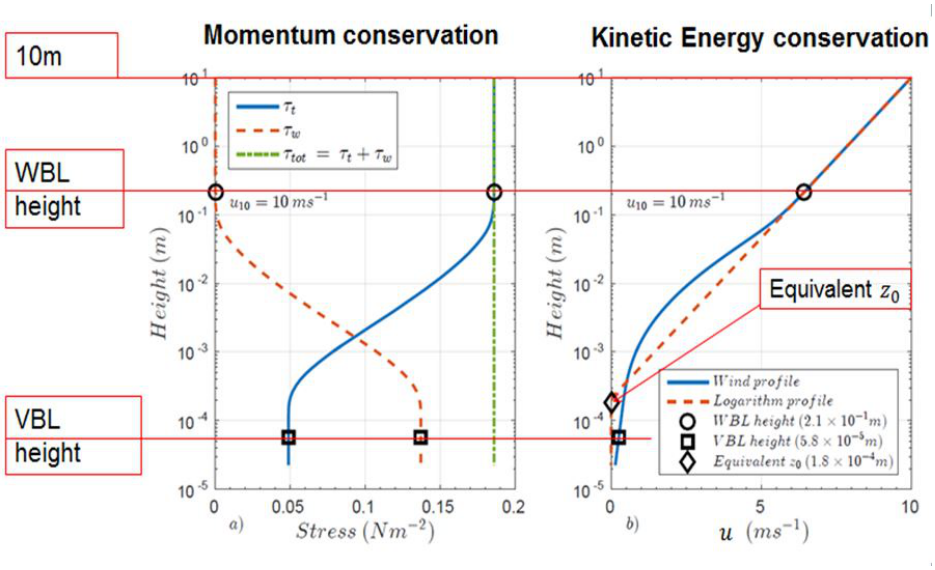

Figure 13: Illustration of the vertical distribution of stress and wind speed profile after 72 hours simulation at long fetch of 3000 km, at wind speed at 10 m of 10 ms^{-1}. WBL means Wave Boundary Layer. VBL means viscous boundary layer. Modified from [62].

thus modified so that the growth rate is proportional to the local friction velocity $u_*^l = \sqrt{|\vec{\tau}_t(z)/\rho_a|}$:

$$\beta_g(\sigma,\theta) = C_\beta \sigma \frac{\rho_a}{\rho_w}\left(\frac{u_*^l}{c}\right)^2 cos^2(\theta-\theta_w) \tag{16}$$

The constant J in the description of the Miles parameter C_β, where $C_\beta = (J/\kappa^2)\lambda \ln^4 \lambda$ with $\lambda \leq 1$, is changed to 1.6 according to [42] instead of the original of 1.2 in [63].

The KE conservation equation reads:

$$\frac{d}{dz}(\vec{u}\cdot\vec{\tau}_{tot}) + \frac{d\Pi}{dz} + \frac{d\Pi'}{dz} - \rho_a\varepsilon = 0 \tag{17}$$

where $\vec{u}$ is the mean wind vector, Π and Π' are the vertical transport of the kinetic energy due to the wave-induced motions and the vertical transport of TKE, respectively, and ε is the viscous dissipation of KE. It is assumed that the wave-induced vertical transport of kinetic energy is mainly from the pressure transport [31], which is equal to the energy flux into the surface waves:

$$\Pi(z) = \int_{\sigma_{min}}^{\sigma} \tilde{F}_w(\sigma)\,d\sigma \tag{18}$$

where $\tilde{F}_w$ is the vertical decay function:

$$\tilde{F}_w(\sigma) = \rho_w \int_{-\pi}^{\pi} \beta_g(\sigma,\theta)\, g\sigma N(\sigma,\theta)\,d\theta \tag{19}$$

The viscous dissipation rate is parameterized as in [31]:

$$\varepsilon(z) = \frac{|\vec{\tau}_t(z)/\rho_a|^{\frac{3}{2}}}{\kappa z} \tag{20}$$

The wind profile inside WBL can be derived through the KE conservation. Assuming that the gradient of the vertical transport of the KE, $d\Pi'/dz$, is small compared to the other terms [31], the wind profile near the sea surface can be expressed as:

$$\begin{cases} \frac{d\vec{u}}{dz} = \frac{u_*}{\kappa z}\frac{\vec{\tau}_{tot}}{|\vec{\tau}_{tot}|}, & z \geq \frac{g\delta}{\sigma_{min}^2} \\ \frac{d\vec{u}}{dz} = \left[\frac{\delta}{z^2}\tilde{F}_w\left(\sigma = \sqrt{g\delta/z}\right) + \frac{\rho_a}{\kappa z}\left|\frac{\vec{\tau}_t(z)}{\rho_a}\right|^{\frac{3}{2}}\right] \times \frac{\vec{\tau}_t(z)}{\vec{\tau}_t(z)\cdot\vec{\tau}_{tot}}, & \frac{g\delta}{\sigma_{max}^2} \leq z < \frac{g\delta}{\sigma_{min}^2} \\ \frac{d\vec{u}}{dz} = \frac{\rho_a}{\kappa z}\left|\frac{\vec{\tau}_\nu}{\rho_a}\right|^{\frac{3}{2}} \times \frac{\vec{\tau}_\nu}{\vec{\tau}_\nu\cdot\vec{\tau}_{tot}}, & z_\nu \leq z < \frac{g\delta}{\sigma_{max}^2} \end{cases} \quad (21)$$

where $z_\nu = 0.1\frac{\nu_a}{\sqrt{|\vec{\tau}_\nu/\rho_a|}}$ is the roughness length of the viscous sublayer where the wind speed turns into zero, and ν_a is the air viscosity.

The calculation of WBLM starts with an initial estimation of $\vec{\tau}_{tot}$, and it calculates S_{in}, $\vec{\tau}_w$, and $\vec{\tau}_t$ at each frequency (height) by Eqs. (14) to (16), and then calculates the wind profile by Eq. (21). The process repeats itself using the Newton-Raphson method until the wind speed at the reference height z_{ref} calculated from Eq. (21) equals to the provided wind speed. In [62], $z_{ref} = 10$ m was used.

5.2 WRF

The WRF model is a next-generation mesoscale numerical weather prediction system [8]. The dynamical solver in WRF integrates the compressible, non-hydrostatic Eular equations. These equations are cast in flux form using variables that have conservation properties such as vector wind, and scalars (temperature and humidity). The equations are formulated using a terrain-following mass vertical coordinate [9].

The following is a description from [25] explaining how WRF modeling is affected by the coupling through WBLM. The momentum flux in the air-sea interface affects the WRF modeling by changing the surface stress which provides the lower boundary of the Planet Boundary Layer (PBL) scheme. Since the input stress to the first model level of WRF is $\tau_t = \tau_{tot} - \tau_w$, the impact of waves is thus introduced into WRF. Here we use the MYNN PBL scheme [64, 65], as it solves higher order Turbulent Kinetic Energy (TKE) equation than other PBL schemes, e.g. MYJ [66]. Here we briefly go through the equations in MYNN PBL scheme that are directly affected by the surface stress. The one-dimensional equations for ensemble-averaged variables are given by:

$$\begin{aligned} \frac{\partial u}{\partial t} &= -\frac{\partial}{\partial z}\left\langle u'w'\right\rangle + f\left(v - v_g\right), \\ \frac{\partial v}{\partial t} &= -\frac{\partial}{\partial z}\left\langle v'w'\right\rangle - f\left(u - u_g\right) \end{aligned}$$

where u and v are the horizontal wind velocity, u_g and v_g are the geostrophic wind velocity, f is the Coriolis parameter. The turbulent flux $\langle u'w'\rangle$ and $\langle v'w'\rangle$ are solved by the Turbulent Kinetic Energy (TKE) equation:

$$\frac{dQ}{dt} - \frac{\partial}{\partial z}\left[LqS_q\frac{\partial Q}{\partial z}\right] = 2\left(P_s + P_b - \varepsilon\right) \quad (22)$$

[8] https://www.mmm.ucar.edu/weather-research-and-forecasting-model

[9] *http://www2.mmm.ucar.edu/wrf/users/docs/arw_v3.pdf*

where $Q = q^2 = \langle u'^2 + v'^2 + w'^2 \rangle$ is the twice-TKE. On the left hand side of Eq. (22) is the time dependence and vertical diffusion terms. On the right hand side are the shear production, buoyancy production and dissipation terms respectively. The two components of the momentum flux are described as

$$\begin{aligned} -\langle u'w' \rangle &= K_m \frac{\partial u}{\partial z} \\ -\langle v'w' \rangle &= K_m \frac{\partial v}{\partial z} \end{aligned}$$

where $K_m = LqS_m$. The master length scale L and q are calculated from Eq. (22), and S_m is solved by MYNN level 2, level 2.5, and level 3 methods which are also functions of L and q. The surface stress affects the solution of TKE equation in two ways. The first way is the kinetic way through changing the shear production P_s. The surface stress (τ_s) is represented by the friction velocity (u_*). $\tau_s = \rho_a u_*^2$, ρ_a is the air density. It directly impacts the first model level of the shear production by:

$$P_{d1} = 2\frac{u_*^3}{\kappa z}(\phi_m - \zeta) - P_{d2} \tag{23}$$

where $P_{d1} = (P_s + P_b)_1$ is the sum of shear and buoyancy production at the first model level. $\kappa = 0.41$ is the von Kármán constant.

$$\begin{aligned} \phi_m &= 1 + (5-1)\zeta, \quad \zeta \geq 0 \\ &= \frac{1}{\sqrt[4]{1-16\zeta}}, \quad \zeta < 0 \end{aligned}$$

where $\zeta = \frac{z}{L_m}$ and L_m is the Monin-Obukhov length, and it is directly impacted by u_*.

$$\begin{aligned} \frac{1}{L_m} &= \frac{B_r \ln\left(\frac{z_{\frac{1}{2}} + z_0}{z_0}\right)}{z_{\frac{1}{2}}}, \quad B_r = 0, u_* < 0.01 \\ &= \frac{\kappa g T_*}{\theta_{\frac{1}{2}} u_*^2}, \quad B_r \neq 0 \end{aligned}$$

In neutral condition, $\zeta = 0$, $\phi_m = 1$, and the production at the first model level will only depend on u_* and the production at the second model level. The impact will transfer to higher levels by the diffusion terms in the TKE equation. The other way that u_* impacts the solution of TKE equation is by changing the master length scale:

$$\frac{1}{L_k} = \frac{1}{L_S} + \frac{1}{L_T} + \frac{1}{L_B}, \tag{24}$$

where L_k is the master length scale at level k, L_T and L_B are the length scale dependent on the depth of ABL and buoyancy. L_S is the length scale in the surface layer which is written as:

$$\begin{aligned} L_s &= \kappa z/3.7, \quad \zeta \geq 1 \\ &= \kappa z\,(1 + 2.7\zeta)^{-1}, \quad 0 \leq \zeta < 1 \\ &= \kappa z\,(1 - \alpha_4 \zeta)^{0.2}, \quad \zeta < 0 \end{aligned}$$

u_* is estimated diagnostically, where the roughness length (z_0) in the atmospheric model is involved:

$$u_*^{n+1} = \frac{u_*^n + \kappa u_{\frac{1}{2}} \psi_x}{2}, \quad \psi_x = \ln\left(\frac{z_{\frac{1}{2}} + z_0}{z_0}\right) - \psi_m \tag{25}$$

Here u_*^{n+1} at the present time step is the average of the previous value (u_*^n) and the new estimation from z_0 to avoid sudden changes.

5.3 SWAN

SWAN is a third-generation wave model, developed at Delft University of Technology, that computes random, short-crested wind-generated waves in coastal regions and inland waters [10].

In the third generation ocean wave model, the evolution of the wave spectrum is governed by a conservation equation for wave action N:

$$\frac{dN}{dt} = S_{in} + S_{nl} + S_{ds} \tag{26}$$

On the right hand side of Eq. (26) are the three source functions of wind-wave generation in deep-water conditions: wave growth induced by the wind S_{in}, nonlinear four-wave interaction S_{nl}, and wave dissipation due to wave-breaking S_{ds}. The surface stress is estimated through S_{in}. There are various ways to estimate the surfaces stress. The simplest, but most commonly used way, is to employ a drag relation that fits measurements. For example, in SWAN's default setting, it uses the 2nd order fit according to Zijlema (2012):

$$C_d = \left(0.55 + 2.97\widetilde{U} - 1.49\widetilde{U}^2\right) \times 10^{-3} \tag{27}$$

where $\widetilde{U} = U_{10}/31.5ms^{-1}$, and $u_* = \sqrt{C_d}U_{10}$. There are also other parameterizations which use Charnock's relation to parameterize z_0 and also take into account of the wave impact (e.g. [20, 67, 18]). Some of them are applied to coupling systems (e.g. COAWST), but they are not always used in wave models. Thus, numerically they are coupled, but physically they are not fully coupled because the wave model and atmospheric model use different surface stresses.

One remarkable approach for coupling follows [63]. The wave model utilizes [63]'s wind-input source function and transfers an effective roughness length z_0, which includes the impact of wave-induced stress (τ_w) in the atmospheric modeling. Thus both models share the same z_0 (or equivalently u_*) and requires fewer assumptions. The effective roughness length is expressed as

$$z_0 = \frac{0.01u_*^2}{g\sqrt{1 - \tau_w/\tau_{tot}}}, \tag{28}$$

where $\tau_{tot} = \rho_a u_*^2$ is the total stress. The friction velocity is calculated from the drag relation

$$u_* = \sqrt{C_d}U_{10}, \tag{29}$$

through the assumption of a logarithmic wind profile Eq. 2. Combining Eqs. (28), (29) and (2), z_0, C_d, and u_* can be obtained for a given τ_w and U_{10}.

[10] *https : //www.tudelft.nl/en/ceg/over − faculteit/departments/hydraulic − engineering/sections/environmental − fluid − mechanics/research/swan/*

The wave-induced stress τ_w is expressed as the model-resolved stress τ_{wl} plus an unresolved (parameterized) high-frequency contribution, τ_{wh}:

$$\tau_{wl} = \rho_w \int_{\sigma_{min}}^{\sigma_c} \int_{-\pi}^{\pi} \sigma^2 \beta_g(\sigma,\theta) N(\sigma,\theta) d\theta d\sigma, \quad (30)$$

$$\tau_{wh} = \rho_w \int_{\sigma_c}^{\sigma_{max}} \int_{-\pi}^{\pi} \sigma^2 \beta_g(\sigma,\theta) N(\sigma_c,\theta) \left(\frac{\sigma_c}{\sigma}\right)^6 d\theta d\sigma, \quad (31)$$

where σ is the radian frequency and c is the phase velocity. $N(\sigma,\theta)$ is the directional wave-action density spectrum. In the wave model, the wave spectra is solved from a minimum (σ_{min}) frequency to a high-frequency limit (cut-off frequency, σ_c). Beyond the cut-off frequency, a σ^{-5} tail is added extending the spectra to a maximum frequency (σ_{max}) where the wave energy is small enough to be neglected. The expression of wave growth rate β_g for JANS wind-input source function is expressed as

$$\beta_g(\sigma,\theta) = C_\beta \sigma \frac{\rho_a}{\rho_w} \left(\frac{u_*}{c}\right)^2 cos^2(\theta - \theta_w), \quad (32)$$

where C_β is the Miles' constant, which is described as a function of non-dimensional critical height λ:

$$C_\beta = \frac{J}{\kappa^2} \lambda \ln^4 \lambda, \quad \lambda \leq 1, \quad (33)$$

$$\lambda = \frac{g z_0}{c^2} \exp\left(\kappa c / |u_* \cos(\theta - \theta_w)|\right) \quad (34)$$

where $J = 1.2$ is a constant.

5.4 MIKE 21 SW

MIKE 21 SW Spectral Wave FM model is developed, supported and maintained by DHI. Like the other modules included in the flexible mesh series of MIKE Powered by DHI, the spectral wave model is based on an unstructured, cell-centred finite volume method and uses an unstructured mesh in geographical space. This approach, which has been available from DHI now for more than a decade and which is thus fully matured, gives the maximum degree of flexibility, and allows the model resolution to be varied and optimised according to requirements in various parts of the model domain. The MIKE 21 SW version 2017 was applied to generate the map of extreme waves around Denmark (section 9). A summary of the model description and capabilities is given below. Note that some of the model features (e.g. diffraction, ice coverage) were not included in this study as they were not relevant for the present application.

MIKE 21 SW is DHI's state-of-the-art third generation spectral wind-wave model. The model simulates the growth, decay and transformation of wind-generated waves and swells in offshore and coastal areas. Due to its unique unstructured flexible mesh technique, MIKE 21 SW is particularly suited for simultaneous, i.e. in one single model domain, wave modelling at regional scale and at local scale. Coarse spatial resolution is used for the regional part of the mesh and a higher resolution is applied in more shallow water environment at the coastline, around structures, etc.

MIKE 21 SW includes the following physical phenomena:

- Wave growth by action of wind
- Non-linear wave-wave interaction
- Dissipation due to white-capping
- Dissipation due to bottom friction
- Dissipation due to depth-induced wave breaking
- Refraction and shoaling due to depth variations and currents
- Wave-current interaction
- Effect of time-varying water depth and currents
- Effect of ice coverage on the wave field
- Wave diffraction
- Wave reflection
- Influence of structures (like piers, wind turbine foundations, WEC, TEC)

Main computational features of MIKE 21 SW are:

- Source functions based on state-of-the-art 3rd generation formulations
- Fully spectral and directionally decoupled parameterised formulation
- In-stationary and quasi-stationary solutions
- Optimal degree of flexibility in describing bathymetry and ambient flow conditions using depth-adaptive and boundary-fitted unstructured mesh
- Coupling with hydrodynamic flow model for modelling of wave-current interaction and time-varying water depth
- Flooding and drying in connection with time-varying water depths
- Water-structure interaction module
- Parallelised using OpenMP and MPI techniques

5.5 Offline wave modeling using MIKE 21 SW

The offline coupling system used enabled the coupling between the atmospheric model WRF (or the wind re-analysis CFSR) and MIKE 21 SW. In the system, WRF uses regular structured grids and MIKE uses unstructured grids. It is called "offline" or "one-way" because the data exchange between the two models is only from the atmospheric model to the wave model. The offline system was used along the project for several objectives:

- to test the sensitivity of the model resolution and different roughness length (z_0)
- to investigate the remapping approach between the two different grid structures, especially in the nested cases (WRF-SWAN)
- to assess impact of online vs offline system
- to assess impact of using WRF or CFSR as an atmospheric forcing fields
- to calibrate/validate MIKE 21 SW for the hindcast of wave storms and extreme value analysis

The offline coupling system was divided into three parts: WRF model, MIKE 21 SW model, and the data interpolation and conversion routine (DIC). To run the system, the first step was to setup and run WRF to get hourly 10 meter wind velocity (U10) for MIKE. Secondly, through a DIC routine, U10 was interpolated to the MIKE unstructured grid and then converted into a "dfsu" format file which was then used by MIKE directly.

Throughout the X-WiWa project, several developments within MIKE21 SW took place to improve wave modelling. These are described in the following sections and include improvements of the forcing and the model itself.

5.5.1 Correction of wind forcing due to atmospheric stability

The Climate Forecast System Reanalysis (CFSR) is a coupled meteorological and oceanographic model system that uses synoptic data for initialization. The data are available on an hourly basis from 1 January 1979 to present. DHI has successfully used CFSR atmospheric data in numerous commercial and research projects worldwide due to their consistency and generally good accuracy. The CFSR reanalysed hindcast data cover the period from 1979 to 2010 (31 years), and since then the operational dataset (denoted CFSR II) was applied. The underlying model in CFSR II is the same as for CFSR; however, the spatial resolution of wind was increased from 0.3° to 0.2°. Hereafter, "CSFR" will refer to the combined CFSR and CFSR2 dataset. CFSR was designed as a global, high-resolution, coupled atmosphere-ocean-land surface-sea ice system to provide the best estimate of the state of these coupled domains. The atmospheric model included in the CFSR modelling complex is GFS. Further details of CFSR are given in [68, 69]. The need of a correction due stability comes from the basis of the wave model equations theoretical derivations (e.g. [70]). The growth rate formulation as implemented in MIKE 21 SW is defined as in Eq. (16) and the stability is described through the Obukhov length L_m as in Eq. (24) in u_*:

$$u_* = \frac{\kappa U(z)}{\ln(z/z_0) - \Phi_m(z/L_m)} \tag{35}$$

Wind speed, air and sea temperature, humidity from CFSR data set are used to calculate u_*.

An example of the impact of the correction due to stability is shown in Fig. 14 at Ekofisk location (see Fig. 6 "Ek") where an improvement in the error statistics is noticeable.

5.5.2 Map of surface roughness approximation

MIKE 21 SW allows the specification of different areas where the surface roughness (and friction velocity) is estimated following different approaches, i.e. Janssen (1991) formulation or a Charnock relation. This is used in an attempt to tackle the known limitation of the spectral models regarding estimate of roughness and surface stress under short fetches. Figure 15 shows an example of such a map where near the coast (blue areas) a Charnock relation is used while in offshore areas (red areas) the Janssen (1991) formulation is used. This model feature has been used in model setting when using Janssen formulation.

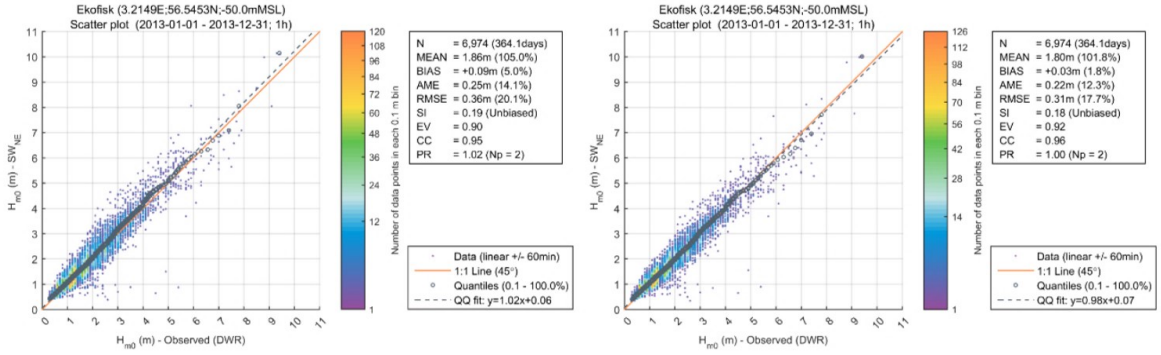

Figure 14: Scatter comparison of modelled significant wave heights (left panel: without taking the atmospheric stability into account. Right panel: taking the atmospheric stability into account) against measurements at Ekofisk for 2013.

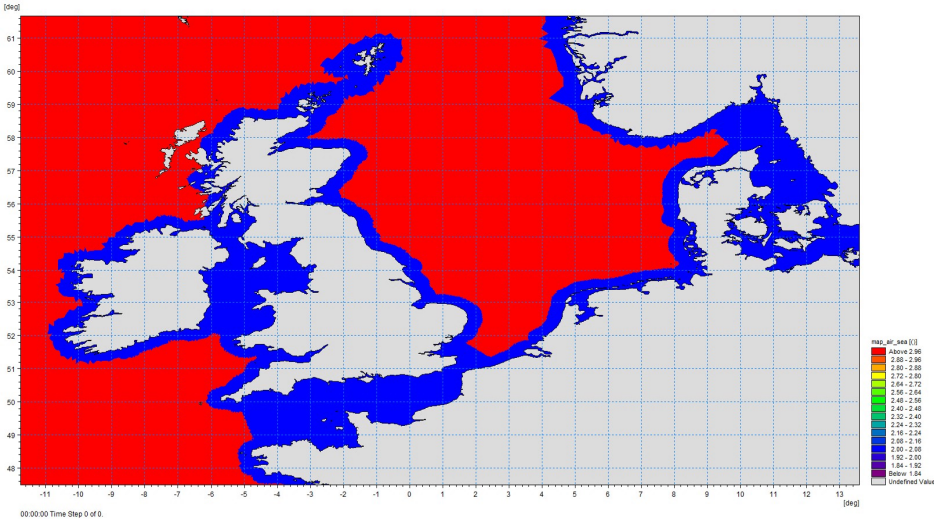

Figure 15: Map of surface roughness approximation. Red areas indicate areas where (Janssen, 1991) formulation is used for estimate of friction velocity and blue areas where a Charnock relation is used instead

5.5.3 Air-water density ratio

Wave growth is dependent on the air-water density ratio (see Eq. (16)). Although variations in the North Sea are relatively small, the project has allowed the development of MIKE 21 SW so that the ratio can be provided explicitly instead of the more traditional constant value ($\sim$ 0.00125). The impact of this new feature is small during storm conditions and thus has not been used for the simulation of storms, see Fig. 16.

5.5.4 Correction of wave celerity due to parametric surface current

The development of spectral wave models has also led to estimates of wind drag and sea surface roughness based on energy balance equation source functions. For example, the (Janssen, 1991) spectral wave formulation (which is the "standard" in models like WAM 4.5 and MIKE 21 SW) considers the interaction of waves and wind to estimate a wind friction velocity (u_*) and roughness length (z_0) dependent on the input source function. However, it has been argued that, although this formulation produces good wave predictions for general operational applications, it over1estimates the drag coefficient when compared with observations [36, 71]. Similar over-estimations were found [72] with the WAVEWATCH III formulation. (Jensen, 2006) proposed the use of a limit on the friction velocity in order to model extreme events. This limitation was in terms of the ratio of friction velocity and wind speed (u_*/U_{10}). A different process that can modify the waves due to the current has been considered within the framework

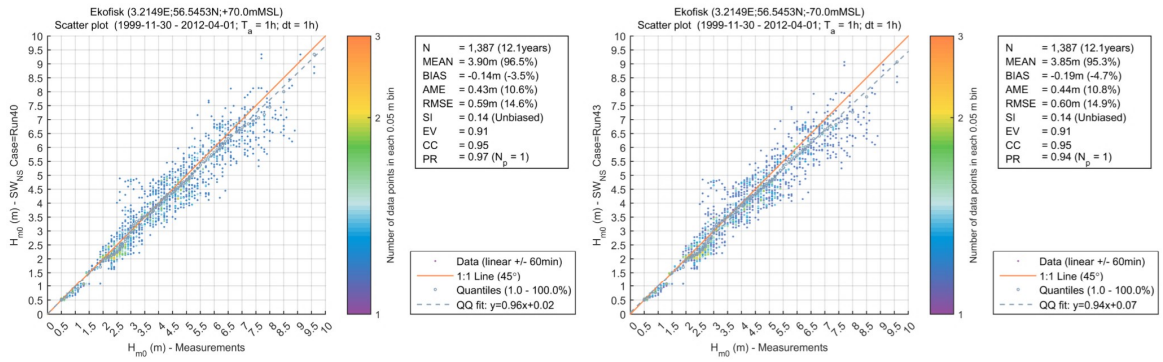

Figure 16: Scatter comparison of modelled significant wave heights (left panel without air-water density and right panel with air-water density input) against measurements at Ekofisk for 15 calibrations storms

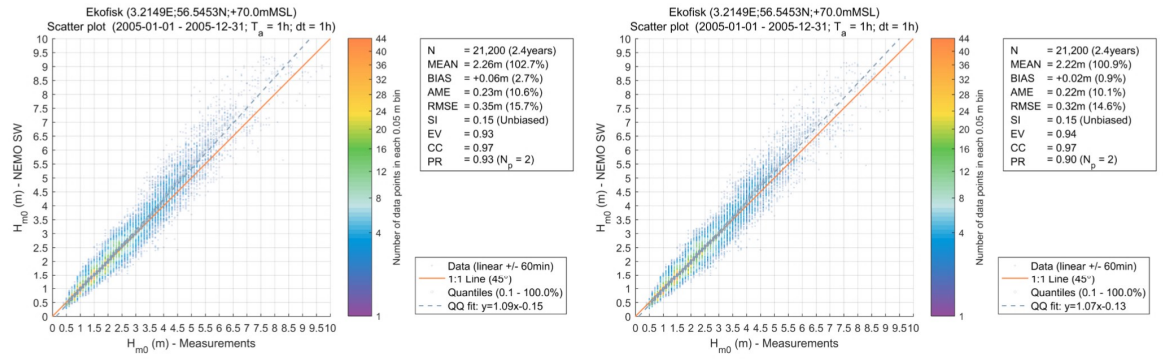

Figure 17: Scatter comparison of modelled significant wave heights (left panel without any current factor applied, right panel with a current factor of 0.01 applied) against measurements at Ekofisk for 2005.

of X-WiWa. This involves the modification of the wave celerity (c) in the wind input source function, see Eq. (16). This correction is of particular importance for small waves (low celerity) within the wave spectrum, as wave growth can be significantly changed. For these small waves, the surface current was more representative than a depth-averaged current. During storms, the surface currents are dominated by wind-induced currents and therefore, it is reasonable to approximate surface current from the wind speed, typically 2-4%. This approximation has been confirmed by observations (e.g. [73]). The inclusion of a parametric current on wave growth tends to reduce wave growth and works in a similar way as a cap to friction velocity. Figure 17 shows a comparison at Ekofisk for the year 2005 where it can be noticed the improvements of the error statistics when using a current factor in the model.

5.5.5 Implementation of Fan 2012 wind drag

Fan et al. (2012) [18] simulated 29 years of waves using a coupled HIRLAM-WWIII model. In their coupled system the roughness length was fed back to the atmospheric model as lower boundary condition. They reported that the WWIII formulation gave values of z_0 of greater than 0.012 m while a new formulation

Table 6: Sediment classes and associated roughness length value.

Sediment class	k_n (m)
Mud/clay	0.01
Sand	0.02
Coarse sediment	0.03

was approximately 0.003 m. The new z_0 formulation depends on wind speed and wave age (c_p/u_*) described as Eqs. (4), (5) and (6).

The Fan formulation is now available within MIKE 21 SW. This however did not show significant advantages over the Charnock relation that was previously implemented in the model. Fig. 4 shows through the measurements from M2 that the Fan formulation and the Charnock formulation are actually quite similar.

5.5.6 Implementation of Ardhuin 2010 physics

Ardhuin et al. (2010) [38] derived parameterizations for the spectral dissipation of wind-generated waves where the rates of dissipation had no predetermined spectral shapes and are functions of the wave spectrum and wind speed and direction. References show good performance of these formulation and thus within X-WiWa, implementation and testing of this formulation were carried. For details of the formulation the reader is referred to the original publication. It is noted here that the paper presents several terms with many constants (about 16 "tuneable") and thus there are details in the implementation that might differ from those done in the WWIII model. In the current implementation the Ardhuin (2010) source terms are more CPU demanding and although in some specific cases it showed some improvements, overall there was no significant benefit. It is important also to notice that Ardhuin et al. (2010) recommend different model setting according to the situation to be used the model, and thus it does not represent a universal formulation.

5.5.7 Map of bottom friction

The ocean bed characteristics are very important in describing the boundary layer of currents and waves and control a large degree the dissipation of flows. The bottom friction is thus typically a calibration parameter in numerical modelling of coastal processes. In this work, a map of varying bottom friction was generated based on ocean bed properties in order to explore the impact of the spatial variability in spectral wave modelling. Results indicate a potential improvement in terms of model skills.

Seabed habitat maps (Fig. 18) have been recently produced by EMODnet through the EUSeaMap project [11], evolving from a prototype to an operational service, delivering full coverage of a broad-scale map for all European sea-basins, along with the dissemination of maps from surveys.

The information obtained from the seabed habitat map from EMODnet (Fig. 18) has been converted into a map (Fig. 19) of Nikuradse roughness length (k_n) with three different values/classes (Table 6). The spatial resolution of the map is of 0.1×0.1 degrees.

[11] http://www.emodnet.eu/seabed-habitats

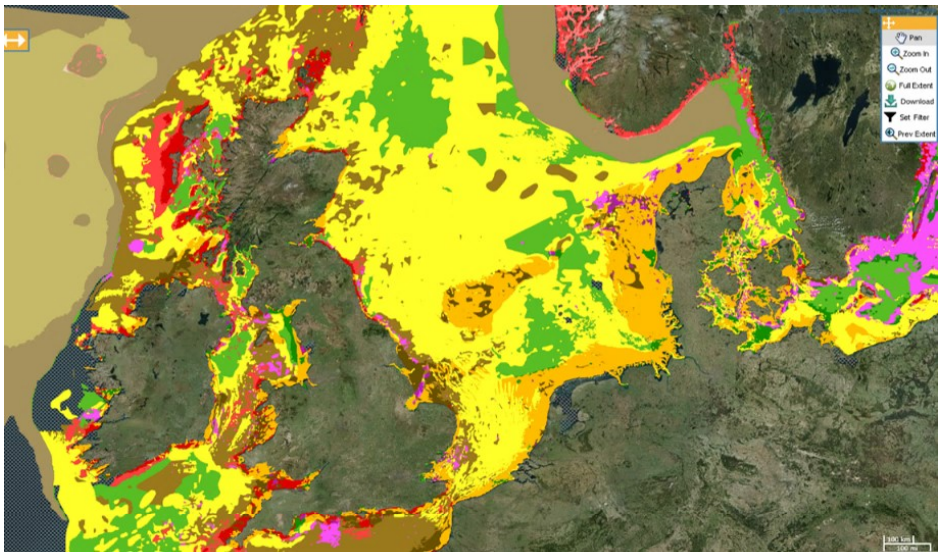

Figure 18: Habitat map from EMODnet

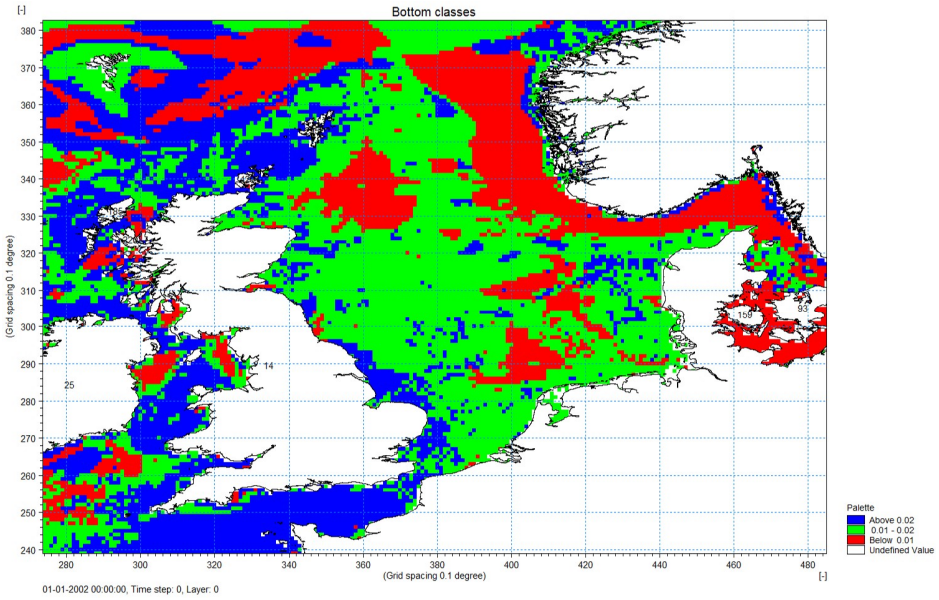

Figure 19: Roughness length (k_n) map based on sediment properties

Table 7: Summary of H_{m0} wave model validation statistics for the three runs with different roughness length.

Location	H_{m0} statistic (m)	Run1 ($k_n = 0.02$)	Run2 ($k_n = 0.03$)	Run3 (k_n map)
Ekofisk	Bias	0.25	0.2	0.22
	RMSE	0.53	0.5	0.51
	SI	0.15	0.15	0.14
Fjaltring	Bias	0.06	-0.07	0.01
	RMSE	0.34	0.33	0.32
	SI	0.14	0.13	0.13
RUNE	Bias	0.12	0	0.07
	RMSE	0.31	0.27	0.29
	SI	0.12	0.11	0.12
K13	Bias	0.1	0.03	0.07
	RMSE	0.33	0.32	0.32
	SI	0.14	0.14	0.13
Nymindegab	Bias	0.1	-0.04	0.13
	RMSE	0.32	0.31	0.33
	SI	0.14	0.14	0.14

MIKE 21 SW was run for three different cases (Bolanos, 2017 [74]) using roughness length as constant (0.02 m and 0.03 m) as well as the values from the map shown in Fig. 19. Significant wave height H_{m0} of approximately 8 m were modelled in the central North Sea during the simulated period (November and December 2015). The eastern part of the North Sea presented larger waves due to winds blowing from the north-west. Differences of up to 0.5 m between those runs were found in the North Sea, specifically in the southeast area.

Table 7 summarizes the model statistics (Bias, Root Mean Square Error (RMSE) and Scatter Index (SI))[12] at the measurement locations. The use of a constant roughness length of 0.02 m produced the worst results at all stations. The constant value of 0.03 m and the map of sea bed roughness seems to produce overall similar results although the model skills vary for different stations.

It is interesting to note the slight reduction in Scatter Index by using a map (Run 3) at Ekofisk and K13 and the general improvement at Fjaltring. While, at the same time, a better performance of Run 2 at RUNE and Nymindegab is obtained. Although those three stations are relatively close to each other, the area is characterized by patches of different sediment sizes. Additionally, model results might be dependent on bathymetry accuracy as the stations are located in water depth shallower than 16 m and close to the coast where some bottom features might not be properly resolved.

5.6 MIKE 21 SW calibration for wave atlas

In order to calibrate the MIKE 21 SW setup (offline model) for the wave atlas, pre-selected storm periods were modelled, with wind forcing from the local WRF

[12]Bias= $\frac{1}{N}\sum_{i=1}^{N}(|Y-X|_i)$; RMSE= $\sqrt{\frac{1}{N}\sum_{i=1}^{N}(Y-X)_i^2}$; SI= $\frac{\sqrt{\frac{1}{N}\sum_{i=1}^{N}(Y-X-Bias)_i^2}}{\frac{1}{N}\sum_{i=1}^{N}|X_i|}$

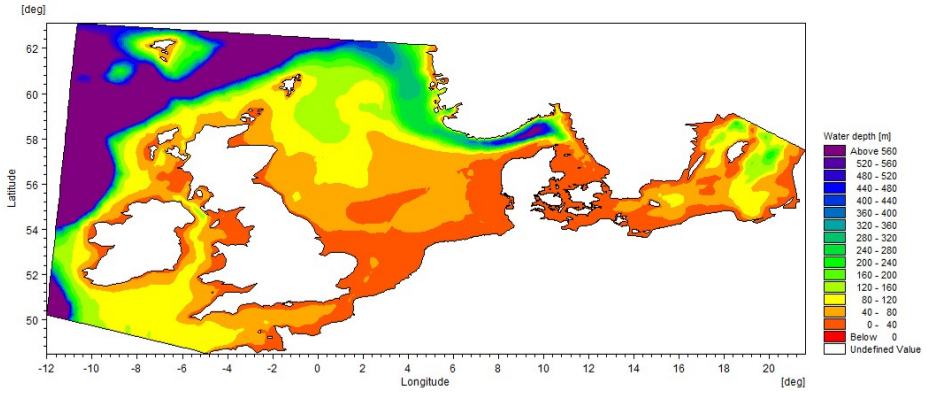

Figure 20: SW domain used during the simulation of wave storms around Danish waters

model, and the model results were compared to available observations within the model domain. The calibration procedure is described in the below sections.

5.6.1 MIKE 21 SW model setup

All model tests were run on a domain, including the Southern Baltic Sea, inner Danish waters, North Sea, Irish Sea, English Channel and the western Atlantic Ocean off the west coast of Ireland, as shown in Fig. 20.

Bathymetric data from Digital Terrain Model (DTM) data products have been adopted from the EMODnet Bathymetry portal [13]. This portal was initiated by the European Commission as part of developing the European Marine Observation and Data Network (EMODnet). The EMODnet digital bathymetry has been produced from bathymetric survey data and from aggregated bathymetry datasets collated from public and private organisations. These have then been processed and quality controlled. The portal also includes a metadata discovery service that gives information about the background survey data used for the digital terrain model (DTM), their access restrictions, originators and distributors.

The open boundaries of the domain in the North Sea, and the west and southwest of UK have been obtained from DHI global wave model while boundary at the Baltic Sea was set as closed. The grid resolution of the domain goes from $\sim$ 20 km at the most offshore areas northwest of UK to $\sim$ 1 km in the Danish waters (see Fig. 21)

[13] http://www.emodnet-bathymetry.eu

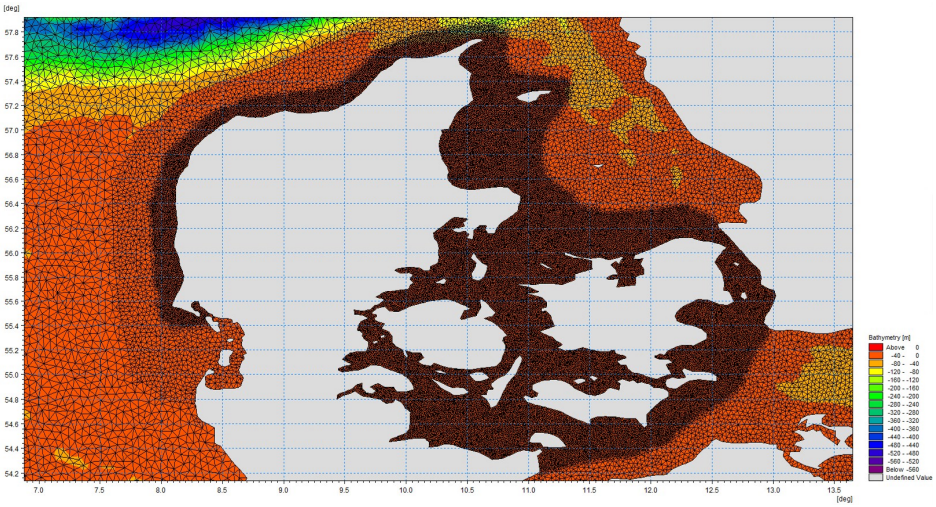

Figure 21: Model mesh around Danish waters

5.6.2 Storms and parameters for calibration

As will be described in section 6, 932 storms were identified between 1994 and 2014 for wave modeling. Due to the large computational time which would be required to run each of these storms for throughout the calibration stage of the project, it was decided that 15 storms out of the predefined storms would be used. The selection of the 15 calibration storms came from the availability of observations across all stations, and all key regions of interest; i.e. North Sea stations, in particular coastal waters off the west coast of Jutland, the inner Danish Waters, and Baltic Sea. The selected handful of storms allowed for the calibration process to become feasible on computational recourses, allowing for the model parameters to be tested more thoroughly.

Each calibration storm was run with a 12 hour warm up period, thus each storm was initialled 12 hours prior to the dates and time stated in Table 8. The warm up period for each storm was discarded prior to analysis. The following parameters were used throughout the calibration process of the offline coupling of the wave atlas. The parameters included:

- Wave growth formulation [26] [38]
- White capping
- Zalpha (constant at the wind input source term)
- Bmax (constant at the wind input source term)
- Bottom friction
- Current factor
- Air-Sea map

Table 8: Start date of the 15 storms used for calibration of the MIKE 21 SW model.

Storm Number	Dates
1	1999-11-30 12:00
2	2000-01-29 12:00
3	2003-04-04 12:00
4	2005-02-21 12:00
5	2005-11-14 12:00
6	2007-01-13 12:00
7	2007-01-20 12:00
8	2009-07-30 12:00
9	2009-10-03 12:00
10	2009-10-14 12:00
11	2011-09-13 12:00
12	2011-11-26 12:00
13	2011-12-09 12:00
14	2011-12-27 12:00
15	2012-01-03 12:00

In addition to the above parameters, the wind field input was also tested. Whilst the MIKE 21 SW model was calibrated with the WRF winds as input forcing, the calibrated model was also run with the CFSR (corrected for stability, see section 5.5.1) as wind forcing for comparison.

5.6.3 MIKE 21 SW calibration results

As outlined above (section 5.6.2), 15 storms were selected out of the 932 identified storms between 1994 and 2014 which were used for the purpose of calibrating the wave model. Forty calibration runs were performed on the 15 storms. Each calibration tested a different combination of the calibration parameters mentioned in section 5.6.2. Taylor diagrams were used to display the modelled significant wave height (H_{m0}) at the observations stations around the Danish coastline and where data were available (Fig. 22 and Fig. 23). On each plot, the black point indicates the statistics from the available observations, the red points indicate the statistics for the 40 calibration runs, while the blue point represents the statistics for the final calibration used for production. It should be noted that there were more observations available for the offshore stations as oppose the coastal stations. In some cases, as few as 1 or 2 storms out of the 15 storms were available for comparison. It is possible to gather this information from the accompanying scatter plots. Additionally, Taylor diagrams do not portray the scatter index between the modelled and observed data. For this, the scatter plots were also consulted. These plots and statistics were used to determine the most suitable calibration across all stations. Presented in this chapter are the scatter plots for the calibration stations from the test with the final model calibration setting.

The final model parameters are summarized in Table 9.

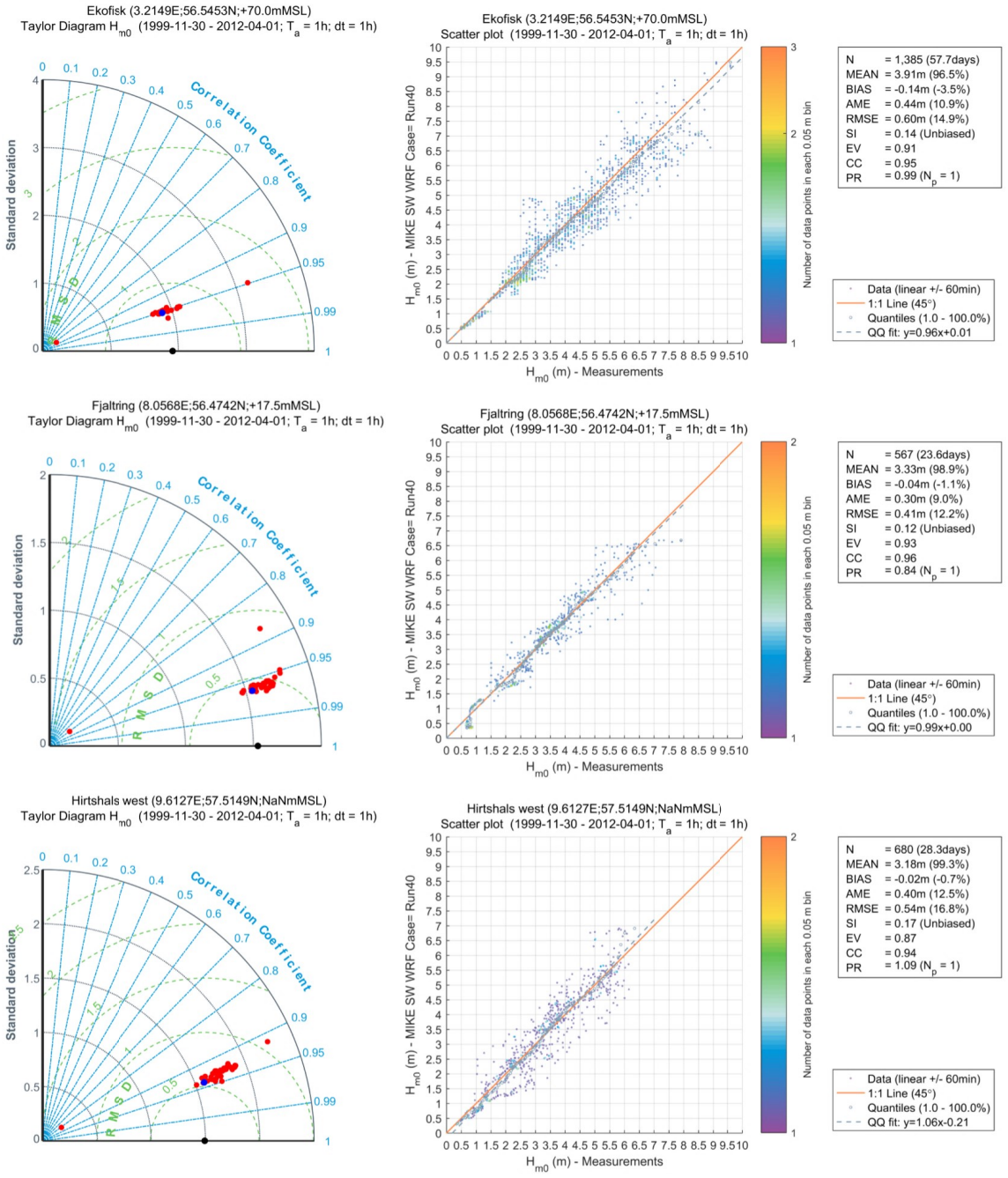

Figure 22: Scatter plot of the modelled significant wave height of the 15 calibration storms between Nov-1999 and Apr-2012 for the final calibration run (right panel, corresponding to blue point in Taylor diagram). A statistical representation of significant wave height (H_{m0}) at Ekofisk (upper panels), Fjaltring (middle panels) and Hirtshals West (lower panels) for the 40 calibration MIKE 21 SW model runs through a Taylor Diagram (left panel). Red points represent the calibrations runs. Black point represents the observations. Blue point shows the final calibration run chosen for production.

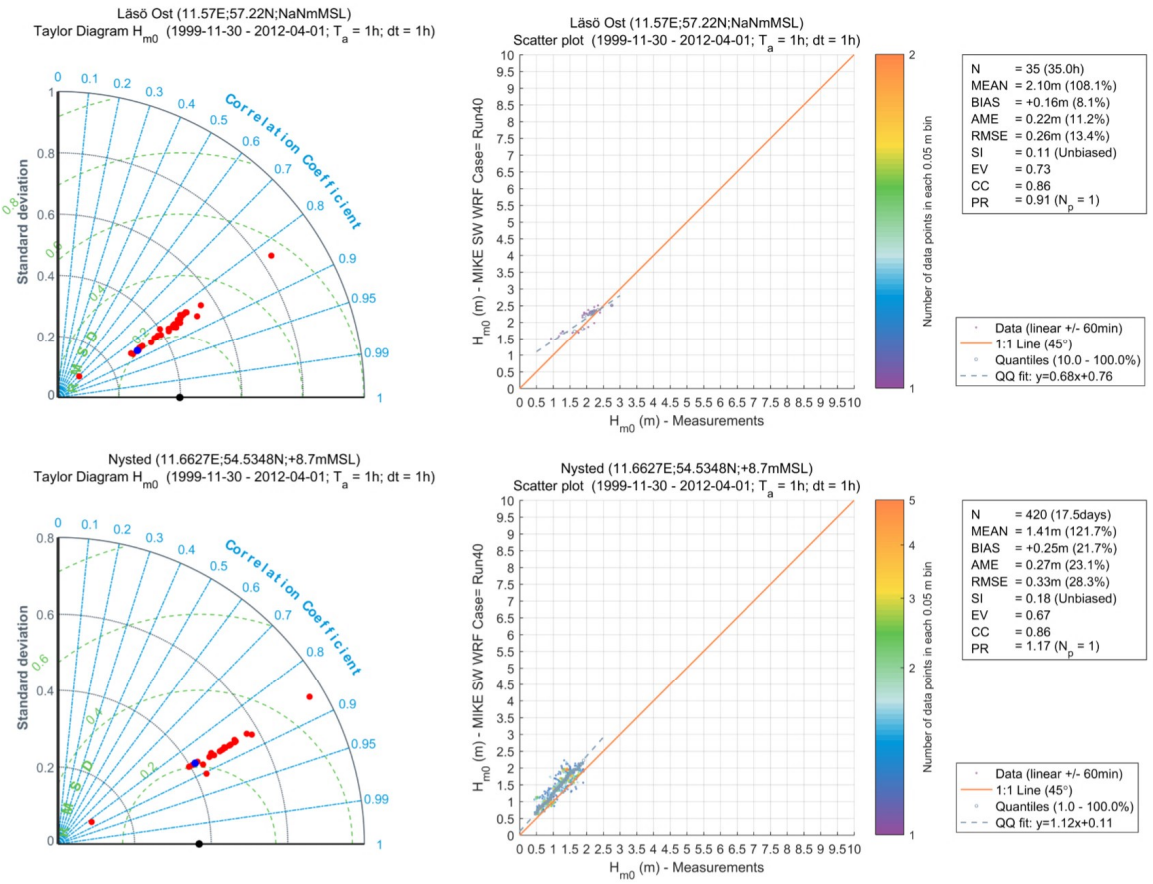

Figure 23: Scatter plot of the modelled significant wave height of the 15 calibration storms between Nov-1999 and Apr-2012 for the final calibration run (right panel, corresponding to blue point in Taylor diagram). A statistical representation of significant wave height (H_{m0}) at Läsö Ost (upper panels) and Nysted (lower panels) for the 40 calibration MIKE 21 SW model runs through a Taylor Diagram (left panel). Red points represent the calibrations runs. Black point represents the observations. Blue point shows the final calibration run chosen for production.

Table 9: Final wave model set-up parameters.

Setting	Value
Mesh resolution	$\sim$ 20 km to $\sim$1 km
Source terms	(Janssen, 1991)
Zalpha	0.011
Bmax	1.2
Current factor	1.2% of wind speed (see section 5.5.4)
Cap to friction velocity	0.053
Discretisation	25 frequencies (1.05 - 30.3s (0.033-0.94Hz) logarithmic frequency increment factor of 1.15), 24 directions
Time step	Adaptive, 0.01-3600s
Water level	DHI regional hydrodynamic model
Wind forcing	WRF alone wind fields
Wave breaking	Included, Specified Gamma, $\gamma = 0.8$, $\alpha = 1$ (Battjes and J.P.F.M., 1978) [75]
Bottom friction	Map (see section 5.5.7)
White-capping	Formulation: (Bidlot et al. 2007 [76]), C_{dis} =2.3, δ_{dis} =0.7
Boundary conditions	2D spectra varying in time and along line from DHI global wave model

On the whole, the Taylor Diagrams show that the majority of the calibration runs were mostly centred around similar statistics. The most ideal calibration would have the correlation coefficient closest to 1, a centred root mean square difference (RMSD) of zero and a standard deviation closest to that of the observations, here the observations statistics are shown as a black point. Thus the closest red point, representing each calibration run, to the black point is statically the best representation of the available observations. The calibration run chosen as the final calibration to be used for production is highlighted as a blue point (and described in Table 9). It should be noted that the final calibration chosen may not have been the best calibration across all stations, but was seen as the calibration which gave the best representation of the observations at each station on the whole. The calibration was focused on the stations closest to the Danish waters and coastlines. It can also be noted the effect of different calibration parameters were more sensitive at some stations than others. This is shown on the Taylor Diagrams as the spread of the red points. There are a number of reasons which could make the model more sensitive to calibration parameters at some location over others, such as fetch, water depth and length of observational time series available.

5.7 In search of a good model setup for COAWST

There are many factors that can affect the model results for a storm. We do not wish that the effect from the coupling is in the shadow of the uncertainties and deviations brought by factors related to the setup of the atmospheric modeling alone. To reduce such uncertainties, we try to first model the large scale key storm properties reasonably well, which will make it easier to quantify the effect from coupling.

X-WiWa, partly through a PhD project [25] and mostly through a master project [77], developed a systematical approach to quantify the quality of a model setup so that the setup can be justified to capture the storm path and intensity. The storm path was examined by comparing the WRF storm center, defined as the position of the lowest mean sea level pressure, with that from the large scale forcing data and, if available, with the XWS track data. The intensity was measured by the value of the lowest mean sea level pressure and, if possible, by wind speed measurements at sites.

The parameters related to the WRF-only setup that are found to affect the model results include the size of the domain, the position of the domain in relation to the path of the storm, the initial time of the model, the simulation period and the resolution. Briefly, the investigations reveal that mesoscale model domains have to be big enough to ensure the storm center is passing the model domain but it should not be too big in order to prevent the development of the mesoscale model's own dynamics from the forcing data. It was found that, for the same reason of preventing such a development of the mesoscale model's own dynamics from the forcing data, it helps using a shorter simulation period such as 36 hours rather than 72 hours. Our spatial spectral analysis suggests that a spin-up time of 12 hours is sufficiently long for the model to build up the top model layers and reach a consistent status with the rest of the vertical layers. Our temporal spectral analysis suggests that in order to capture the wind variability of the storm over the Denmark, a spatial resolution of 2 km is necessary. [77] also found that the location where the storm enters the model domain yields to an

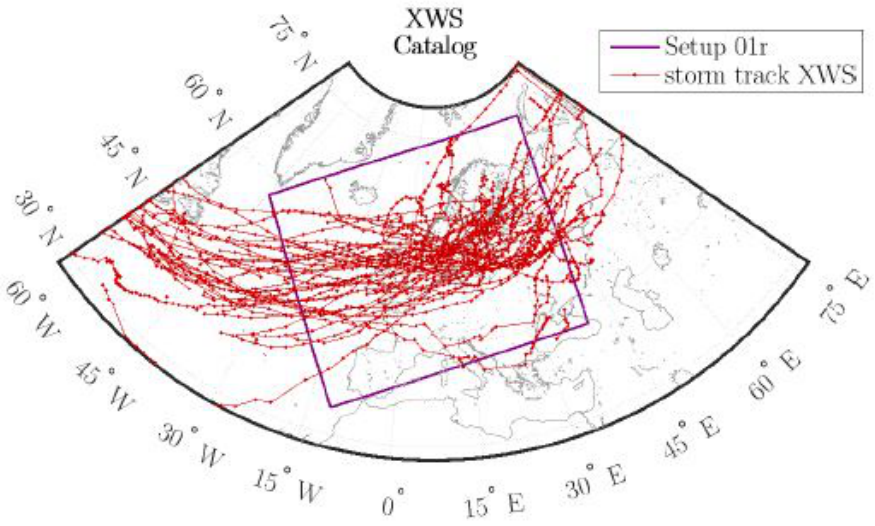

Figure 24: Storm track of all 52 available extreme weather events in the XWS catalog with X-WiWa model domain I setup. A copy of Figure 4.25 From [77].

underestimation of the storm intensity if it is very close to the corner.

The above findings are used to set up the modeling system for X-WiWa. First of all, the model domain setup is guided by the extreme weather events (XWS) catalog from which the storm paths of entire 52 events are plotted together in Fig. 24 (see also the outermost domain in Fig. 5). This figure at the same time shows our outmost model domain setup allows these storms enter away from the corners and they pass the center of the domain.

The model domain setup is the same for WRF and SWAN, with three nested domains (Fig. 5) and spatial resolutions of 18, 6 and 2 km for domain I, II and III, respectively. For WRF, the domains are two-way nested. There are 52 vertical sigma levels for all WRF domains, with the lowest model level at a height of 10 m, and an interval of about 10 m up to 100 m. We used MYNN 3.0 PBL scheme [78], Thompson microphysics scheme [79], and RRTM long wave and short wave radiation physics schemes [80]. The Kain-Fritsch cumulus scheme [81] was used for domain I but was deactivated for domain II and III. The Corine land use data were used. We used CFSR data as the initial and boundary forcing for WRF modeling. The 0.312° CFSR SST data were used.

In SWAN, the 1/8 arc-minute bathymetry data from the EMODnet Digital Terrain Model (DTM) were used. SWAN is initiated with the output spectrum of a previous SWAN simulation 30 hours before. The open boundaries of the outer domain are set to be zero. We used 36 directional bins. The frequency exponent was 1.1 and the lowest frequency was set to be 0.03 Hz.

The time step for SWAN and the coupling to WRF is 5 minutes. Each simulation covers 36 hours.

6 The selective dynamical downscaling method for extreme wind and extreme wave estimation

We use the "selective dynamical downscaling method" to obtain the extreme wind and extreme wave atlas. This method was first developed, applied and validated in [3] for extreme wind atlas. There are three main steps in applying the method.

The first one is to identify the extreme wind events. In connection with the statistical approach for the estimation of the 50-year wind, the Annual Maximum Method (AMM), we identify cases that contribute to the Annual Maximum wind samples. First of all, we define the area of interest, which for this project is the water area around Denmark. We defined the area as shown as domain III in Fig. 5. The CFSR 10-m wind data are used to find the dates of the yearly strongest wind at each grid point in domain III. The CFSR data are hourly. There are two phases of the CFSR data, CFSR I is from 1979 to 2010 and CFSR II is from 2011 to 2017. We use the period 1994 to 2016, in total 23 years. The spatial resolution is about 38 km for CFSR I and 25 km for CFSR II. In total there are 735 grid points for CFSR I and 1728 grid points for CFSR II where the annual maximum winds and their corresponding dates are identified. The dates are eventually merged together, suggesting 321 individual storms for the period 1994 to 2016 that have contributed to the estimate of the extreme wind. The list of these storms can be found in www.xwiwa.dk/data. Since in this area, the extreme wind events are related to the synoptic weather system, these CFSR data (hourly, 38 km and 25 km) are considered to be adequate for the purpose of identification. The measurements from several sites are used to identify the most important storms for the extreme wind calculation and they are all included in the storm list from CFSR data.

The second step is the modeling of the 321 storms. The model setup has been introduced in section 5.7. By running each simulation for 36 hours starting from 12:00 the day before the storm peak day, the 321 storms, with some more than two days, there are altogether 429 simulations. These storms have been simulated using WRF-WBLM-SWAN as well as WRF only.

The third step is to use the Annual Maximum Method, applying Gumbel distribution to the 23 samples to obtain the 50-year wind. The 50-year wind has been calculated for 10 m, 50 m and 100 m.

For further applications, for data over land, they will go through the "generalization" process and be corrected to 10 m over homogenous surface with a roughness length of 5 cm [3]. These generalized data can be further downscaled through microscale modeling through e.g. the Linear Computational Model LINCOM. For data over water, they do not need to be generalized.

Similar concept has been applied here for the estimation of the extreme wave atlas. A database of wave storms were selected in the long term DHI regional hindcast wave dataset. Dates corresponding to the times with maximum significant wave heights at each model element around Denmark (see Fig. 25) were found between 1994 and 2014. A total of 1006 "wave-maxima" dates were identified. The combined dates of the wave maxima with the wind speed maxima was produced, with simultaneous dates being considered as one single storm. A total of 932 storms were identified and simulated with atmospheric parameters from the WRF model alone. The storm list of the extreme wave modeling can be found in www.xwiwa.dk/data.

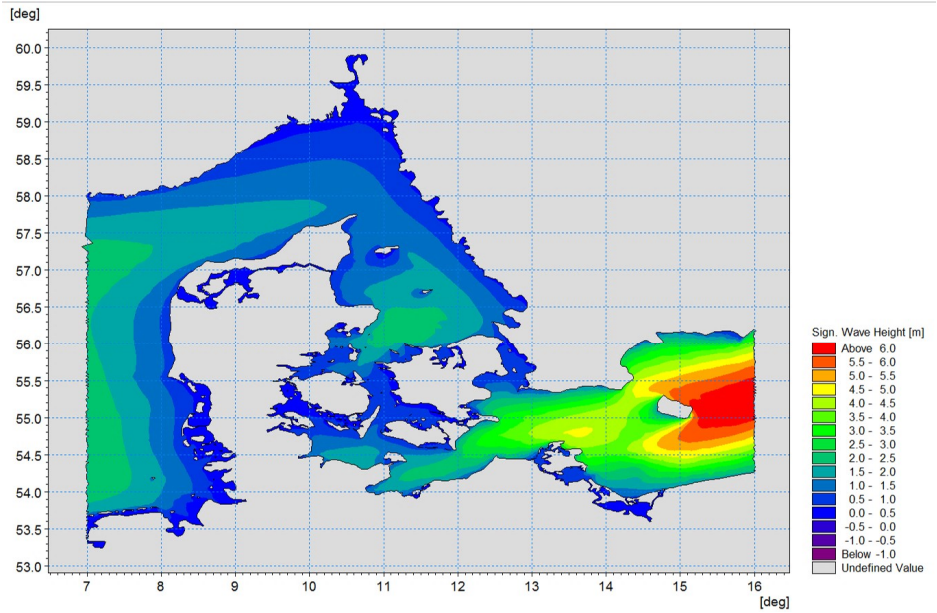

Figure 25: Area used in the DHI hindcast data for selection of storms for X-WiWa extreme wave atlas.

7 Calculating the 50-year return values

7.1 The 50-year wind

For estimating the extreme winds, the generalized extreme value distribution (GEVD) and the generalized Pareto distribution (GPD) are the most used distribution functions.

The generalized extreme value cumulative distribution (GEVD) for fitting the extreme wind values in the form of wind maxima from a basis period T_{BP} takes the form:

$$F(U) = \exp\left(-\left(1-\alpha k(U-\beta)\right)^{1/k}\right), \tag{36}$$

where $F(U)$ is the probability that wind speed U is not exceeded during the basis period, k is a shape factor, α and β are distribution parameters. For $k > 0$, GEVD is known as a Type III (or Reverse Weibull) extreme value distribution. For $k < 0$, GEVD is known as a Type II (or Frechet) extreme wind distribution. For $k = 0$, GEVD becomes Type I, also known as the Gumbel, distribution:

$$F(U) = \exp\left(-\exp(-\alpha(U-\beta))\right). \tag{37}$$

Note, Eqs. (36) and (37) are the integration of the corresponding probability density functions for the extreme wind samples U, given that these samples are independent and identically distributed. Due to its association to a certain basis period T_{BP}, the method is denoted the Periodic Maximum Method (PMM) or, in the case of a basis period of one year, Annual Maximum Method (AMM). [82] shows that the uncertainty related to the determination of the k-factor is too

big compared to other sources of uncertainty and it was found that $k = 0$ is a good approximation for the distributions. Here we use $k = 0$. The algorithms for AMM will be introduced in section 7.1.1.

The generalized Pareto distribution (GPD) is used to describe the wind speed exceedances over a threshold and it takes the form:

$$\begin{aligned} F(U, u_0) &= 1 - \left(1 - \frac{k(U - u_0)}{A}\right)^{1/k}, \quad k \neq 0 \\ &= 1 - \exp\left(\frac{U - u_0}{A}\right), \quad k = 0, \end{aligned} \tag{38}$$

where u_0 is the speed threshold, A is a scale factor and k is a shape factor. A poisson-process has been found to be a suitable way to describe how the individual exceedances occur randomly in time, independent of each other (e.g. [83]). This has resulted in the name peak-over-threshold (POT). For the same wind climate the shape factor k has in fact the same value as that of GEVD due to the mathematical relationship between PMM and POT distributions as shown in [82] in their appendix. $k = 0$ is used in relation to POT. The algorithms for calculating U_{50} using POT are introduced in section 7.1.2.

7.1.1 Annual Maximum Method

The annual wind maxima from n years are first sorted in ascending order as U_i^{max}, where $i = 1, ..., n$. Then, the Gumbel extreme wind distribution is used to fit the set of annual wind maxima ([84, 85]) and eventually the T-year wind speed, U_T, is obtained from

$$U_T = \alpha^{-1} \ln T + \beta, \tag{39}$$

where the coefficients α and β are obtained through the probability-weighted moment procedure

$$\alpha = \frac{\ln 2}{2b_1 - \overline{U^{max}}}, \ \beta = \overline{U^{max}} - \frac{\gamma_E}{\alpha}, \tag{40}$$

where $\gamma_E \approx 0.577216$ is the Euler constant, $\overline{U^{max}}$ is the mean of U_i^{max} and b_1 is calculated from

$$b_1 = \frac{1}{n} \sum_{i=1}^{n} \frac{i - 1}{n - 1} U_i^{max}. \tag{41}$$

According to [83] and [86], the probability weighted moment procedure gives little bias and variance on the parameter estimates and is very efficient for small size samples.

Mann et al. [87] gave the estimation of uncertainty of U_T, which is calculated from uncertainties on α and β:

$$\sigma(U_T) = \frac{\pi}{\alpha} \sqrt{\frac{1 + 1.14k_T + 1.10k_T^2}{6n}} \tag{42}$$

with

$$k_T = -\frac{\sqrt{6}}{\pi} \left[\ln \ln \left(\frac{T}{T - 1}\right) + \gamma_E\right] \tag{43}$$

The uncertainty due to the fitting is estimated as the 95% confidence interval here and it is obtained by $1.96 \cdot \sigma(U_T)$ and $\sigma(U_T)$ decreases with increasing sample number n. [88] showed that the T-year estimate can be considered to be normally distributed and accordingly, the 95%-confidence interval can be calculated to be $U_T \pm 1.96 \cdot \sigma(U_T)$ ([83]).

7.1.2 Peak-Over-Threshold Method

If the exceedance rate of the level u_0 is λ per year, then the mean crossing rate of the level U_T is $\lambda(1 - F(U_T - u_0))$. Relating $\lambda(1 - F(U_T - u_0))$ to $1/T$, together with Eq. (38), gives

$$U_T = u_0 + A\frac{1 - (\lambda T)^{-k}}{k} \tag{44}$$

which, for $k = 0$, simplifies into

$$U_T = u_0 + A\ln(\lambda T), \tag{45}$$

which can be written in a form similar to Eq. (39):

$$U_T = A\ln T + B, \tag{46}$$

with $B = u_0 + A\ln\lambda$. [87, 83] used the Poisson process and properties of the exponential distribution; together with the propagation of variance formula, they obtained the uncertainty in relation to Eq. (45):

$$\sigma(U_T) \approx \frac{A}{\sqrt{\lambda L}}\sqrt{1 + \ln^2(\lambda T)}, \tag{47}$$

where L is the data length. Similar to GEVD, the 95% confidence interval can be obtained as $U_T \pm 1.96 \cdot \sigma(U_T)$, under the assumption that the estimate of U_T is normally distributed ([88]).

7.1.3 Uncertainties

One of the major sources of uncertainties as studied in [82] is the strong wind climatological representativity as in the data we used for the estimation of the extreme wind.

[82] shows that a short time series has a high chance to fail representing the climatology of extreme winds, regarding the inter-annual variation and long-term trend. Figure 26 shows when using AMM, shorter time series have a larger chance for biased estimates and at the same time have much higher uncertainty. The spread of U_{50} is much more significant when using data shorter than 10 years. The results are similar when using POT method, except that the spread of U_{50} is slightly smaller. This is due to the fact that with a suitable selection of the threshold which provides a stationary estimate with a good number of samples, more samples can be collected in comparison with AMM. For instance, for a data of 6 years, using AMM gives only 6 samples, a careful use of POT can provide double number of samples, which gives higher certainty. Note that we are addressing the analysis of data from Denmark.

In our estimates of U_{50} from measurements, when the data length is shorter than 10 years, we weight more to the estimates from POT than AMM (section 8.2.2).

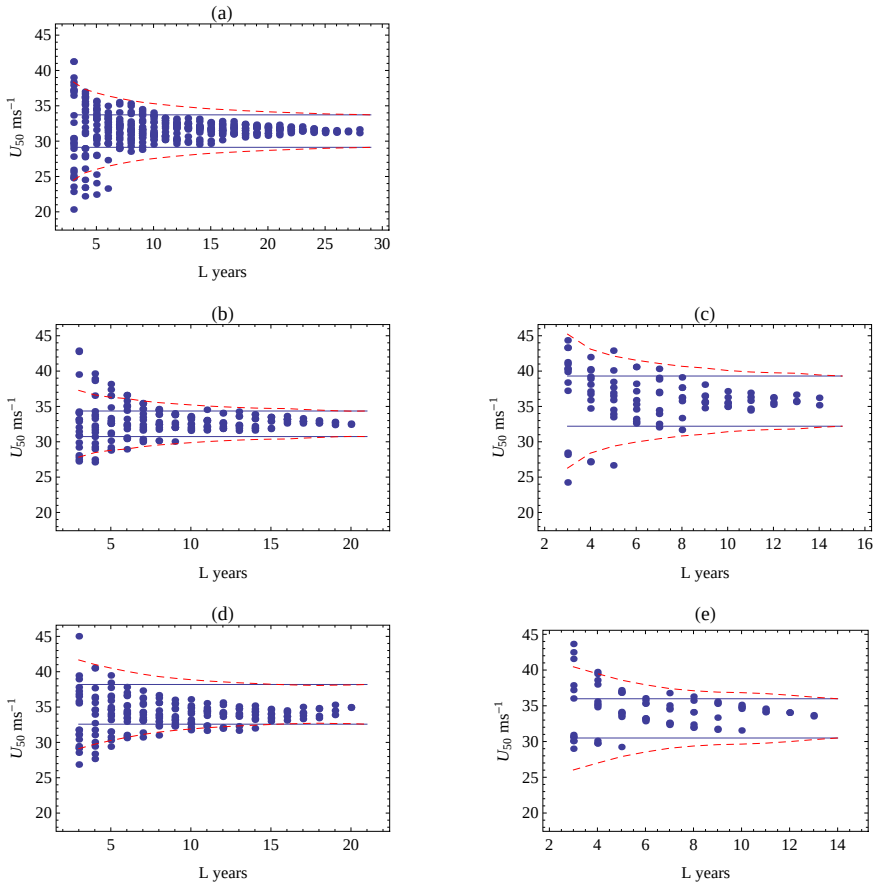

Figure 26: The 50-year wind U_{50} from AMM with data length L ranging from 3 years to the record length at five sites over Denmark. In each sub-plot, the right-most dot is the estimate based on the entire time series, the solid straight lines show $\sigma(U_T)$ (Eq. (42)) centered at U_{50} from the entire time series, and the two dashed curves show $\sigma(U_T)$ at $L = 3$ to n, centered at U_{50} from the entire time series. A copy of Figure 7 From [82].

7.2 The 50-year significant wave height

Several standard approaches are applied to estimate the 50-year significant wave height. Some of them are the same as those used for the extreme values for the wind as shown in section 7.1 and some are used by DHI for waves. Due to the fact that the atmospheric field and the wave field may use different phrases for the same concept, e.g. we used "Annual Maximum Method" while DHI uses "Annual Maximum Peak" (AMP), here we adopt the corresponding expressions as used by DHI for readability. There might be repeatation here to section 7.1 to certain degree.

Three types of extreme data section methods are used for the extreme wave analysis:

- Annual Maximum Peak (AMP)
- Average Annual Peaks (AAP)
- Peak over Threshold (POT)

AMP is the same as AMM. AAP refers to the method which uses a fixed number n of exceedances per year. The n largest values are extracted, implying that the threshold levels becomes a random variable. POT is the same as that used for wind in section 7.1.2. In relation to AAP and POT, to ensure the selected events to be independent of each other, some restrictors have to be imposed on the time and level between two successive events. Here an inter-event time and an inter-event level criterion can be defined:

- Inter-event time criterion: two successive events are independent if the time between the two events is larger than the specified inter-event time.
- Inter-event level criterion: two successive events are independent if the level between the events becomes smaller than specified inter-event level (between 0 and 1) times the lower of the two events

The following probability distributions are used here for the extreme wave analysis:

- 2-parameter Weibull distribution
- Truncated Weibull distribution
- Exponential distribution
- General Pareto distribution
- Gumbel distribution

where point 3 to 5 have been introduced in section 7.1 with wind as the variable.

The 2-parameter Weibull distribution is given by:

$$P(X < x) = 1 - \exp\left(-(\frac{x}{\beta})^{\alpha}\right) \tag{48}$$

where α and β are the two distribution parameters. This is used in connection with POT analysis where the threshold was subtracted from data prior to fitting.

The 2-parameter *truncated* Weibull distribution is given by:

$$P(X < x) = 1 - \frac{1}{P_0}\exp\left(-(\frac{x}{\beta})^{\alpha}\right) \tag{49}$$

where P_0 is the exceedance probability, described by

$$P(X < x) = \exp\left(-(\frac{\gamma}{\beta})^{\alpha}\right) \tag{50}$$

where γ is the threshold. Compared to the non-truncated 2-parameter Weibull, the distribution is fitted directly to the data without subtraction of threshold from the time series.

8 Results: Wind

8.1 Model performance for individual storms

A number of scientific issues were investigated during our modeling and data analysis. One of the main topics is how the use of the interface parameters (e.g. z_0 or stress) between the wind and wave modeling affect the results for wind and waves. Our studies show that the effect of coupling on the wind modelling is most important for coastal areas and for strong wind conditions; the studies will be presented here in section 8.1.1 and 8.1.2. In relation to offshore functions, there have been many studies related to storm simulations, among many, over the North Sea. We have, as shown in section 5.7, analyzed individual storm simulations in the framework of finding the best model setup. Some of the storms are interesting due to the presence of special atmospheric features, such as gravity waves [89, 90], boundary-layer rolls [91] and open cellular structures. One of the famous storms, Britta, that happened end of October and beginning of November in 2006, has obtained a lot of attention in research due to extreme significant wave height measured at FINO 1 under not-so extreme wind conditions and the simultaneous appearance of open cells over the North Sea. X-WiWa studies the many pieces of puzzles from a large number of research articles regarding this storm and investigated the existing model ability in capturing this storm [43]. This case was briefly introduced in section 8.1.3. Section 8.1.4 presented some statistics from the entire simulation for the stations where measurements are available for the validation.

8.1.1 The effect of coupling in coastal areas

Popular description of the atmospheric and wave modeling interface parameters such as drag coefficient C_D or roughness length z_0 as a monotonic function of wind speed at 10 m U_{10} alone is a quite good approximation when other relevant parameters are highly correlated with U_{10}, such as over open and wind sea conditions, which is also the condition for the Charnock parametrization to work. This charming simple approach is seen to be representable of measurements collected over open sea conditions when winds are light to moderate, see Fig. 2, if we assume the spread of C_D at certain U_{10} is not important. However, such an assumption becomes obviously questionable when wind exceeds about 20 ms^{-1} where a variety of simple dependence of C_D on U_{10} have been suggested. Fig. 2 also suggests that when U_{10} becomes larger than about 40 ms^{-1}, the uncertainty is so large that C_D can simply not be described by U_{10} any longer. It is other parameters than U_{10} that define C_D or z_0 under these conditions.

Figure 4 shows several layers of information. Firstly, consistent with the coastal study by [15], at this coastal site Horns Rev I (see Table 4), z_0 is a function of fetch, which, at the same wind speed less than approximately 13 ms^{-1}, corresponds to rougher surface when the winds are from land to sea than from sea to land. However, at the same wind speed stronger than approximately 13 ms^{-1}, the sea surface is rougher when the winds are from sea to land than otherwise. Secondly, the dependence of z_0 on U_{10} for winds from the open sea follows very well with the parameterizations for the open sea conditions (cf. COARE 3.0 and Zijlema), but it is not the case for the short fetch cases. Thirdly, the difference in z_0, in terms of absolute magnitude, is very small between the five parametrization schemes when $U_{10} < 10$ ms^{-1} but the difference increases

with increasing U_{10}.

It is generally speculated that when the simple dependence of C_D or z_0 on U_{10} breaks down, parameters that affect the water surface waves start to play a more relevant role, such as fetch and wave state. Figure 27 [62] shows the ideal SWAN modeling through WBLM for a range of wind speed and fetch. Here it is shown that C_D is a function of wind speed U_{10}, fetch x (km) and developing time t that are related to the wave state. The dependence of C_D on U_{10} is compared with measurements from Fig. 2, some often-used $C_D - U_{10}$ relationships and the model results using the Janssen scheme. Even though the performance of these $C_D - U_{10}$ relations for $U_{10} > 40$ ms^{-1} is still hard to evaluate, it is reasonably good for wind speed smaller than 40 ms^{-1}.

The water surface in the coastal areas is more likely to be dependent on a number of other parameters than the wind speed only due to the presence of land and variation in water depth. Take the area around Horns Rev I as an example, Fig. 28a [25] shows that here the water depth could be very shallow and it is not homogenous in space. One example as shown in Fig. 28b is the radar backscatter data corresponding to a background wind from the north (see the black arrows from the modeled data CFSR) at 9 : 49 : 09 on 2004-02-23. The backscatter data are somehow reflecting the wind strength, the larger values corresponding to stronger winds. One can see that the wind field reflects the bathymetry to some degree. This case was chosen because of this character. The modeling system WRF-WBLM-SWAN is used to model the wind and wave field for the period 2004-02-22 to 2004-02-24. Details of the simulation can be found in chapter 8 in [25]. Here we briefly present the effect of 8 schemes for the interface parameter z_0 on the wind field. The 8 schemes include those 5 as introduced in section 3.2 which are shown in Fig. 2 and 4, one from WBLM, one from Janssen's scheme and one from COARE 3.0 the uncoupled version.

The modeled roughness lengths z_0 at corresponding time of the radar backscatter data in Fig. 28b are shown in Fig. 29 using the 8 schemes. There is no wave information feed in the use of COARE 3.0, so that z_0 in Fig. 29a reflects only the surface wind speed conditions. As we learnt from section 3.2 and Fig. 4 the Fan scheme, even though has a wave age dependence, the overall magnitude of z_0 is rather close to the Charnock parametrization, and hence COARE 3.0. This is also the case here shown in Fig. 29b. To quantify these spatial distribution of z_0 from the different schemes and thereafter to judge which one is the best, positions A to E, representing different bathymetry conditions, are selected to spot on the correspondence of the modeled z_0 to the ASAR backscatter data. Quite obviously Fig. 29h gives best correspondence to Fig. 28b. Detailed analysis can be found in [25]. This serves as the first data validation.

The drag coefficient C_D and wind speed from the entire simulation time for the innermost domain are used to perform their relationship based on the 8 schemes, shown in Fig. 30. As expected, COARE 3.0 gives one line (the red curve in all subplots). Note the measurements from Fig. 2 are borrowed here presented as dots and error bars. The purple line shows the mean values of wind speed bins of the scatters. Considering the magnitude, the dependence, the values for strongest winds and the spread, Fig. 30h corresponds to the best performance. This serves as the second data validation.

Further validation is done to the time series measured at Horns Rev, including wind speed, direction, H_{m0} and T_p, see sections 8.1.4 and 9. Note that the wind speed during this period is not very strong since the criteria for choosing this

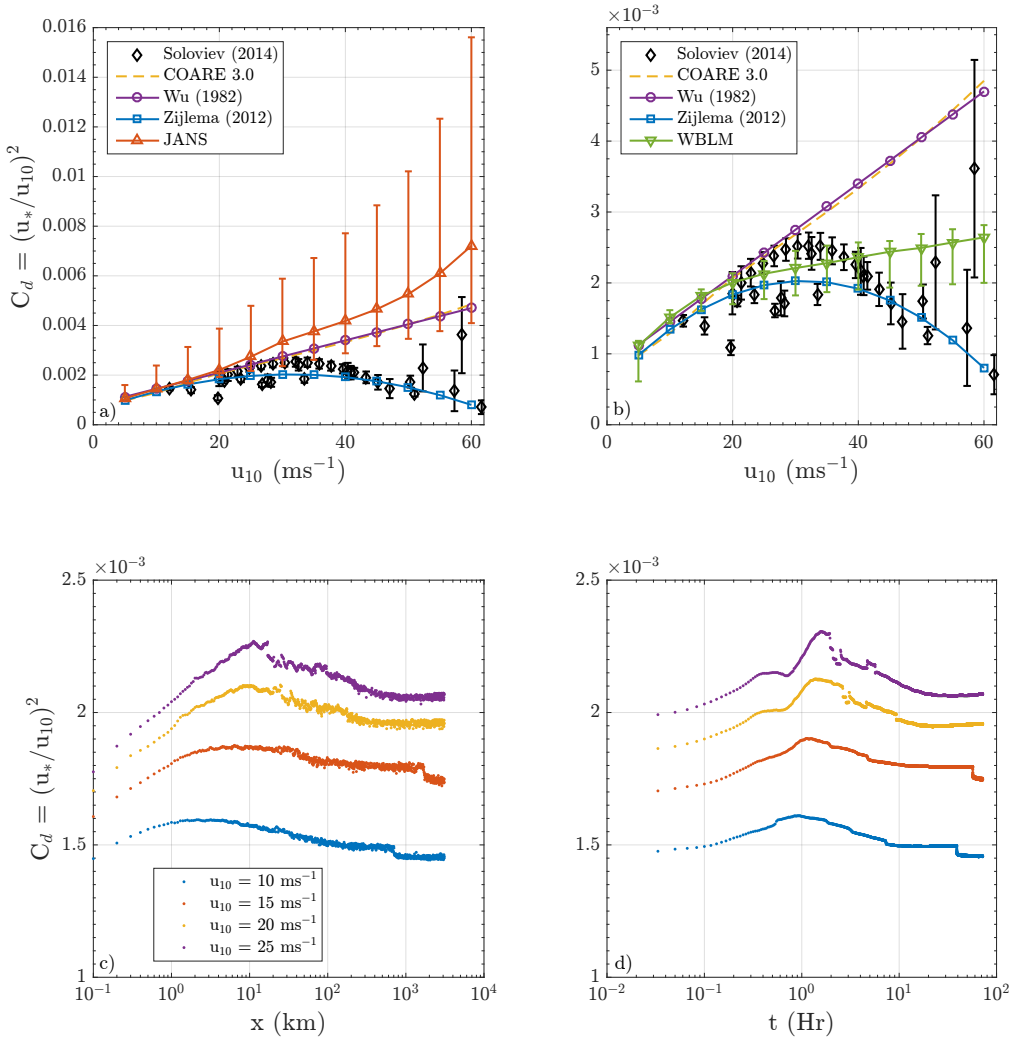

Figure 27: Drag coefficient C_D as a function of U_{10} (a, b), fetch (c) and simulation time (d). data in (c) are after 72 hours' simulation time and data in (d) are at a fetch of 3000 km using WBLM. A copy of Fig. 6.9 in [25].

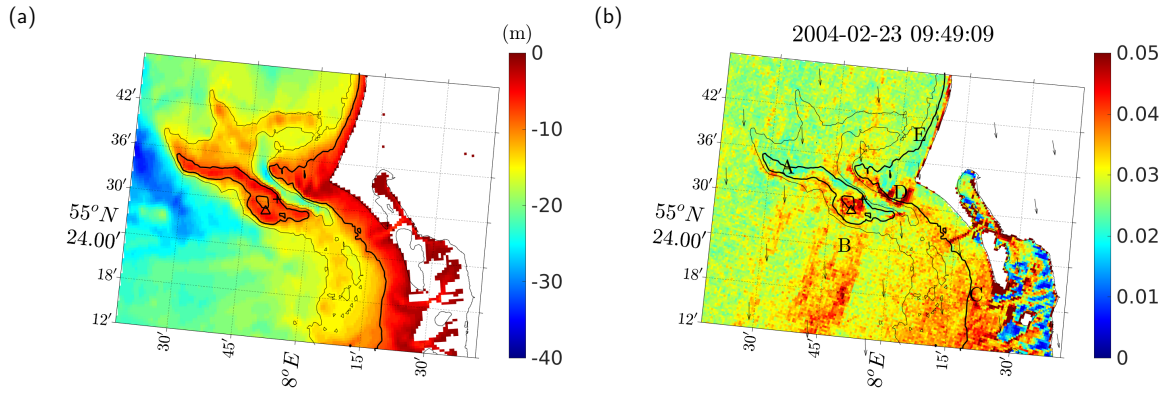

Figure 28: (a) Bathymetry around Horns Rev I where cross and triangle mark the positions of M2 and buoy, respectively. Contours of water depth of 9 m and 15 m are shown in thick and thin lines, respectively. (b) Radar backscatter measured by ASAR at 9:50 on 2004-02-23. Letters A to E represent areas where the backscatter is larger or smaller than surrounding areas. Black arrows show the 10 m wind vectors from the CFSR data. A copy of Fig. 8.1 in [25].

case is the coastal feature shown in the ASAR data. In this range of wind speed up to 15 ms^{-1}, the difference caused by the different z_0 is expected to be small to moderate. At 15 ms^{-1}, the difference in U_{10} is as large as 4 ms^{-1} by using different schemes for z_0, quite considerable (see Fig. 8.6 in [25]).

Figure 31 shows another case where the wind speed around Horns Rev was about 20 ms^{-1} and here the coupled modeling using WBLM gives in general larger wind speed in comparison with the non-coupled version. The effect of the bathymetry is clear where about 6% difference can be seen from the coupled and non-coupled version.

8.1.2 The effect of coupling for strong winds

Measurements shown in Figs. 2 and 4 have suggested higher modeling uncertainty in using z_0 parametrization at strong winds. Figure 30 indicates that WBLM outperforms the other 7 schemes for strong wind conditions in describing the dependence and spread of C_D on the wind speed.

Figure 4 also suggests that the differences in z_0 between difference schemes are of much larger magnitude at stronger winds and there larger effect is expected on the wind field simulation.

For the case 2004-02-22 to 2004-02-24, we now shift the focus to the storm center as in the outer model domain where the wind is stronger. A cloud picture exists at 20:40 on the 23rd, and it is used to verify the modeled storm center. The storm center was well captured. To see the impact of coupling, differences of C_D between the coupled and the non-coupled modeling are calculated for this time slot 20:40 and they are shown in Fig. 32 for the seven schemes for coupled modeling. The corresponding differences in U_{10} caused by coupling are shown in Fig. 33. The difference in U_{10} can be 10% or larger, which is not negligible, suggesting the effect of coupling can not be neglected. Note that in Fig. 32, schemes using parametrization have the artificial patterns showing discontinuity

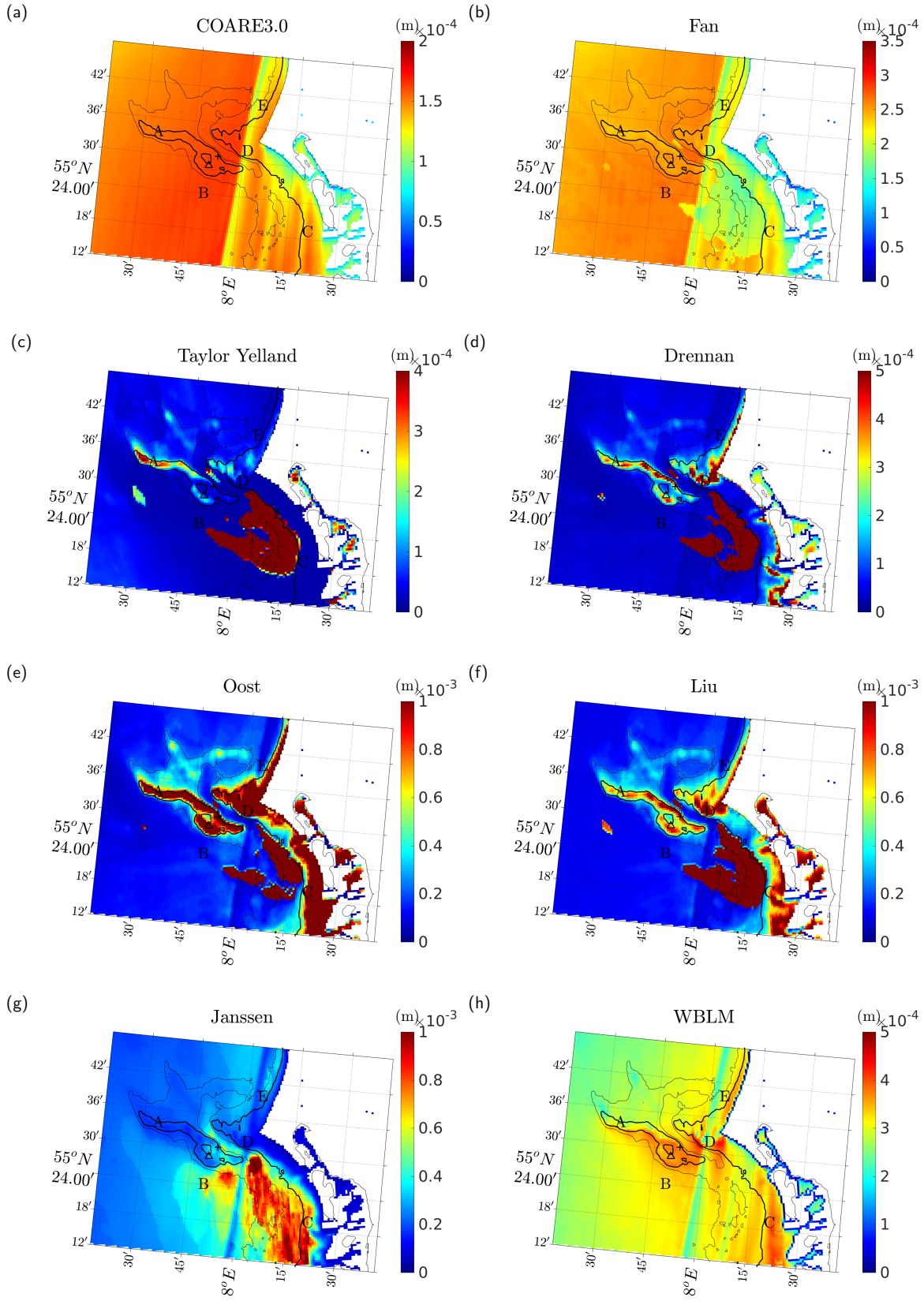

Figure 29: Roughness length z_0 at 9:50 on 2004-02-23, corresponding to the time shown in Fig. 28b. The names of the eight schemes are given in the plot label. A copy of Fig. 8.7 in [25].

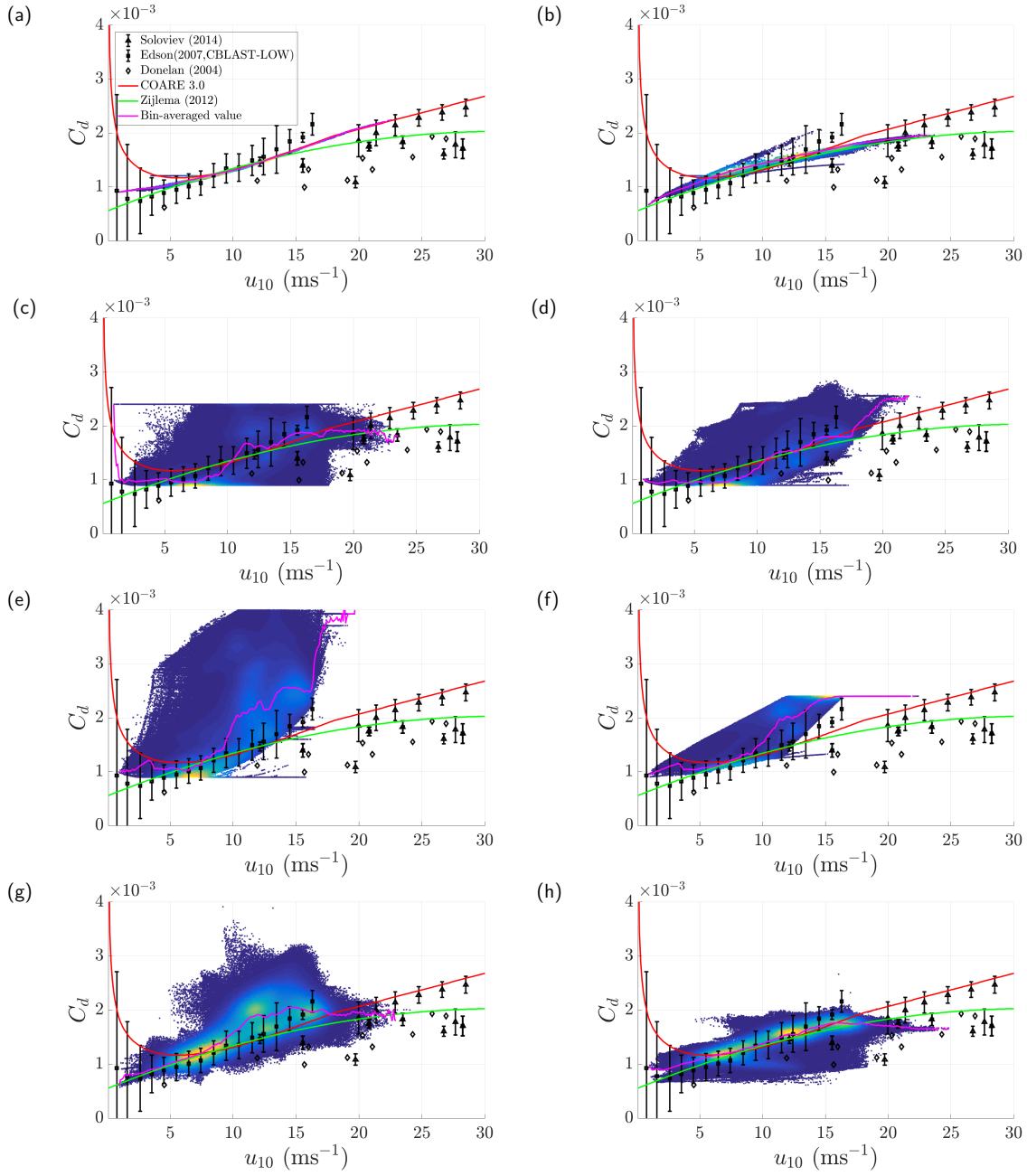

Figure 30: Scatter plot of C_D as a function of wind speed at 10 m for all grid points in domain III as in Fig. 6 from 2004-02-22 6 am to 2004-02-24 6 am, using eight different schemes for coupling WRF and SWAN. Each subplot corresponds to one scheme, same as in Fig. 29. a-CORARE; b-Fan; c-Taylor-Yelland; d-Drennan; e-Oost; f-Liu; g-Janssem; h-WBLM. A copy of Fig. 8.11 in [25].

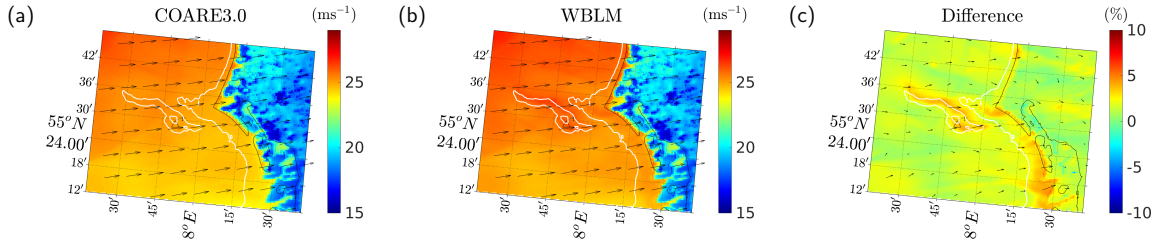

Figure 31: Spatial distribution of U_{10} at 21:00 on 2002-01-28, (a): using COARE 3.0 not coupled; (b): WBLM; (c): the difference between (a) and (b). A copy of Fig. 8.15 in [25].

in the drag coefficient, which is absent in the stress-based method Janssen and WBLM (Fig. 32f and g).

The analysis in section 8.1.1 and 8.1.2 suggests that (1) WBLM outperforms the other coupling schemes in describing the drag coefficient (2) the effect of coupling is important in coastal zones (3) the effect of coupling is important in strong winds.

8.1.3 The storm Britta

The case study of the storm Britta not only shows the skill of one of the modeling systems of X-WiWa in capturing the special strong wind and wave fields but also investigated a general issue of how the modeling system handles wind "gustiness" related to open cell structures in wave modeling. This study was published as [43].

As introduced in [43], Storm Britta is characterized by strong and highly fluctuating mean wind speed and usually high waves in the North Sea, where FINO 1 experienced a 20-year return value for H_{m0} and where the platform was damaged at a 15 m tall working deck [46]. This storm also caused a remarkable storm surge on the coast of the Netherlands, Germany and southern Baltic Sea [92]. Since a large number of offshore wind farms are planned in the southern North Sea where the design specifications for the offshore wind turbines outlined smaller extreme waves, storm Britta represents a challenge but also an opportunity for us to examine our modeling ability, to understand the physics and to better allocate our modeling efforts.

One specific research topic addresses this question: the wind speeds during Britta are strong but not extreme, and similar strength of wind speeds is observed in many other storms, such as Erwin from 8th January 2005, what caused the extreme H_{m0} at FINO 1? Was it the convective condition [93]? Or was it related to the presence of the open cell structures as several groups of researchers noticed [94, 95]? [94] noticed the highly fluctuating mean wind speed and [95] examined the "gustiness" of the open cell wind field on the wave modeling using the K-spectral model [96] with a special resolution of 1 km. In their modeling, the open cells are described as "rapid moving gust structure" and they are artificially implemented by updating the wind field every 5 minutes, formulated as an idealized hexagon-ring pattern that is superimposed to the existing mean wind field. However the findings from these studies are not conclusive in explaining the Britta wave field in response to the wind field.

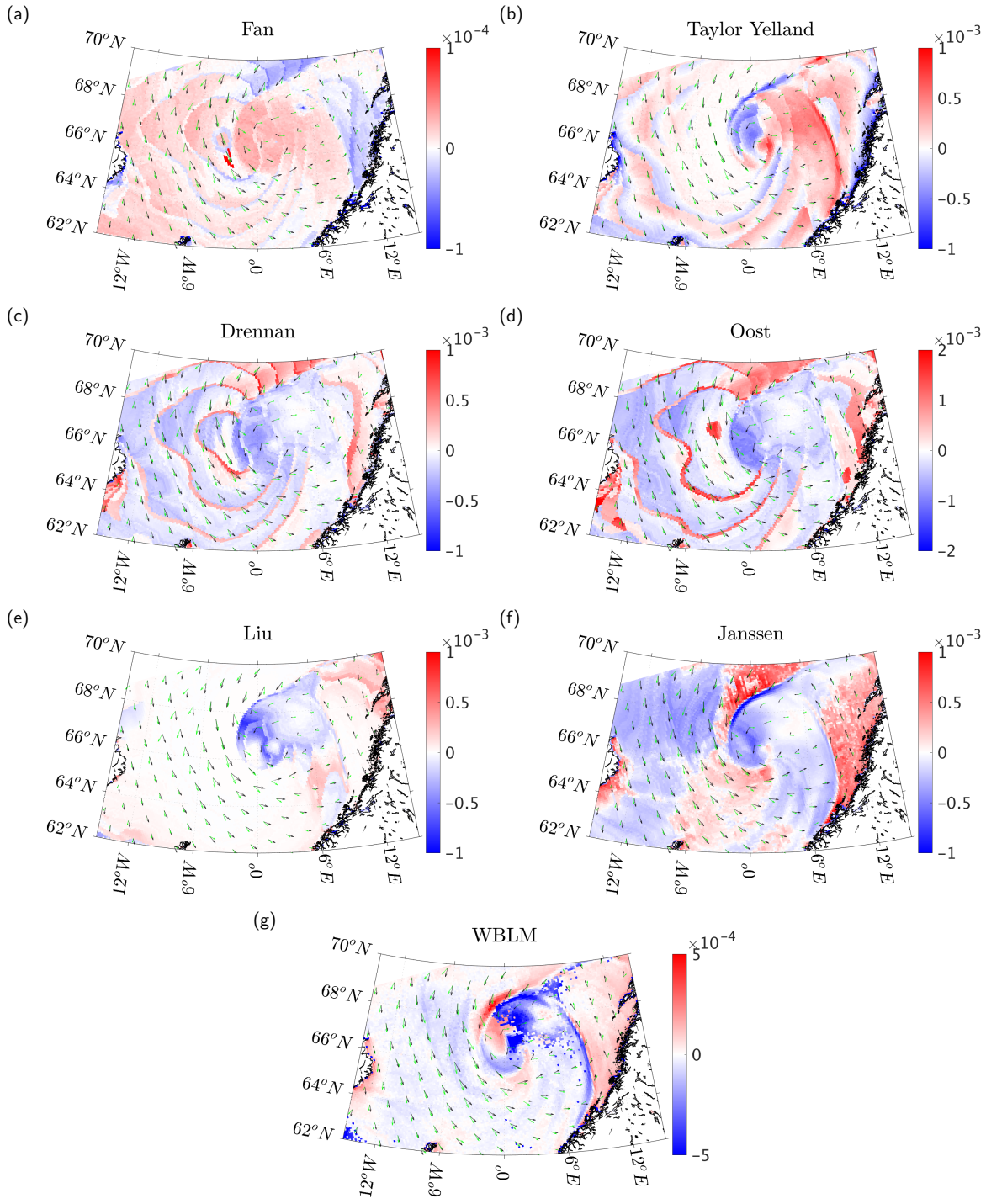

Figure 32: Difference of C_D between z_0 schemes of coupled modeling and the non-coupled COARE 3.0 scheme for 20:40 on 2004-02-23. A copy of Fig. 8.12 in [25].

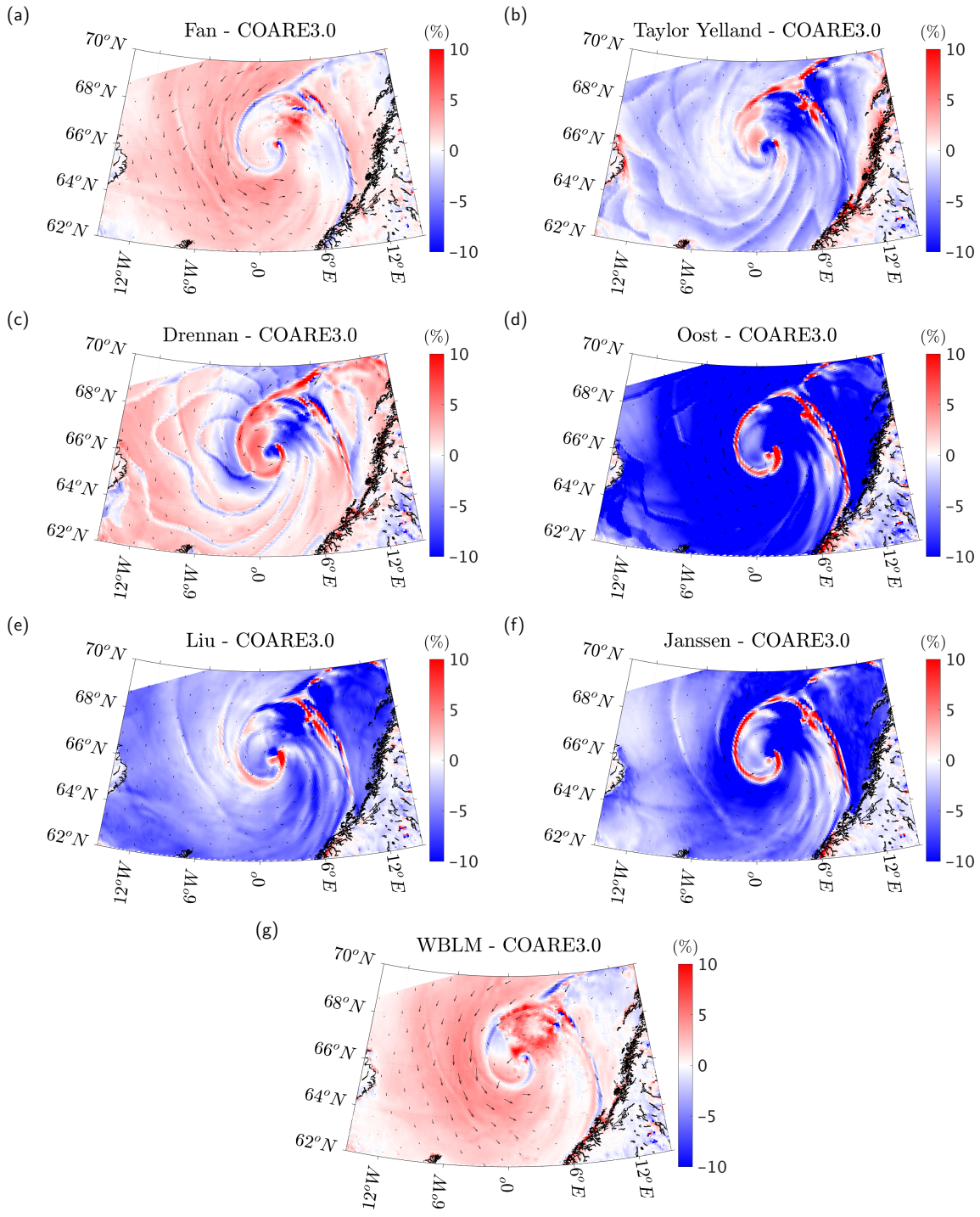

Figure 33: Difference of U_{10} in percentage between z_0 schemes of coupled modeling and the non-coupled COARE 3.0 scheme for 20:40 on 2004-02-23. A copy of Fig. 8.13 in [25].

In [43] we used the COAWST modeling system with WRF and SWAN activated to model the wind and wave field from 2006-10-30 00:00 to 2006-11-02 00:00. In this experiment, SWAN is initiated with a JONSWAP spectrum and the outer domain open boundaries are set to the JONSWAP spectrum with $H_{m0} = 0.5$ m and $T_p = 1$ s, where T_p is the wave period at the spectral peak. We used 36 directional bins and a frequency resolution of 0.1 f with f the frequency and it is between 0.03 and 1.02 Hz. One-way nesting is used in SWAN. The wind input and dissipation source functions are based on the studies of [16]. WRF transfers winds at 10 m to SWAN and SWAN feeds back with T_p, which will be used to calculate the wave age c_p/u_*, with c_p the phase velocity of waves at the peak frequency, which then will be used to calculate z_0 following the Fan's scheme with Eqs. (4), (5) and (6). Data are exchanged between WRF and SWAN in an so-called "online coupling" on a 90 s basis.

This study shows an example of how data analysis and model validation is done within X-WiWa. We use all measurements available to examine particular wind or wave behaviors. Point measurements of wind and waves as shown in Fig. 6 and Table 2 are used to examine the variation of wind and wave vectors with time during the storm. Measurements at particular site provides important time-varying parameters such as wind speed, direction, temperatures and pressures, to validate our model results. Cloud pictures are used to trace the track of the storm center and special atmospheric features. SAR data are used to compare the wind speed patterns over the North Sea with model results and to calculate the spatial spectrum in comparison with model outputs. These data suggest that the wind fields during Britta are reasonably well simulated, including the storm peak values and the open cell wind fields (Figs. 6 to 9 in [43]). Figure 34 is an example of the model performance at FINO 1 during storm Britta and Fig. 35 shows the open cell structure development in the wind field where Fig. 35b corresponds to the wind field shown in the SAR image in Fig. 11.

To understand the uniqueness of Britta, [43] studied altogether 17 North Sea storms from 2005 to 2013, with most of them named in the literatures. The study includes the storm path, the wind and respective wave field, stability conditions and it suggests that, while stability is a secondary condition and open cells are under convective conditions, the necessary conditions for the development of the extreme H_{m0} as in storm Britta are primarily (1) persistent strong mean wind and (2) long and undisturbed fetch during a long period that allows the development and propagation of strong waves. Though in the North Sea strong winds do often accompany cold fronts, namely unstable conditions and often open cells are produced. That open cells are not cause to the extreme H_{m0} is supported by the fact that our COAWST modeling successfully captured the extreme H_{m0} at FINO 1 and the effect of the gustiness related to open cells is not expected to be included in the standard setup of a spectral model SWAN.

This study also suggest that using not coupled version, with WRF only, gives smaller estimate of the wind speed by 2 ms^{-1} in comparison with the coupled version and smaller estimate of H_{m0} by about 1 m at the storm peak, see Fig. 36.

Note that this study was submitted for publication before WBLM was successfully implemented. There haven't been time so far to do a similar analysis with WBLM modeling, but it will be followed up. This also tells that the roughness length in [43] was not from WBLM; the Fan et al (2012) scheme was used.

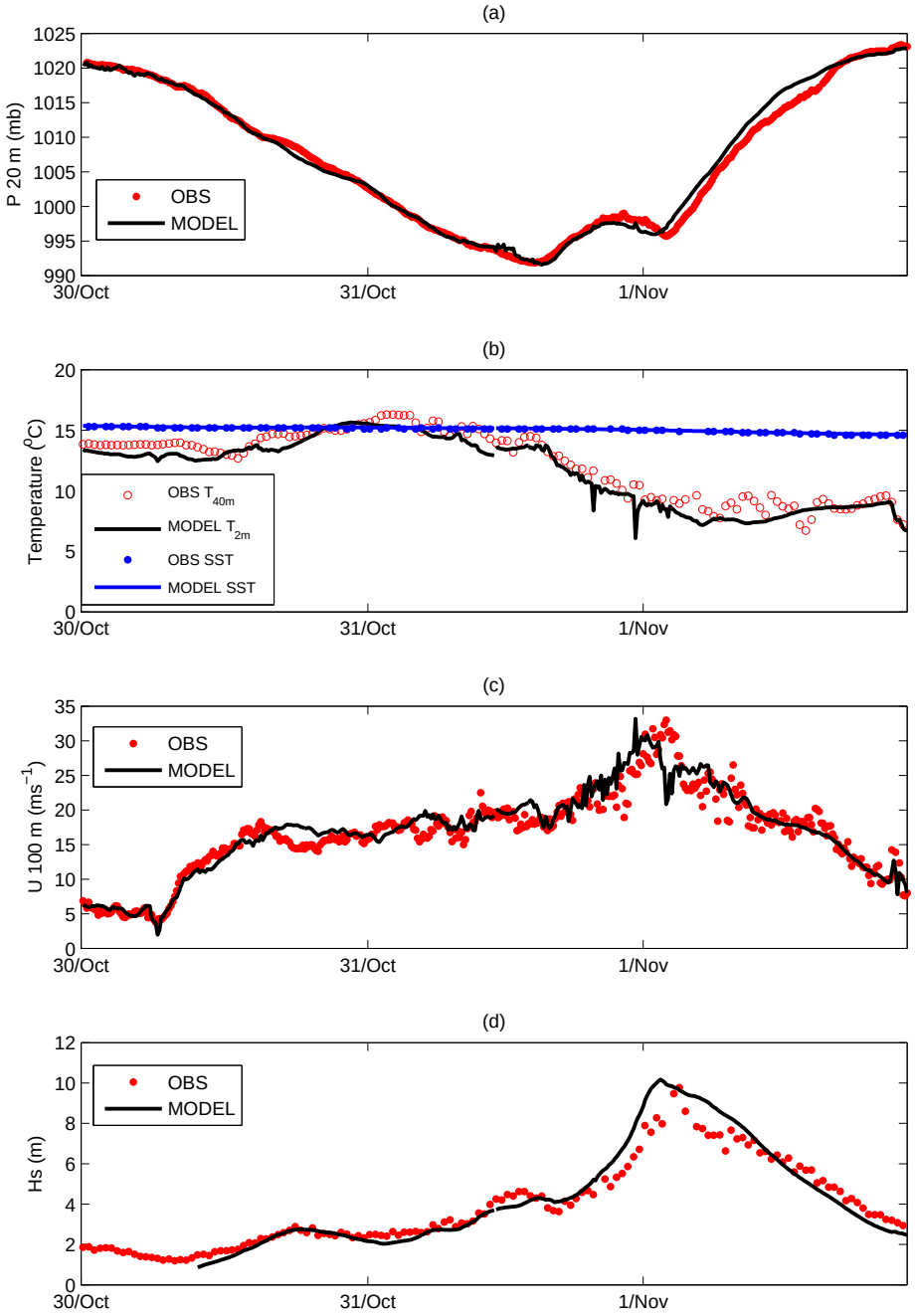

Figure 34: At FINO 1, time series of pressure at 20 m (a), temperatures (b), wind speed at 100 m (c) and significant wave height (d), measured and modeled. A copy of Fig. 6 from [43].

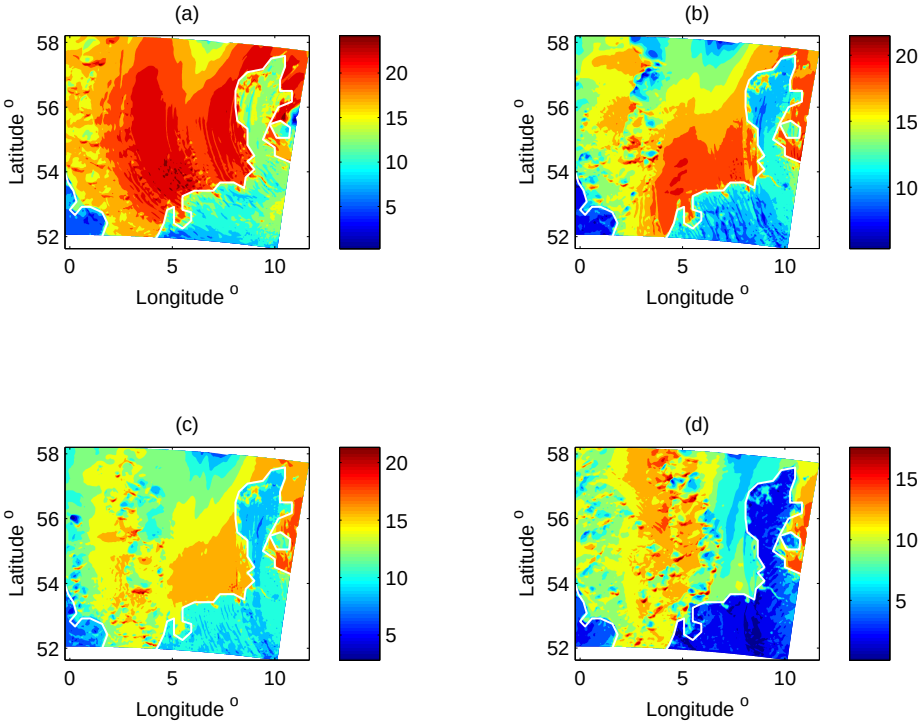

Figure 35: Modeled wind speed at 10 m on 2006-11-01 at (a) 4:00; (b) 10:00; (c) 13:00 and (d) 22:00. A copy of Fig. 7 from [43].

8.1.4 General validation

This section presents the general performance of the wind fields from all the coupled modeling using WRF-WBLM-SWAN in comparison with measurements. Fig. 37 shows the measured and modeled wind speed time series at six sites for all the simulations where measurements are available. Here the modeled data are from the coupled modeling. The difference in coupled and uncoupled will be discussed in connection with the calculation of extreme wind in section 8.2.1. Modeled data are extrapolated linearly to the corresponding measurement heights. The mean error (ME), mean absolute error (MAE) and root-mean-squared error (RMS) all each site are printed on each plot. The same data are plotted as density scatter in Fig. 38 where it can be seen that (1) majority data follow the 1:1 distribution, except for RUNE where lidar data are few; (2) most strongest winds scatter around 1:1. The strongest wind from each storm was identified from both the measured and modeled time series and plotted together for all sites in Fig. 39. The largest bias at strong winds from Fig. 39 are from RUNE and Anholt, where both measurements are short and from lidars and the uncertainty in the measurements has not been assessed.

The drag coefficient C_D has been calculated from the modeled u_* and U_{10} for four sites, two relatively open sea conditions (FINO 1 and FINO 3) and two coastal sites (Horns Rev M2 and Anholt) and its distribution with wind speed at 10 m is presented as density scatter plot in Fig. 40. On these plots, the black symbols are reference measurements from the literature as discussed in section 3.2.1 and most of them are for open sea conditions, especially for strong winds. The modeled data at FINO 1 and FINO 3 show a good agreement with these

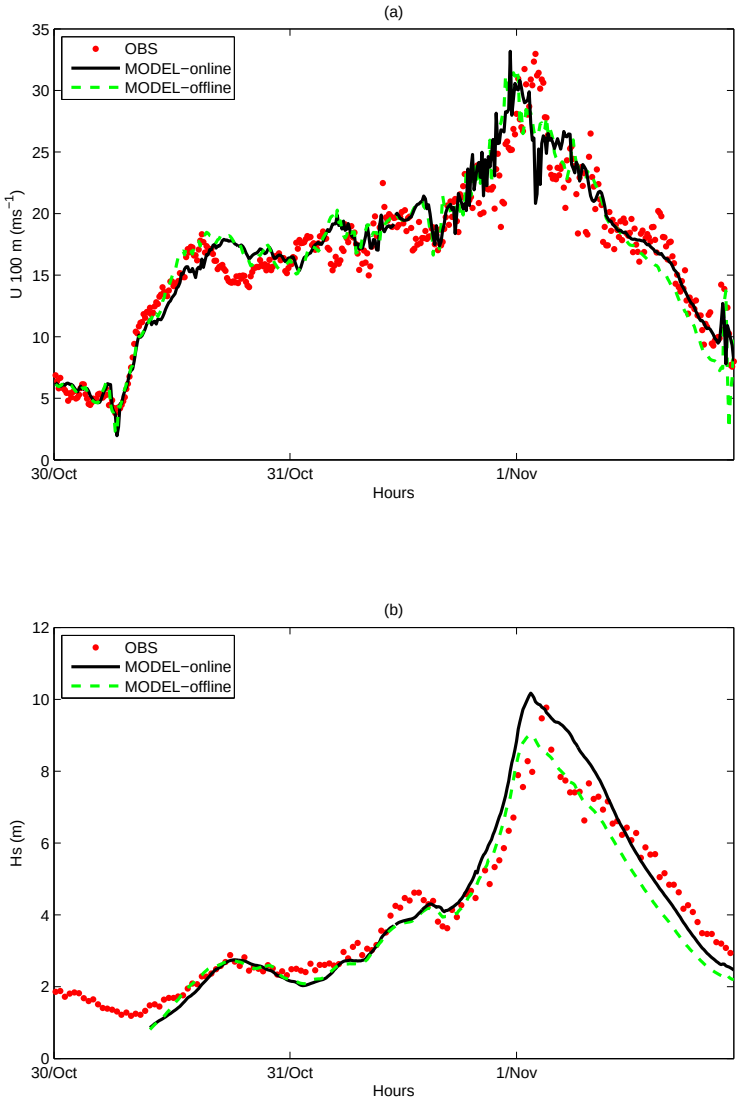

Figure 36: Time series from measurements and the two-way online coupling (legend "MODEL-online") and the one-way offline coupling (legend "MODEL-offline") during storm Britta (a) wind speed at 100 m at FINO 1. (b) significant wave height H_{m0} at FINO 1.

open sea data, regarding the mean value and the level of scatter at the same wind speed, while at the two coastal sites M2 and Anholt, the majority of modeled data suggests higher drag in comparison with these open sea data.

8.2 The extreme wind atlas

Storm Britta is one of the hundreds of storms that contributed to the extreme wind samples for the estimate of the 50-year wind over the Danish waters.

All extreme wind events in this area are the mid-latitude cold front systems. In cloud pictures such as the one shown in Fig. 8, along with the front, there are open cell structures. In fact, out of the 429 simulations of our extreme wind storms, during 45% of the cases, open cells are present. This was examined through looking at the wind field of the model outputs.

Open cells frequently occur within cold air outbreaks [97]. The cold air advects over warm water surface, becomes modified and forms clouds which frequently take the form of cloud street which roughly orients along winds in the outbreak. Further downwind in the outbreak, the cloud street transforms into 3-dimensional open cells [98]. When moving along with the weather system, in the center of open-cell circulation, there is downward motion and clear sky, surrounded by cloud associated with upward motion [97]. Accordingly there is both spatial and temporal significant variation in the wind speed, as shown in Fig. 11 (wind speed difference over 5 ms^{-1} over 3 km distance) and Fig. 34 (ΔU over 10 min can be as large as 7 ms^{-1}).

Figure 41 shows two more examples from our 429 storms when open cell structures are present. Those open cells have a diameter of tens of kilometers. One can see hot spots of high winds over the space, as also present in the SAR image (Fig. 11).

8.2.1 Extreme winds from modeling

As introduced in section 6, the 429 storms are run both with WRF-WBLM-SWAN and with WRF only. Over domain III, with a spatial resolution of 2 km, there are 339×342 grid points. At each grid points, all storm simulations over one year are put together and the maximum value of the year is identified. Thus for each grid point, we have 23 values (1994 - 2016), which will be used to fit a Gumbel distribution to obtain the 50-year wind. Figure 42 shows such an example for the site FINO 1 from WRF-WBLM-SWAN (left) and WRF modeling (right).

The 50-year wind atlases for 100 m and 10 m over the waters around Denmark are shown in Fig. 43 and 44, respectively. In each of the two plots, there are four subplots, where subplot-a is the calculations from the coupled modeling and subplot-b is from the non-coupled, WRF-only modeling, subplot-c is the difference between the coupled and non-coupled modeling. Subplot-d is a smoothed version of subplot-c, which is a conservative estimate of that in subplot-c: the maximum difference in U_{50} across 13 grid points, namely 12 grid boxes corresponding to 24 km, is chosen and presented all grid points, except the 6 rows on the boundaries.

The following can be observed from Fig. 43 and 44:

- U_{50} is in general strongest over the open North Sea than the Baltic Sea. There is a gradient of U_{50} from land to coastal zones to open sea.

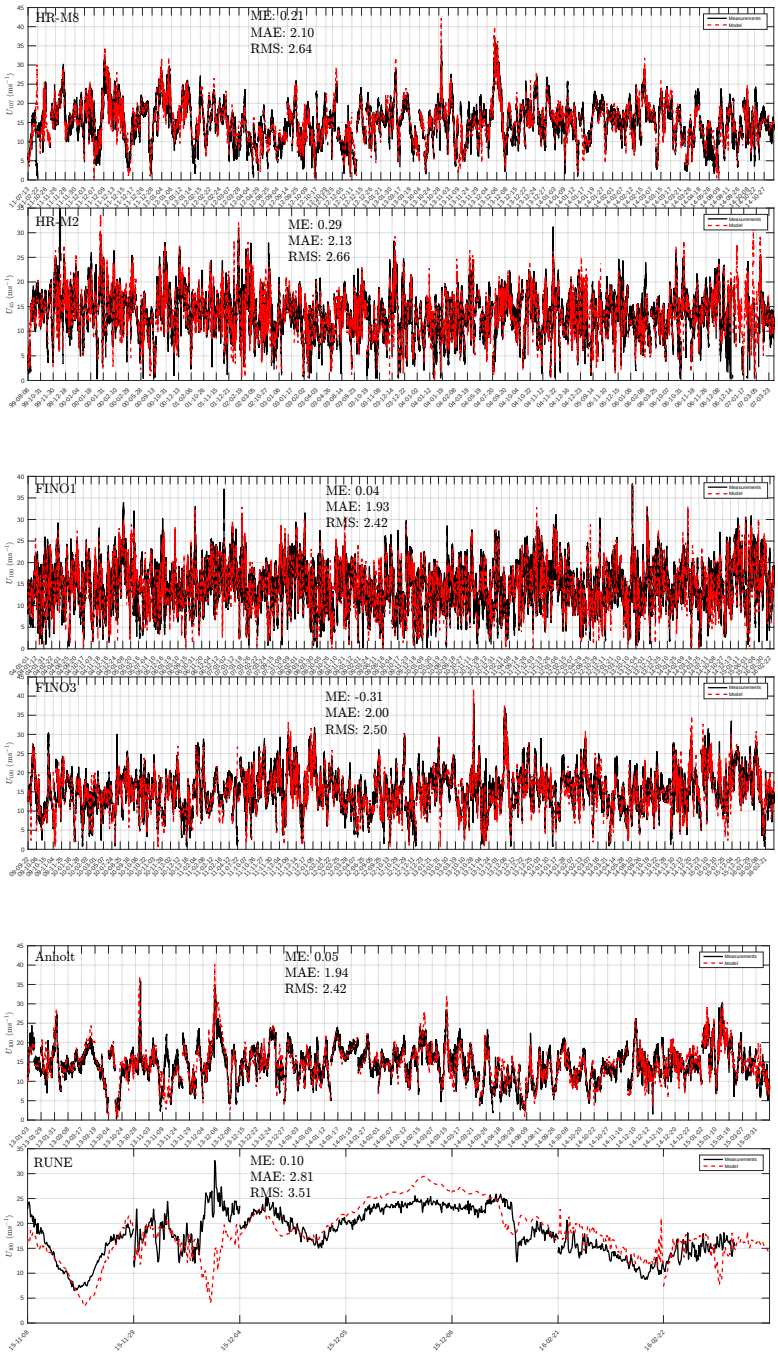

Figure 37: Time series of wind speed at measurement heights of all days when measurements are available for validation, from above to below: Horns Rev M2, M8, FINO 1, FINO 3, RUNE and Anholt. The model data are from the coupled modeling.

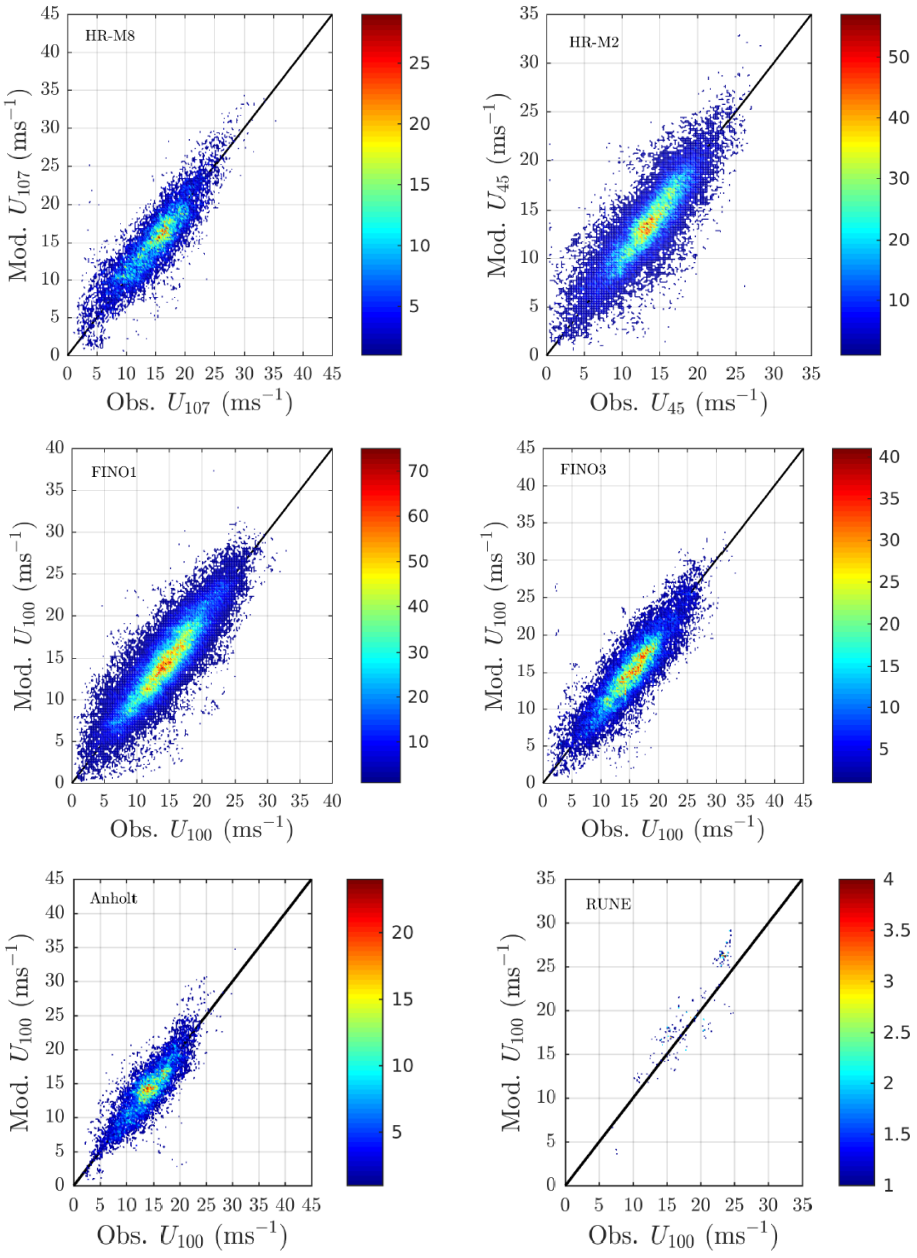

Figure 38: Same data as Fig. 37 but as scatter density plot with coupled modeled winds vs measured winds at corresponding measurement heights at the six sites. The color shows the number of points at one coordinate.

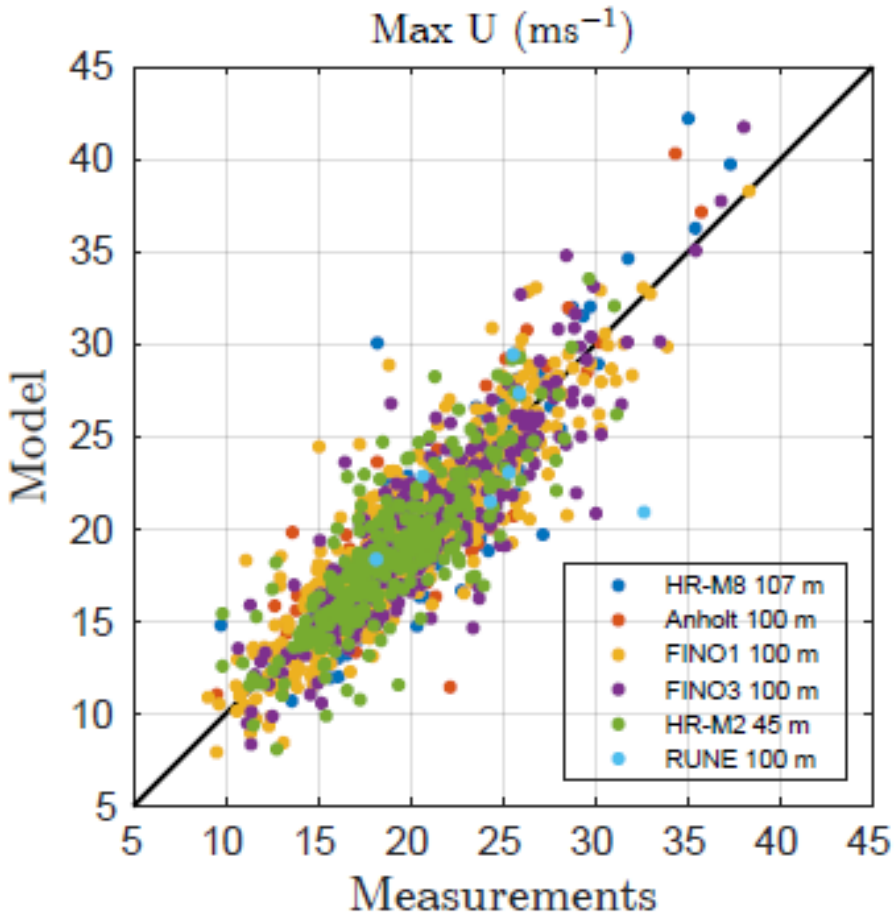

Figure 39: Comparison of the coupled modeled and measured wind maxima of each simulation (36 hours) at all stations if measurements are available.

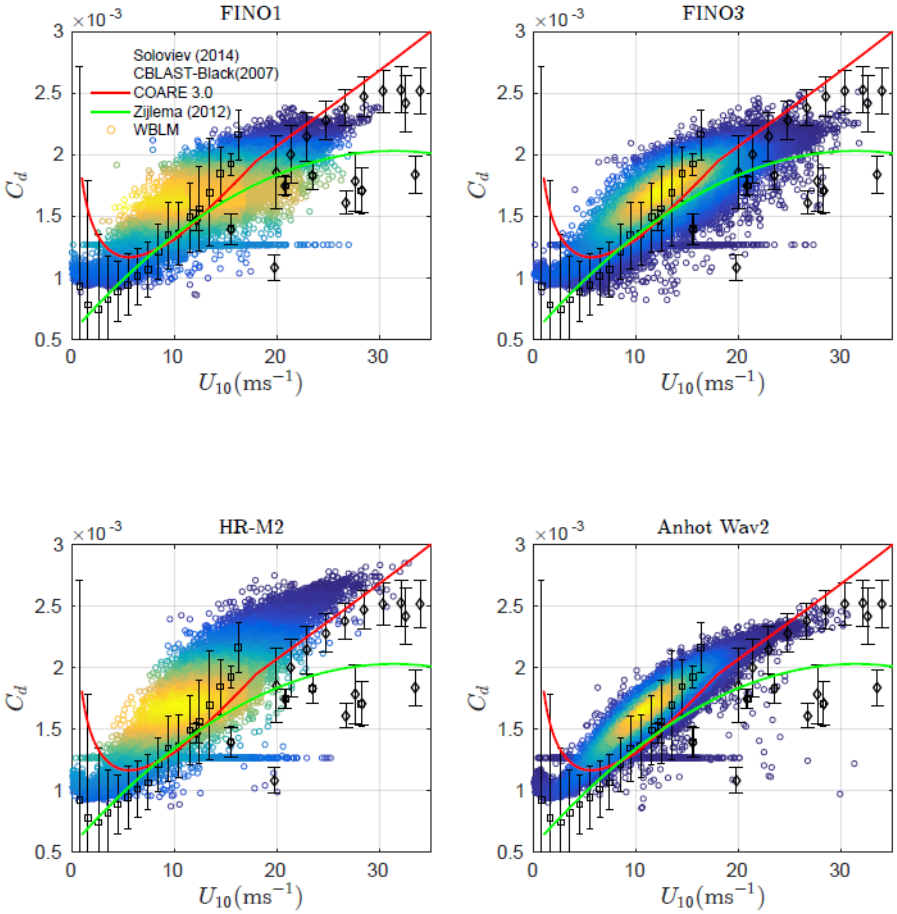

Figure 40: Density scatter plot of drag coefficient vs 10-m wind speed from the coupled model data at four sites: FINO1, FINO3, Horns Rev M2 and Anholt, on top of reference measurements from Fig. 2

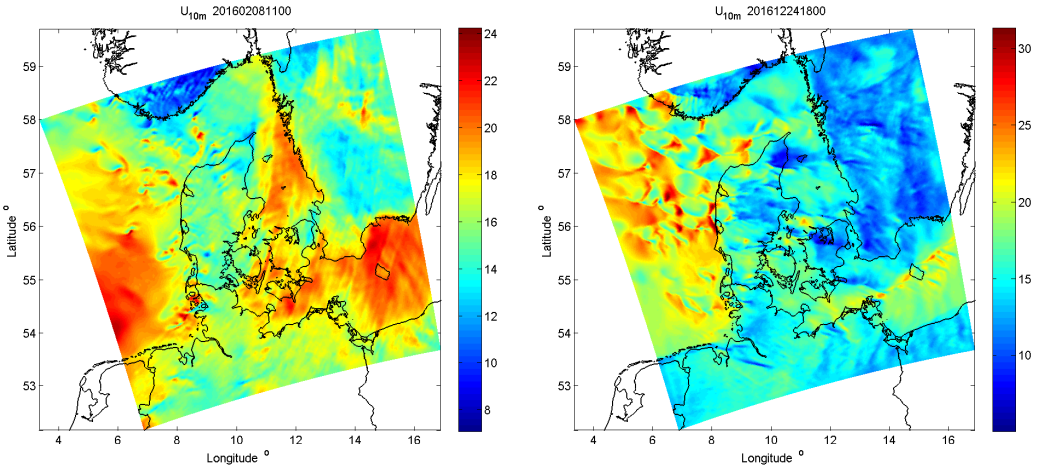

Figure 41: Examples of spatial wind variation: 10-m wind field at 11:00 on 2016-02-08 and at 18:00 on 2016-12-24.

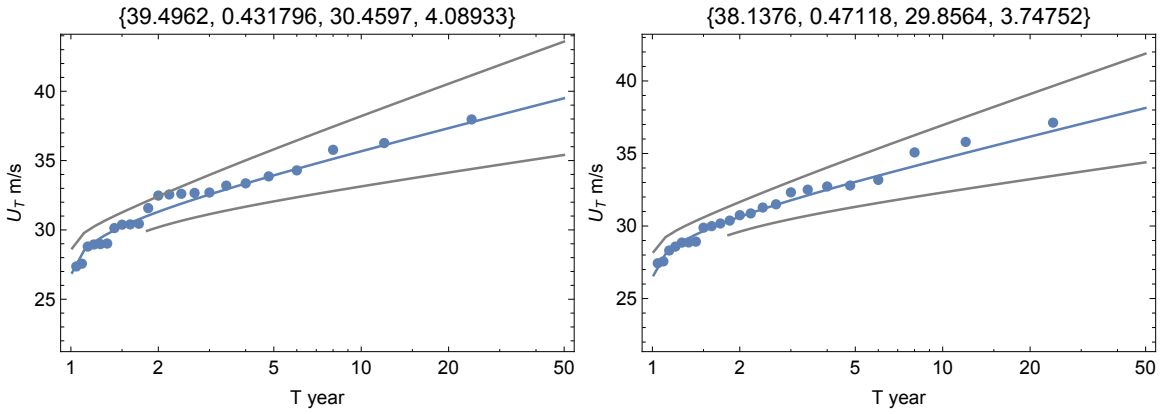

Figure 42: Gumbel distribution and the estimate of U_{50} for FINO 1 using X-WiWa model output using (left) WRF-WBLM-SWAN and (right) WRF. The four numbers on the label of the two plots are: U_{50}, α, β and $1.98\sigma(U_T)$ as in Eq. (39), (40), (42)

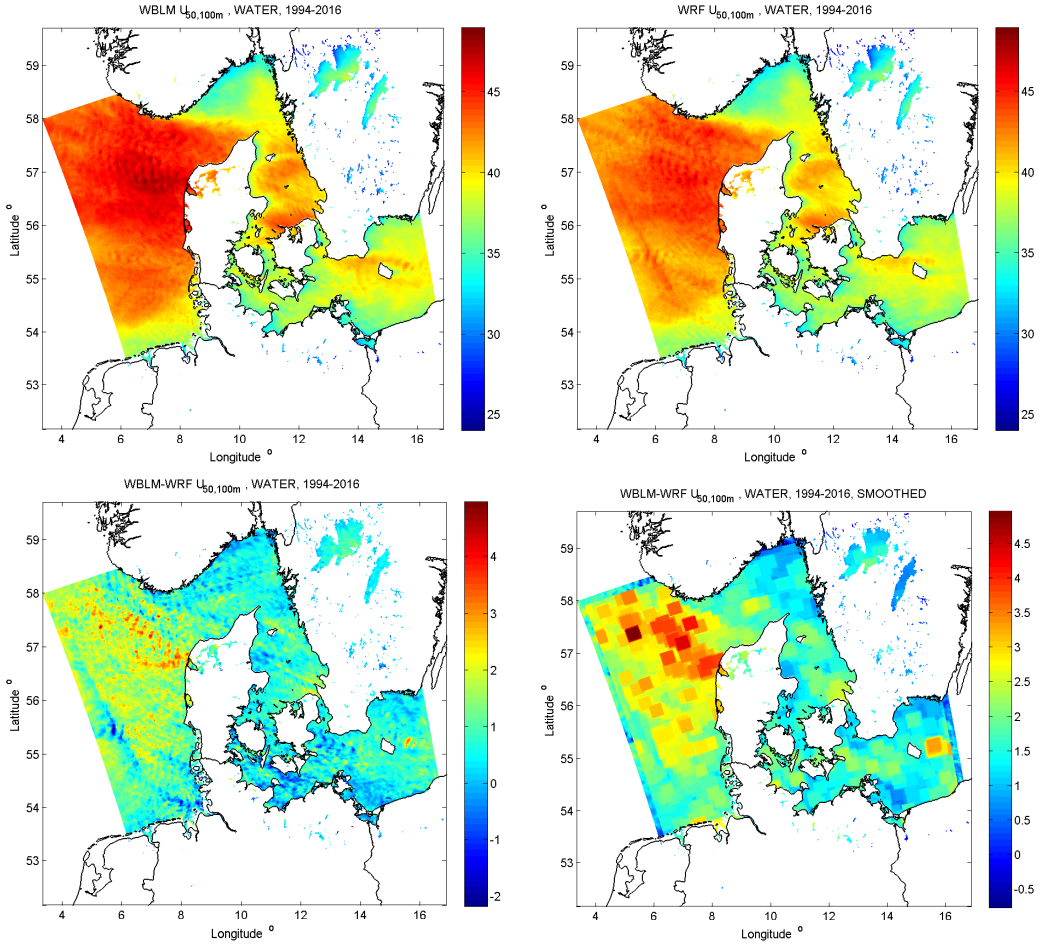

Figure 43: The 50-year winds at 100 m over waters around Denmark. (a) from WRF-WBLM-SWAN modeling; (b) from WRF modeling; (c) difference between (a) and (b) (a minus b); (d) maximum of wind speed difference over 13 by 13 grid points around each grid point (apart from the boundaries)

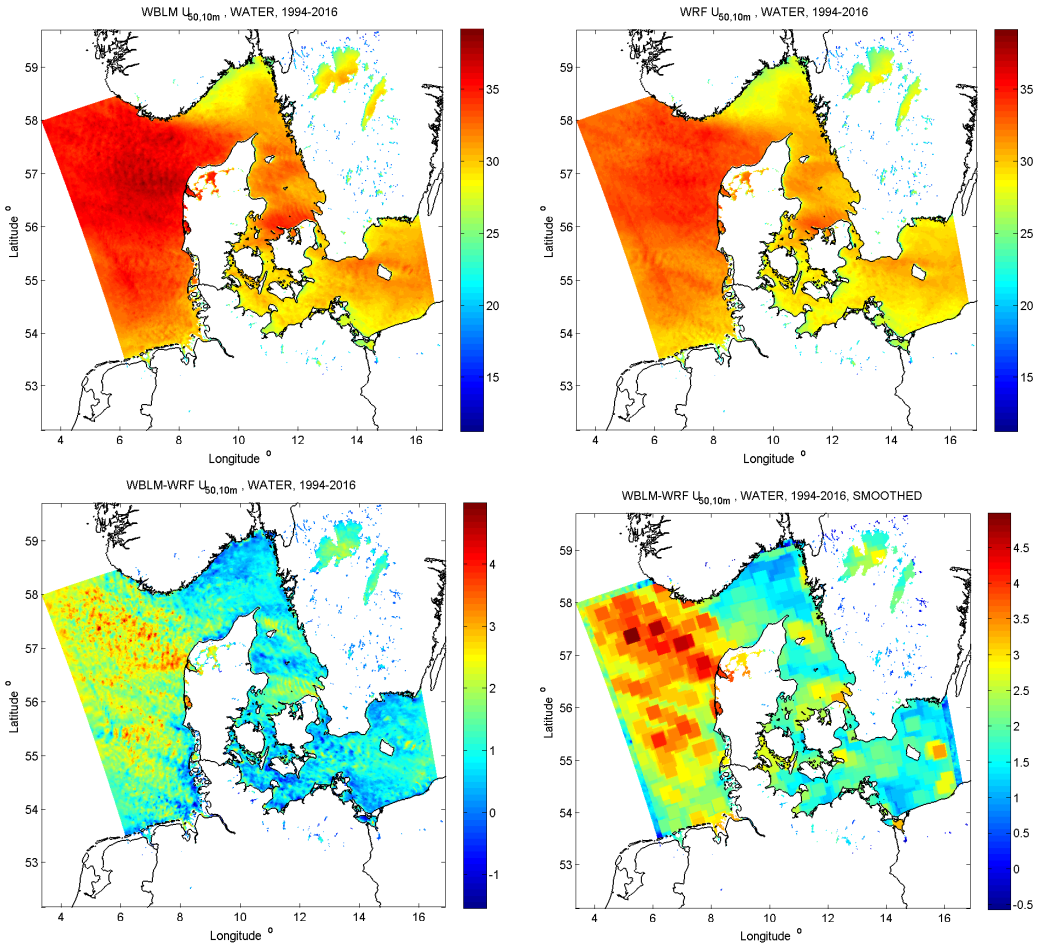

Figure 44: Same as Fig. 43, except for at 10 m.

- There is difference in U_{50} calculated from the coupled and non-coupled simulation, with stronger extreme wind from the coupled system.
- There is perturbation-like patterns in the extreme wind field.

Accordingly, the following question are investigated:

1. Are the estimates reasonable?
2. Which U_{50} is better, the coupled or non-coupled modeling?
3. Are the differences between the coupled and non-coupled modeling important?
4. What are the perturbation-like pattern in the wind field and what's the indication?

The first to third questions will be answered through validation with comparison with estimates from measurements in section 8.2.2 .

The fourth question is to be answered by the fact that 45% of our simulated storms have the open cell structure. Bakan and Schwarz [99] examined the cellular convection over the north-eastern Atlantic using satellite data over four years 1980 to 1983 and found that "only 111 days out of 4 years the satellite image did not display convective phenomena over the oceans". These perturbation-like patterns are directly caused by the high spatial variation in the wind field, with examples as shown in Fig. 11, Fig. 35 and Fig 41. This is examined through the step-by-step calculation of the maximum wind during individual storms, which is one major step in identifying the annual maximum winds at each grid point. Even though the modeling is capable of capturing the open cell structure up to a horizontal size of about 15 km [43], the exact position of each cell is not necessarily captured. Fig. 34c shows that at FINO 1, the storm peak offsets by a couple of hours. This fact affects our evaluation and application of the individual value at each grid point, since its uncertainty is related to the spatial structure (e.g. size) of open cell wind field. The smoothed version shown in Fig. 43 and 44 show that the coupled modeling provides systematically stronger winds and the largest difference in the extreme wind caused by model coupling is located at strongest wind field in the northern part of the North Sea, which is as expected, as analyzed in section 8.1.2. The largest difference is about 13% at 10 m and 10% at 100 m. This difference is significant as we evaluated in the preparation of the current project (see also section 1) and it should not be ignored.

8.2.2 Extreme winds from measurements and validation

Measurements from Horns Rev M2, FINO 1, FINO 2, FINO3 and Høvsøre (see Table 4) have relatively long records for the estimation of extreme wind. Note that the mast from Høvsøre is land-based with a few kilometers away from the shoreline, but the wind at 100 m is representing the sea condition when it is from the sea [100], as most extreme wind samples are from the sea. The data length at these sites are 5, 13, 9, 7 and 12 years at M2, FINO 1, 2, 3 and Høvsøre, respectively. In section 7.1 it is discussed that in the North Sea area, data length shorter than 10 years has high chance in providing biased estimate of U_{50} and when data length is shorter than 10 years, using POT gives smaller uncertainty due to much more samples can be used. At the same time, in case of using an incomplete time series (here we have data coverage less than 95% in general), POT is less critical to the missing of the annual maximum wind peak. Figure 45

Table 10: U_{50} (ms^{-1}) from measurements and from modeling (1994 - 2016).

Site	Measurements	coupled modeling	non-coupled modeling
M2 (62 m)	44.3	40.0	40.0
FINO 1 (100m)	41.2	39.5	38.1
FINO 2 (100m)	38.3	38.6	37.3
FINO 3 (100m)	43.9	43.0	41.6
Høvsøre(100m)	45.0	44.6	42.0

shows such an example for FINO 3 where data are of 7 years using AMM (Fig. 45a) and POT (Fig. 45b) method. As also discussed in section 7.1.2 as well as originally in [82] that the estimate of U_{50} using POT method is related to the selection of the threshold, the interval between two consecutive storms to ensure the sample are independent of each other and the data length. Here we use the interval of 7 days, which is typically long enough to separate individual storms for the area of North Sea. By requiring an exceedance rate greater than 2 per year, we average the estimates using a range of wind speed thresholds whichever is within 95% confidence interval. Such a requirement of 2 events per year is to make sure the sample size is at least double that of using AMM.

The 50-year winds are calculated from measurements using POT method for Horns Rev M2 (top level 62 m), FINO 1 (100 m), 2 (100 m), 3 (100 m) and Høvsøre (100 m). The 50-year winds at 100 m are also calculated using AMM for FINO 1 and Høvsøre where the data length is longer than 10 years and they are 41.0 ms^{-1} at FINO 1 and 44.0 ms^{-1} at Høvsøre, close to the estimates from POT. The estimates from modeled data are prepared using the entire measurement period (1994 - 2016) as well as the overlapping period as the measurements. The results from modeled data and measurements (using POT) are shown in Table 10 and 11 for the entire period and the overlapping period, respectively. For the modeled data, there are two estimates, one is from the coupled modeling and one from the non-coupled modeling. These estimates are again presented in Fig. 46a for the entire period and Fig. 46b for the overlapping period, respectively. One can see that in general, the coupled system provides larger U_{50} and better agreement with measurements. The difference is though small at some places, for instance, Horns Rev M2, which can also be seen in Fig. 43 and 44.

Now we can answer the questions 1 to 3 from section 8.2.1. The estimates from our modeling are reasonable. The coupled system provides better estimates than the non-coupled modeling system. The difference can be as large as 15% (10 m) and 10% (100 m), which is significant. In the IEC standard 61400-1 (Ed.3), turbine class is defined into type-I, II, III and S, where the recommended values for the hub-height 50-year winds are 50 ms^{-1}, 42.5 ms^{-1}, 37.5 ms^{-1} and "values specified by the designer". A systematic deficit by 15% or 10% has a significant meaning for defining the wind turbine class when the 50-year winds at 100 m are about 40 ms^{-1}, see Fig. 43 and Table 10 and 11. For instance, for FINO 3, the non-coupled modeling suggests a type-III turbine ($U_{50} = 41.6$ ms^{-1}), while both measurements and the coupled modeling suggest a type-II turbine ($U_{50} = 43.9$ and 43.0 ms^{-1}, respectively).

Table 11: U_{50} (ms^{-1}) from measurements and from modeling (overlapping period).

Site	Measurements	coupled modeling	non-coupled modeling
M2 (62 m)	44.3	43.0	43.0
FINO 1 (100m)	41.2	39.1	37.1
FINO 2 (100m)	38.3	36.1	35.8
FINO 3 (100m)	43.9	45.5	41.9
Høvsøre(100m)	45.0	45.5	42.6

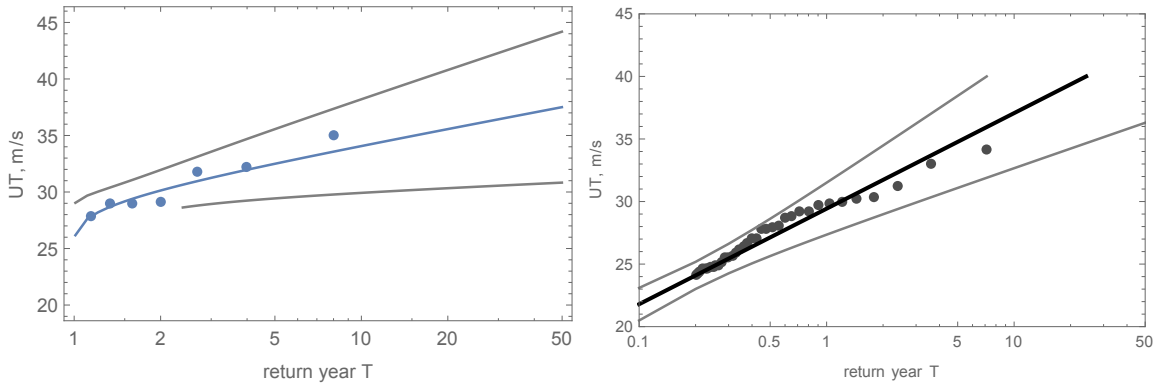

Figure 45: Illustration of problems in using short time series for the estimation of U_{50}. The 50-year wind at 100 m from measurements from FINO 3, using Annual Maximum Method (a, left) and Peak-over-threshold method (b, right).

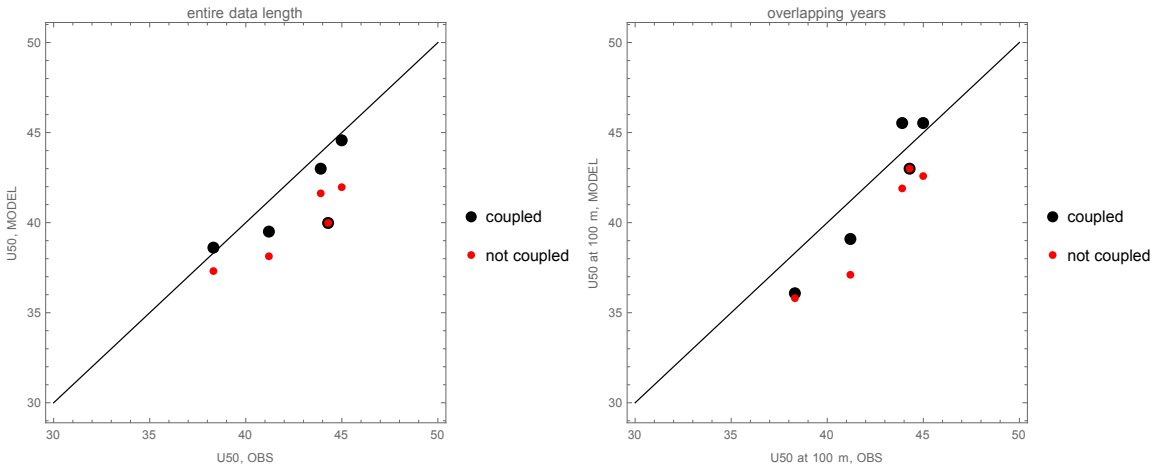

Figure 46: Comparison of U_{50} at 5 stations, measured (x-axis) vs modeled (y-axis), coupled (black dots) and non-coupled (red dots), see also Table 10 and 11. The measurement height is 100 m at FINO 1, 2, 3 and Høvsøre and 62 m at Horns Rev M2. (a. left) using entire modeled data. (b. right) using modeled data overlapping with measurements.

9 Results: Wave

This section presents the results obtained with the production run of the storms (section 9.1), together with assessment of the impact of different wind forcing (WRF and CFSR, section 9.2), and brief comparison of online and offline coupling (WRF-WBLM-SWAN vs WRF/CFSR-MIKE, section 9.2)

9.1 Offline WRF-MIKE modeling all storms: Validation of calibrated results

Presented in this chapter are the comparison of the full 932 storms against the available observations for each key calibration stations. Fig. 47 and Fig. 48 show the scatter plot comparisons for the selected stations. On the whole, the scatter plots for all the stations within the area of interest show a good overall representation of the modelled significant wave height against the available observations, although the scatter index is typically higher than 0.15. In the case of the largest H_{m0} in Fig. 47 and 48, in general they are well represented. However, there are also some cases that show slight misrepresentation by the model. This can be seen as both an under representation and overestimation of the H_{m0} in comparison with the observations depending on the location.

9.2 Offline CFSR-MIKE modeling 15 storms: assessment of CFSR wind forcing

The calibrated MIKE 21 SW model was also forced with the global CFSR wind field (corrected for atmospheric stability, see section 5.5.1) for the 15 calibration storms. The results are presented in the following sections. It should be noted that the wave model was calibrated to the WRF wind field (see section 5.6) and not the CFSR wind field, however a comparison was still made to assess the impact of the different wind fields.

The results from the model test are presented in Fig. 49 to 50. The significant wave height produced from the CFSR wind field forced MIKE 21 SW model produced a reasonable representation of the observations for the North Sea and western Danish Coastline. From the Taylor diagrams on the left hand side of Fig. 50 and Fig. 51, a comparison to the final calibration of the WRF forced model can be made. Of these stations, neither the CFSR or WRF forced wave model is suggested to outperform the other. Note that the full storm list cannot be compared as CFSR forced model was only run for the 15 calibration storms, and thus comparisons are limited, however with these results there is no strong evidence of significant differences on wave modelling when using CFSR reanalysis or WRF downscaling.

9.3 Online WRF-WBLM-SWAN modeling all storms

In this section we first show comparison of H_{m0} modeled from the online COAWST (WRF-WBLM-SWAN) modeling for all the storms at buoy stations from Horns Rev, FINO 1 and 3, Anholt and RUNE, where measurements are available.

Further analysis of H_{m0} has been done to stations where results from the offline WRF/CFSR-MIKE 21 SW modeling are prepared in previous sections, for sites Ekofisk, Fjaltering, Hirtshals, Läsö Ost and Nysted. For the comparison,

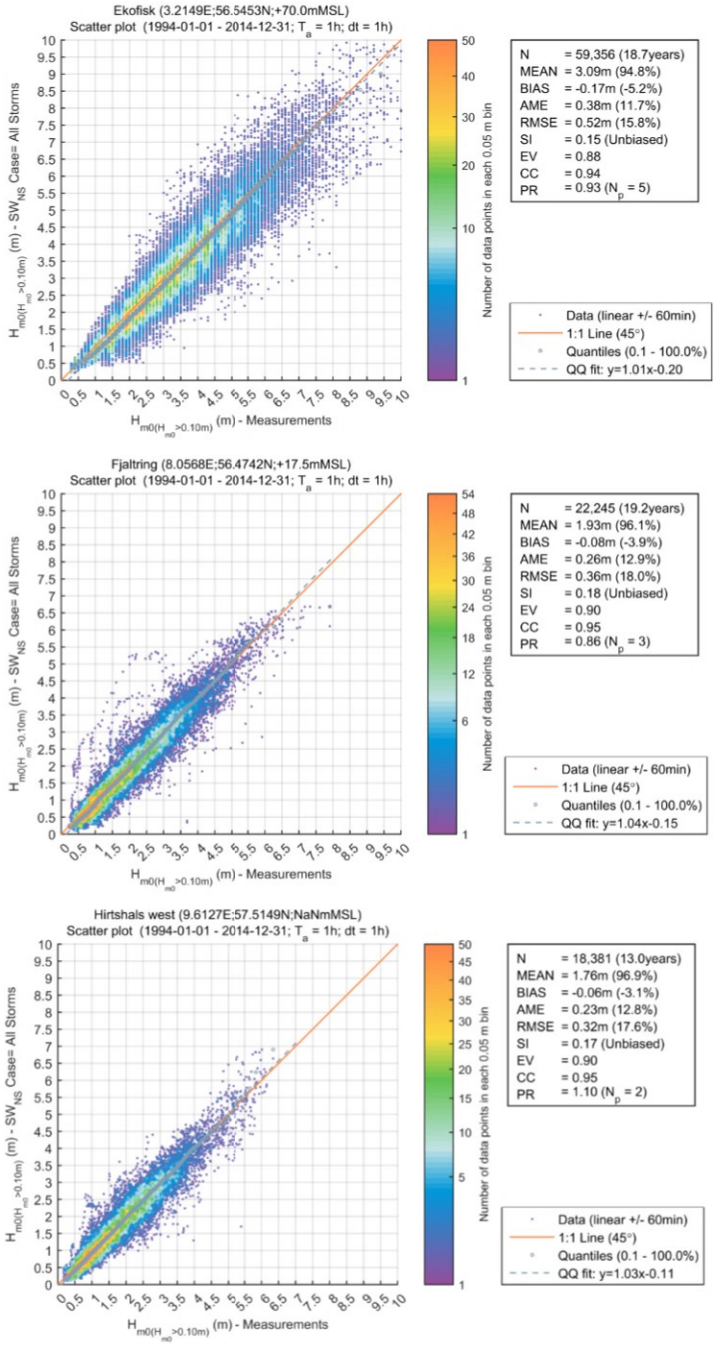

Figure 47: Validation of all storms from WRF-MIKE. Scatter plot of the MIKE 21 SW modelled significant wave height with forcing from the local WRF wind field for the all storms between 1994 and 2014 at Ekofisk (upper panel), Fjaltring (middle panel) and Hirtshals West (lower panel).

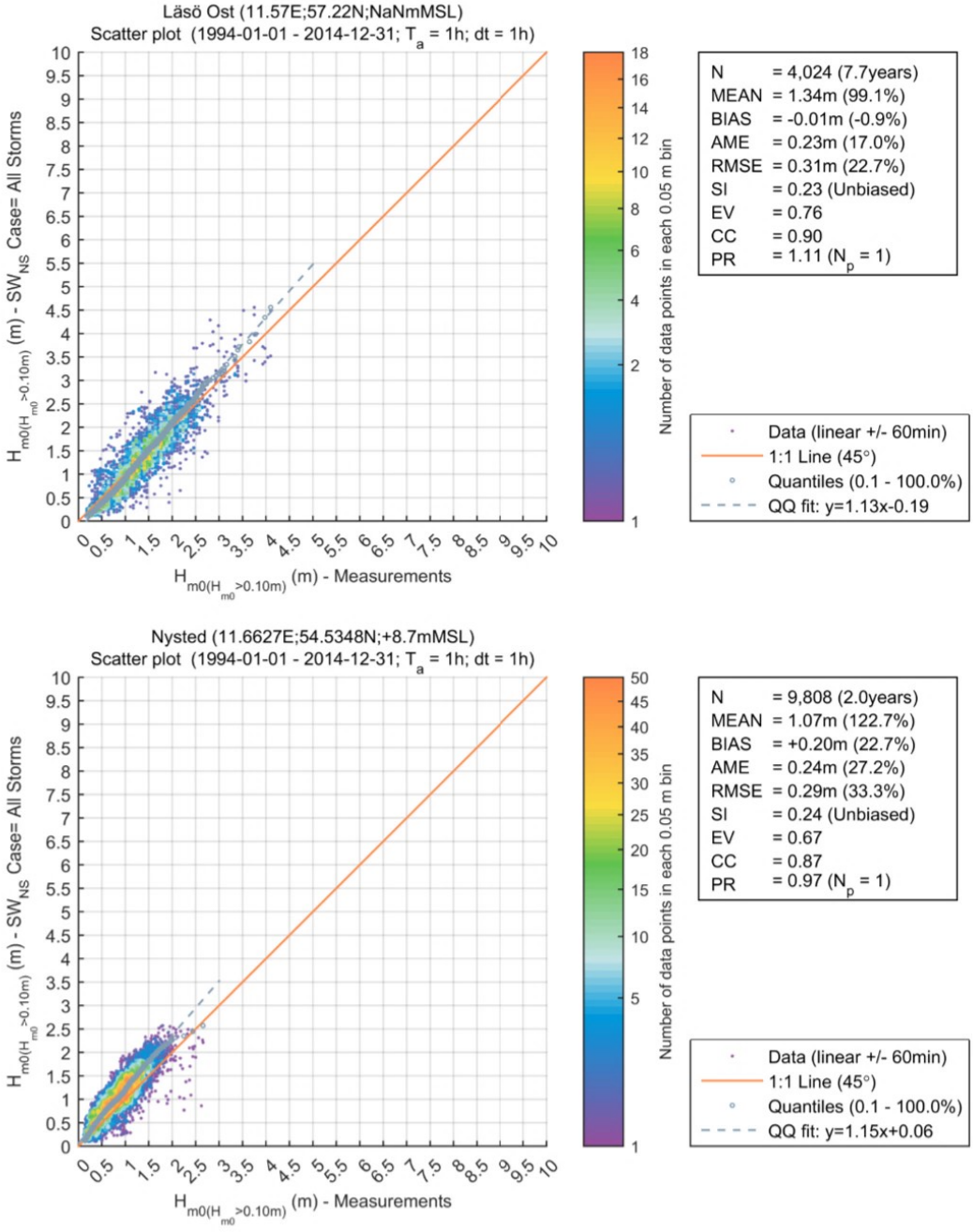

Figure 48: Validation of all storms from WRF-MIKE. Scatter plot of the MIKE 21 SW modelled significant wave height with forcing from the local WRF wind field for the all storms between 1994 and 2014 at Läsö Ost (upper panel) and Nysted (lower panel).

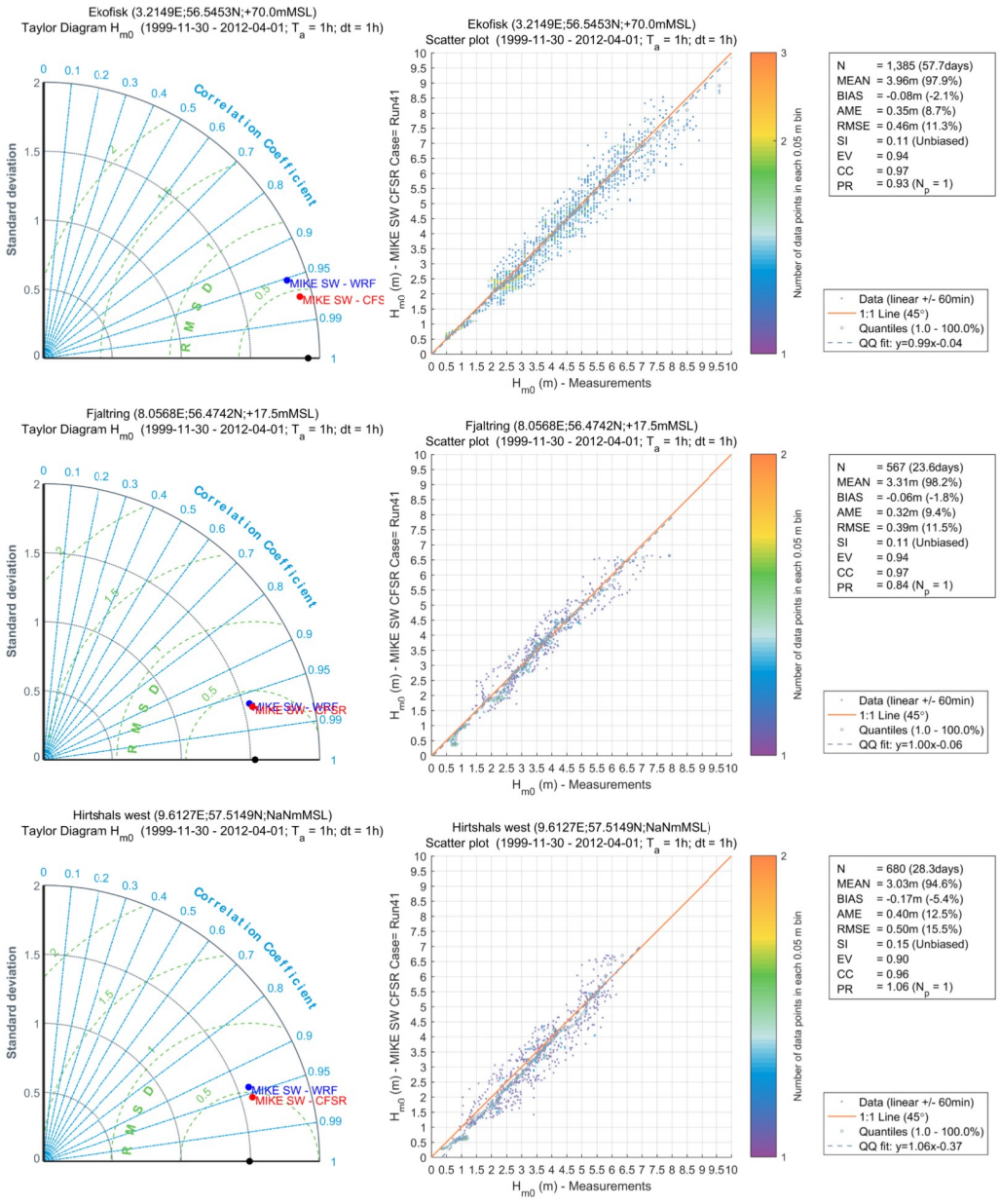

Figure 49: Comparison between WRF-MIKE and CFSR-MIKE over 15 storms. A statistical representation of significant wave height (H_{m0}) at Ekofisk (upper panels), Fjaltering (middle panels) and Hirtshals West (lower panels) for the two offline MIKE 21 SW model with WRF (blue) and CFSR (red) wind forcing through a Taylor Diagram (left panel). The black point represents the observations. Scatter plot of the modelled significant wave height with forcing from the global CFSR wind field for the 15 calibration storms between Nov-1999 and Apr-2012 (right panel, corresponding to red point in Taylor diagram).

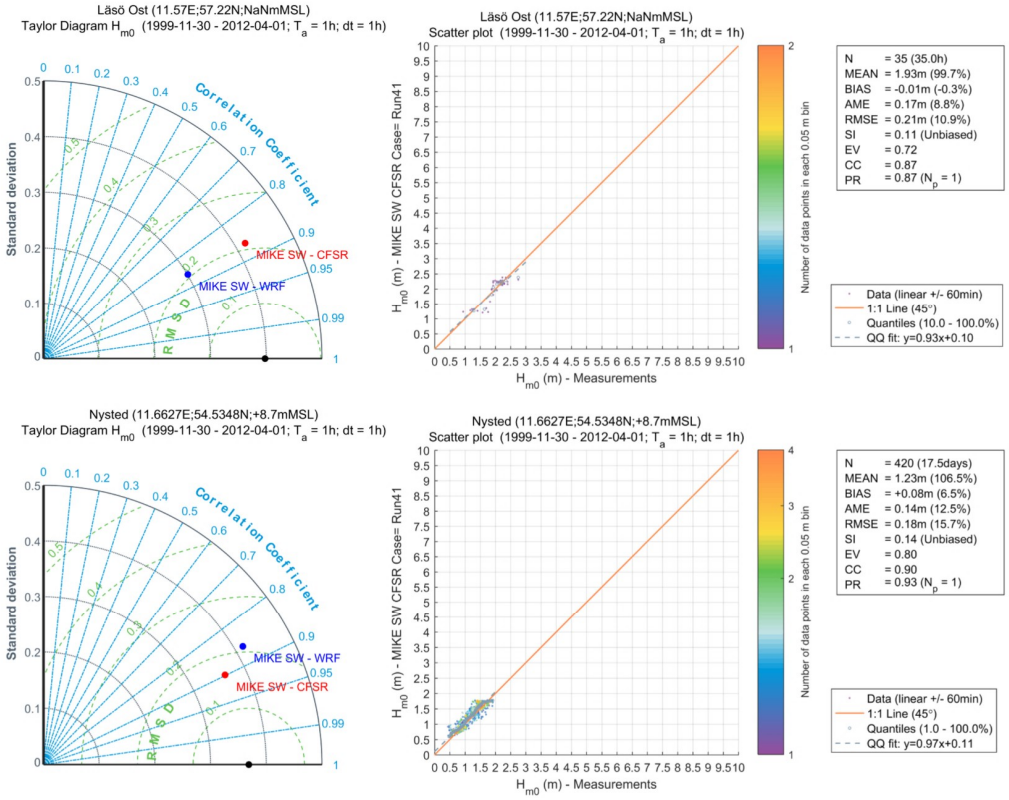

Figure 50: Comparison between WRF-MIKE and CFSR-MIKE over 15 storms. A statistical representation of significant wave height (H_{m0}) at Läsö Ost (upper panels) and Nysted (lower panels) for the two offline MIKE 21 SW model with WRF (blue) and CFSR (red) wind forcing through a Taylor Diagram (left panel). The black point represents the observations. Scatter plot (right) of the modelled significant wave height with forcing from the global CFSR wind field for the 15 calibration storms between Nov-1999 and Apr-2012 (right panel, corresponding to red point in Taylor diagram).

most data used was extracted from the inner most domain domain III, except for Ekofisk, which is outside of domain III of the COAWST modeling. Thus the data used for the comparison at Ekofisk was extracted from the coarser domain II of the COAWST model. Comparison of data at sites inside domain III with the output from domain II only give much smaller difference than the bias shown in Fig. 51a for Ekofisk.

In addtion, Taylor diagrams have been prepared for five more sites: FINO 1, FINO 3, Väderöarna, Trubaduren and Nymindegab. Detailed analysis can be found in [101]. Briefly, for the online model results, see Fig. 51 and 52, better results are seen for the shorted fetch location of the inner Danish waters, with poor agreement with the observations seen for Ekofisk. It is difficult to draw conclusions on any final ranking of the two modeling systems with data analysis from only five sites. Though, at Ekofisk and Fjaltering, results from WRF-MIKE 21 SW modeling are better than WRF-WBLM-SWAN, particularly for high H_{m0}, which are important for the estimation of the extreme values.

Figure 54 shows the comparison of WRF-WBLM-SWAN modeled and measured H_{m0} at other seven buoy stations. The corresponding scatter plot for each of the site are shown in Fig. 55. The agreement is in general good, though it is seen that the peak values of H_{m0} are underestimated, particularly at FINO 1. In Figs. 54 and 55, all available measurements for the 1080 storm days from 1994 - 2016 are used for the validation.

9.4 Extreme Conditions and Wave Atlas

An extreme value analysis (EVA) was performed on the significant wave height (H_{m0}) from the X-WiWa storm database at all elements in the MIKE 21 SW model domain. The methodology for analysis of extreme conditions is described below. Estimates of extremes values were based on the methodology outlined in section 7.2 and in [**?**], in short, as:

- Extraction of independent identically-distributed events by requiring that events were separated by at least 36 hours, and that the value between events had dropped to below 70% of the minor of two consecutive events.
- Fitting of extreme value distribution to the extracted events. Distribution parameters were estimated by the maximum likelihood method. For this study the following approaches were tested:

  a. Fitting different distributions depending on the water depth; These included truncated Weibull, 2-parameter Weibull and Gumbel distributions

  b. Fitting a singular Gumbel distribution for all water depths to annual maximum peaks (AMP) and annual maximum peaks squared
- Estimating the uncertainty due to sampling error

Due to the nature of waves in shallow waters a truncation in extreme H_{m0} is expected. In order to identify which distributions were on average suited to different water depths, several analysis locations around the Danish waters were selected. All locations had varying depths and fetch distances. Further details on the analysis points can be found in Fig. 56 and Table 12 and appendix in [101].

Following a sensitivity test of a sample of locations in Table 12, it was possible to identify that the optimum EVA distribution was not the same for all water

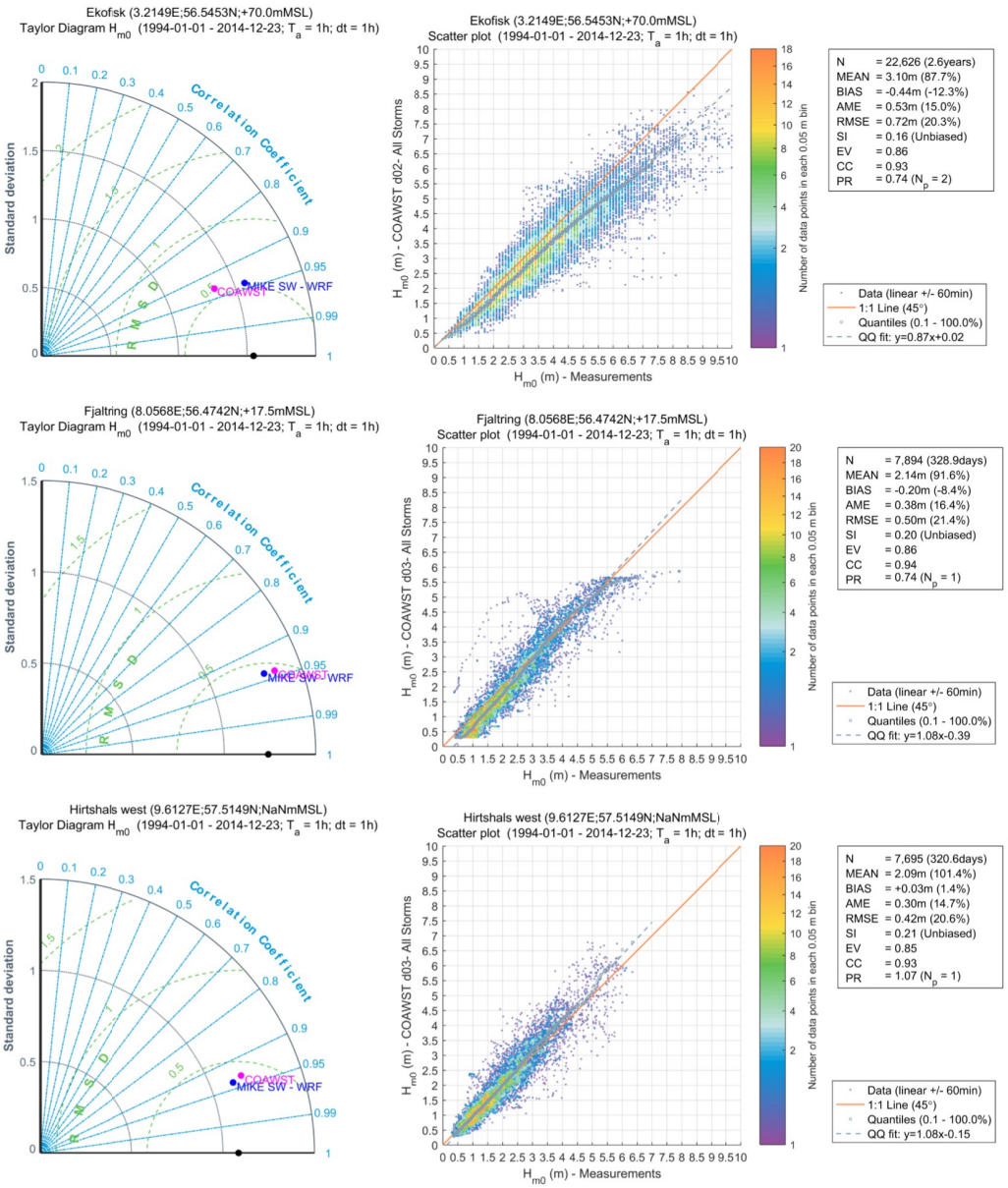

Figure 51: Comparison of WRF-MIKE and WRF-WBLM-SWAN for all storms. Left: A statistical representation of significant wave height (H_{m0}) at Ekofisk (upper panels), Fjaltring (middle panels) and Hirtshals West (lower panels) for the offline MIKE 21 SW model with WRF (blue) and wind forcing and the online WRF-WBLM-SWAN model (pink) through a Taylor Diagram. Right: The black point represents the observations. Scatter plot of the COAWST modelled significant wave height for storms between 1994 and 2014 (corresponding to pink point in Taylor diagram).

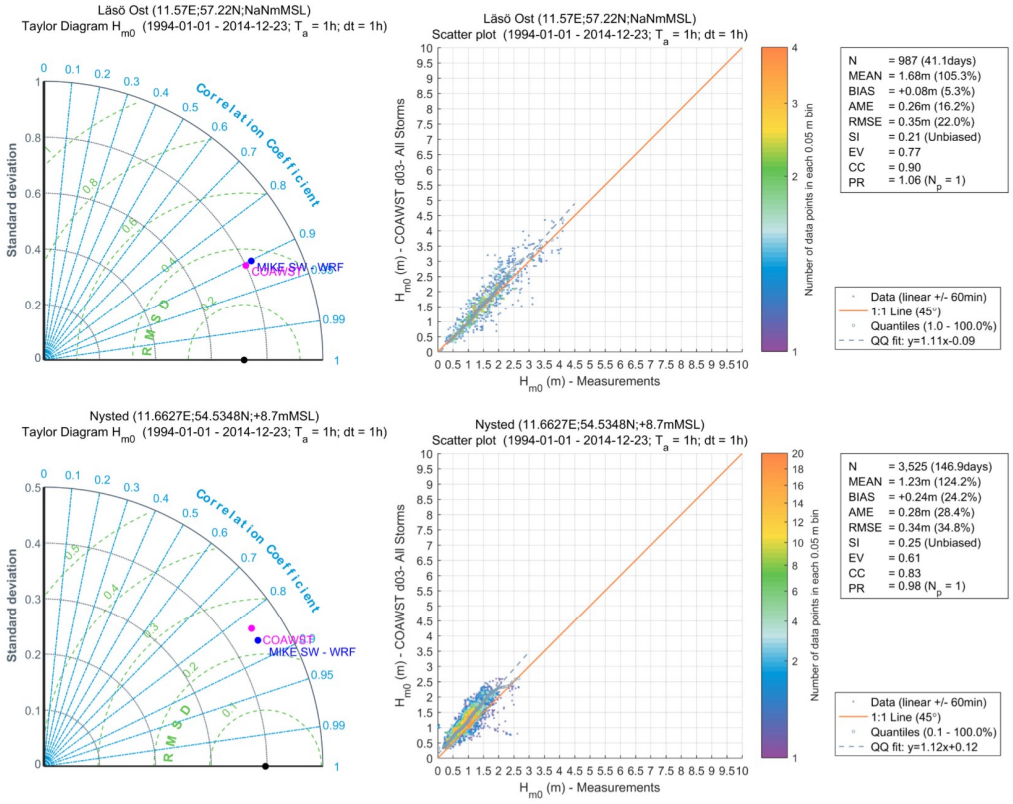

Figure 52: Comparison of WRF-MIKE and WRF-WBLM-SWAN for all storms. Left: A statistical representation of significant wave height (H_{m0}) at Läsö Ost (upper panels) and Nysted (lower panels) for the offline MIKE 21 SW model with WRF (blue) and wind forcing and the online COAWST model (pink) through a Taylor Diagram. Right: The black point represents the observations. Scatter plot of the WRF-WBLM-SWAN modelled significant wave height for storms between 1994 and 2014 (corresponding to pink point in Taylor diagram).

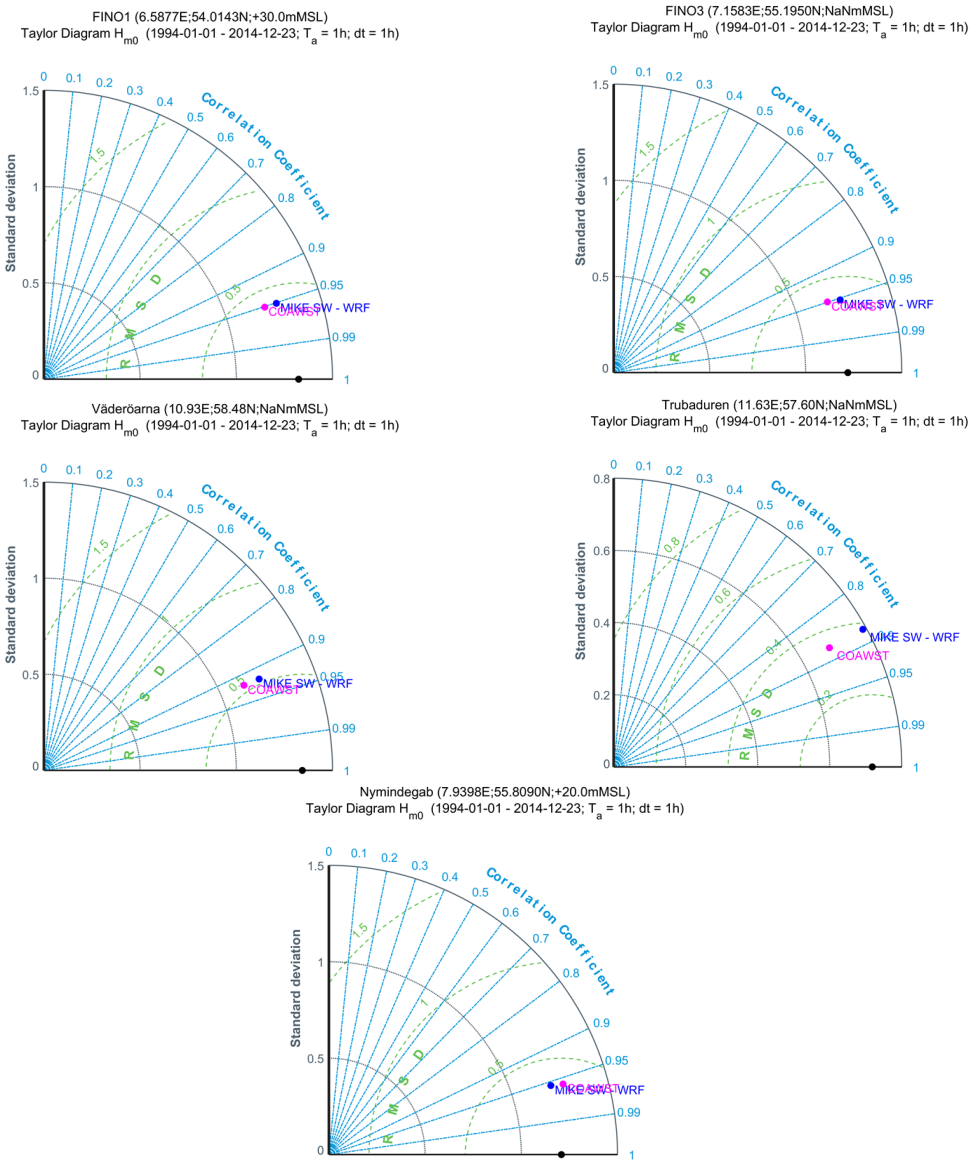

Figure 53: Comparison of WRF-MIKE (denoted as MIKE SW-WRF on the plots) and WRF-WBLM-SWAN (denoted as COAWST on the plots) for all storms through a Taylor Diagram for FINO 1, FINO 3, Väderöarna, Trybaduren and Nymindegab.

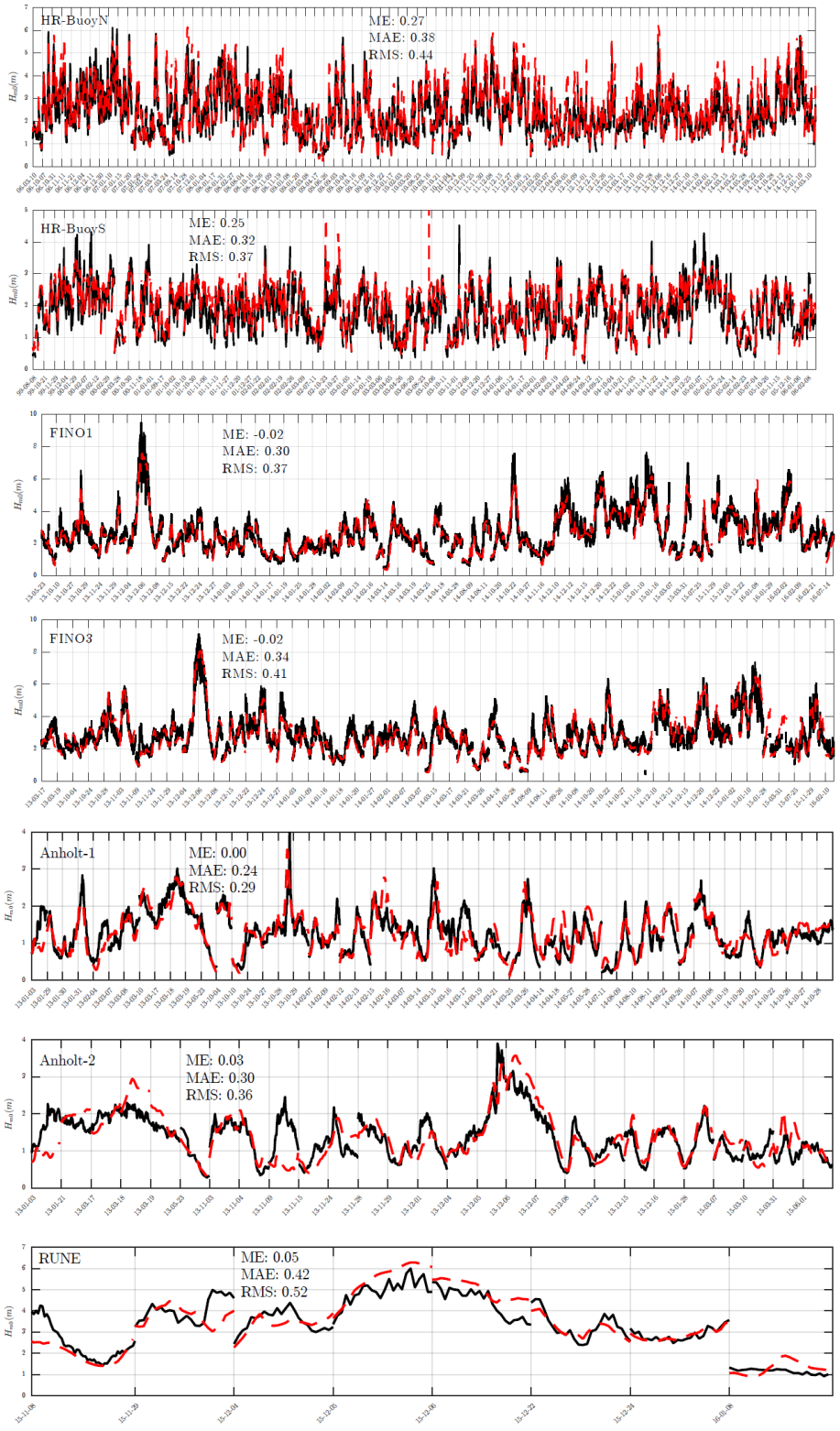

Figure 54: Validation of all storms from WRF-WBLM-SWAN. Time series of the significant wave height H_{m0} at, from above down, Horns Rev buoy North, Horns Rev buoy South, FINO 1, FINO 3, Anholt 2, Anholt 1 and RUNE. Measurements vs modeled data from WRF-WBLM-SWAN. The mean error (ME), mean absolute error (MAE) and toot-mean-square error (RMS) between measurements and modeled data for each station are printed on the plots.

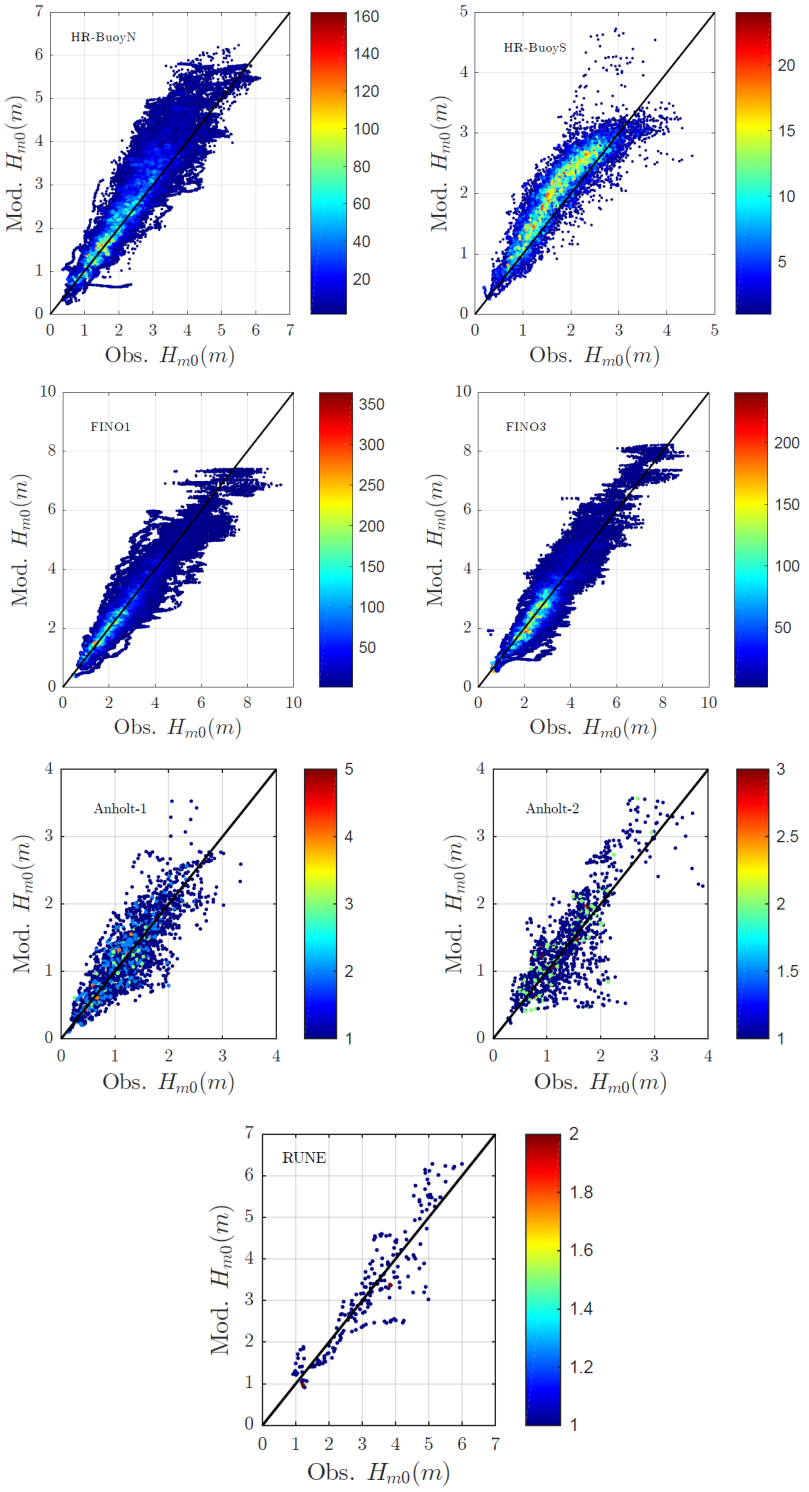

Figure 55: Density scatter plot of the WRF-WBLM-SWAN data from Fig. 54 for each site.

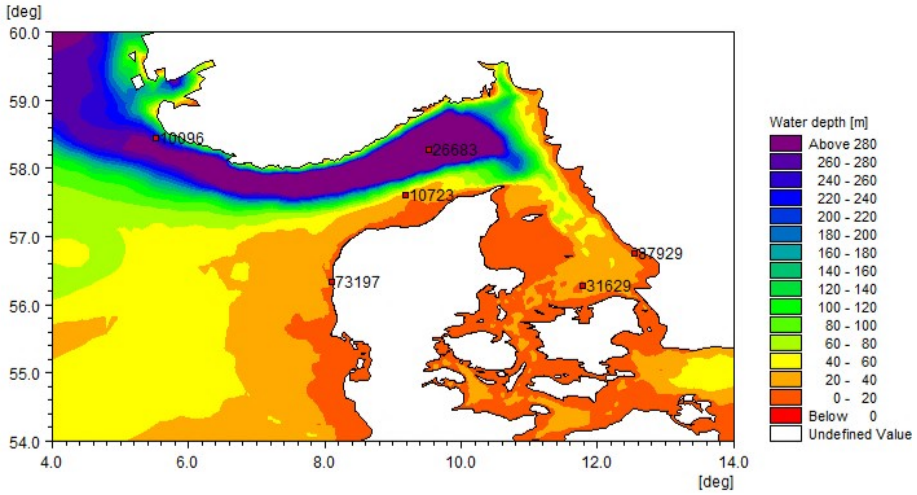

Figure 56: Sample locations around the Danish waters used to assess the extreme analysis. The numbered point represents the grid element number within MIKE 21 SW for the corresponding location

depths. The distribution which fit the extreme significant wave height data for the sample locations was identified for the different water depths. Using this information, different water depth categories were assigned the distribution which fit best to the sample data in that category. Thus, different distributions were applied to each element depending on its water depth. A summary of the EVA is presented in Table 13.

A comparison between using the same distribution across all water depths against using different distributions for varying water depths are shown in Fig. 57, 58 and 59. In the left hand columns the varying distributions depending on water depths are shown, and in the right hand columns are the comparative constant distribution for all water depths at the analysis points described above.

In general, it can be seen that using the Gumbel distribution for all water depths was not best suited. It can be seen that the shallower water depths benefit from a distribution with a truncation, as it tends to fit the extreme events tail better. In the deep water, a similar result for both extreme value methods can be seen, since the two methods have very similar distributions properties at deep water depths. Table 14 summarizes the 50-year return period $H_{m0,50yr}$ for both methods at the 6 locations (Table 12). The use of three AAP events per year in the depth dependent method could be considered to underestimate values, since the method used to compile the storm database was obtained by only identifying the annual maximum event of each element (see section 7.2 for more details). However, a better fit was produced when AAP was taken to be three. Additionally, when analysing the results from both methods, an underestimation from the depth dependent method was not evident at all locations.

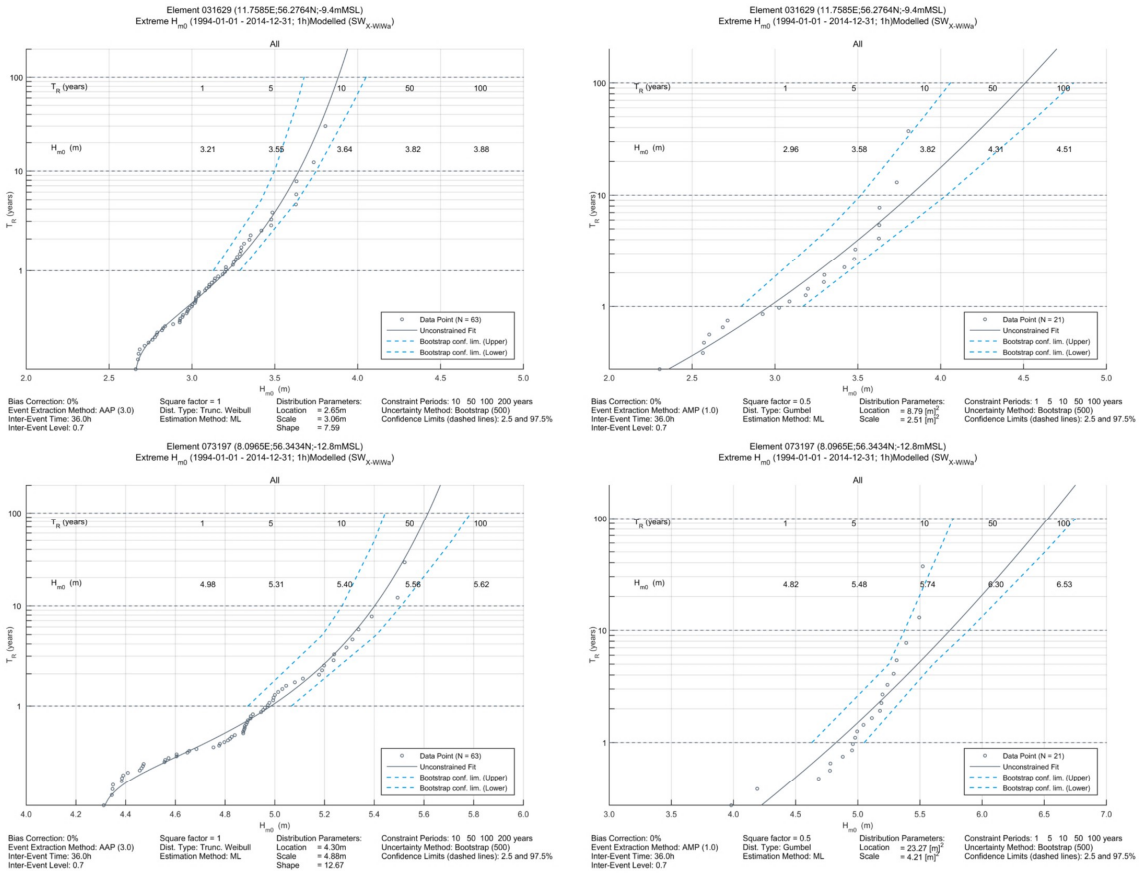

Figure 57: Extreme value distribution profile fit to the data of shallower water locations (water depth <15m). Varying distributions with water depth can be seen of the left hand side. In this case the distribution fit to the data was the Truncated Weibull. On the right hand side is the constant distribution with water depth (squared Gumbel).

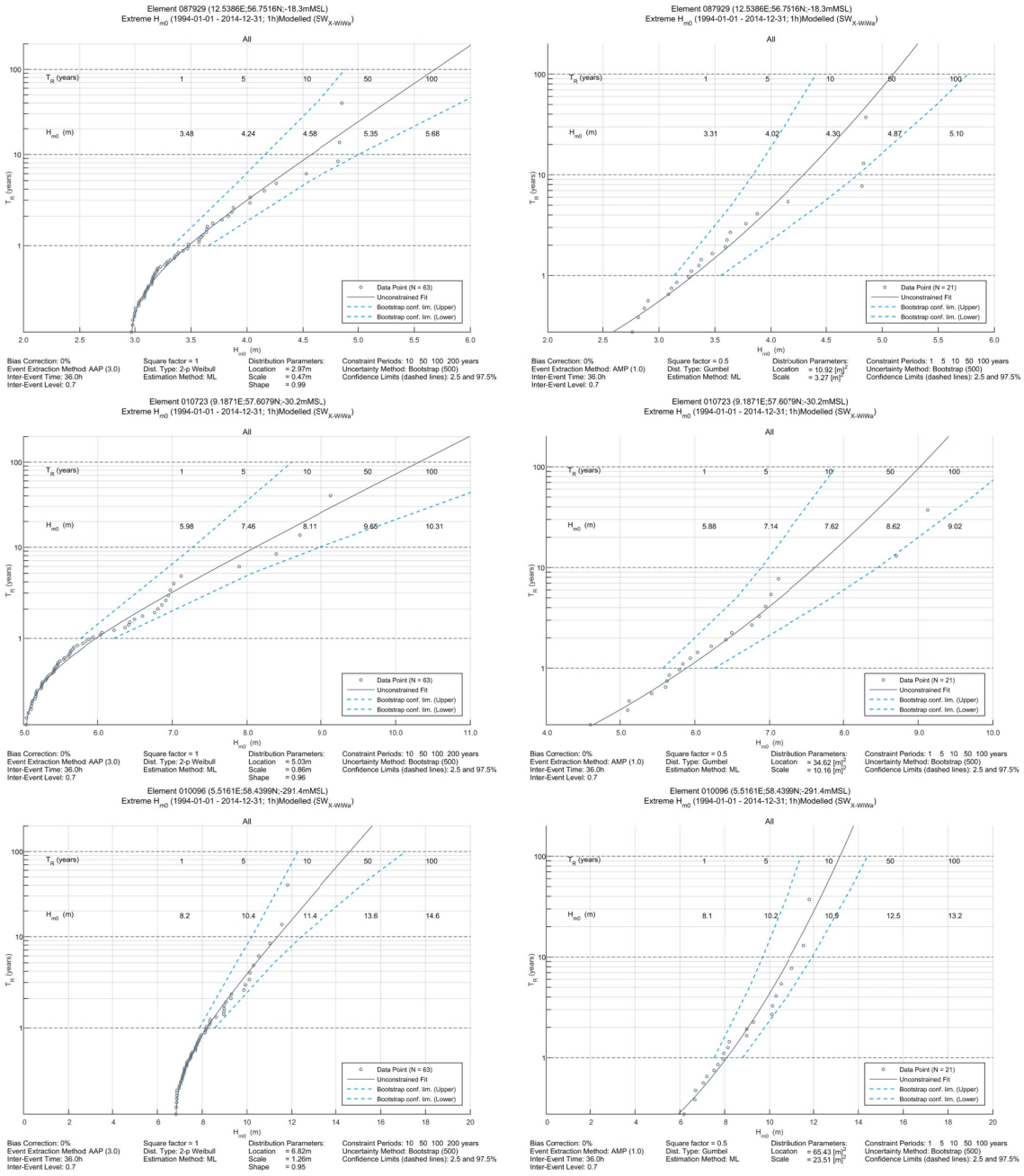

Figure 58: Extreme value distribution profile fit to the data of intermediate water locations (water depth 15<x<300m). Varying distributions with water depth can be seen of the left hand side. In this case the distribution fit to the data was the 2-parameter Weibull. On the right hand side is the constant distribution with water depth (squared Gumbel)

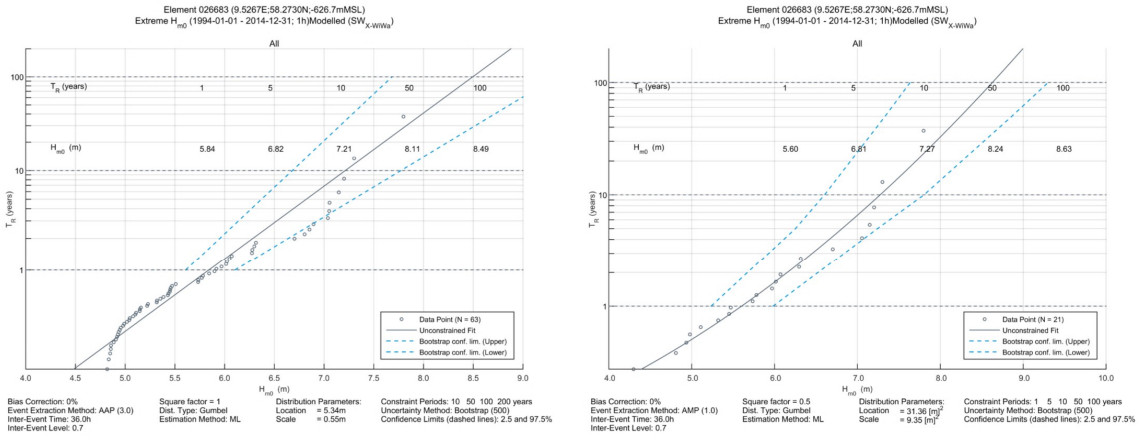

Figure 59: Extreme value distribution profile fit to the data of deep water locations (water depth >300m). Varying distributions with water depth can be seen of the left hand side. In this case the distribution fit to the data was the Gumbel. On the right hand side is the constant distribution with water depth (squared Gumbel).

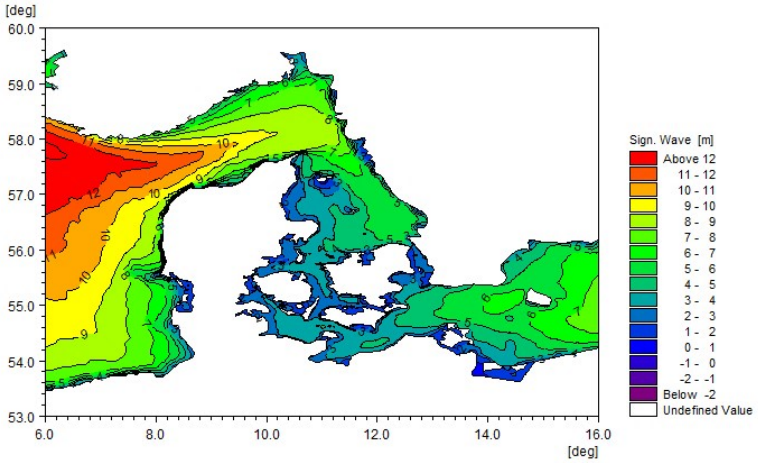

Figure 60: Wave atlas of the 50yr return period for significant wave height using varying distributions with water depths.

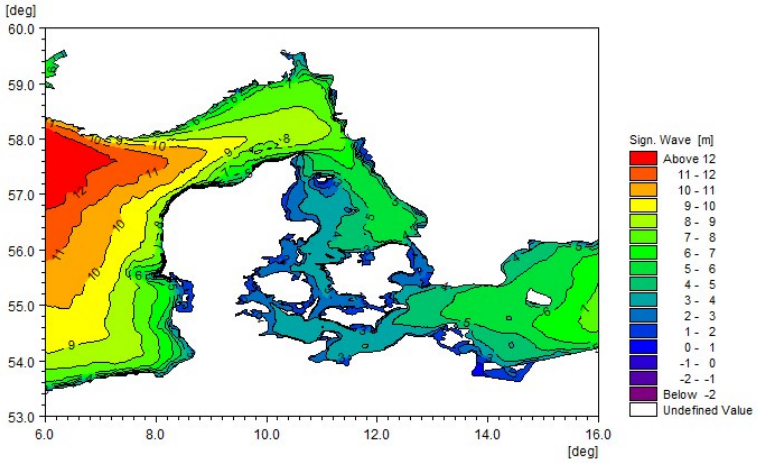

Figure 61: Wave atlas of the 50yr return period for significant wave height using the same distributions for all water depths.

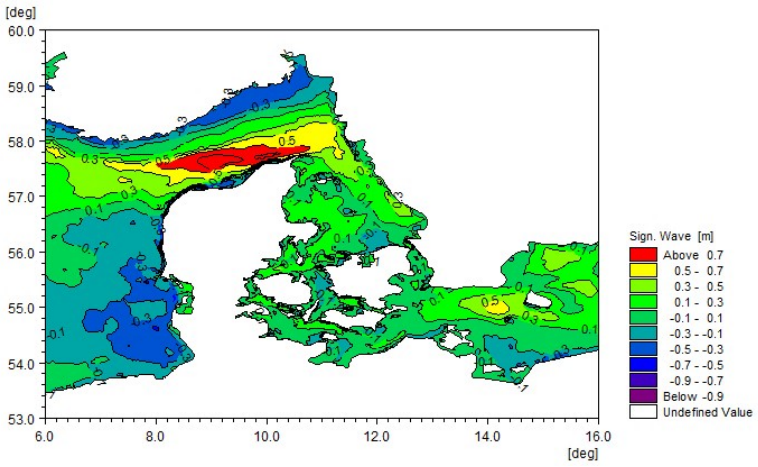

Figure 62: Difference map of the 50yr return period significant wave height for the varying distribution method minus the constant distribution method.

It is important to note that although the use of different distributions depending on water depth provide a better estimate, it still does not guarantee a good performance at all locations. For a more accurate EVA in a specific point in the domain, a detailed EVA should be done, assessing the best distribution of the interested location.

A wave atlas containing the significant wave height 50-year return period for the waters surrounding the Danish coastlines was compiled for both methods. The results for the depth dependent method can be seen in Fig. 60, and the results for the singular Gumbel distribution method can be seen in Fig. 61. The difference between the two methods was calculated and presented in Fig. 62. From this difference map, it can be concluded that the depth dependent method results in a more conservative $H_{m0,50yr}$ in the Skagerrak region (north of Denmark) while giving a less conservative approach along the southern Norwegian coastline of Skagerrak, as well as in the North Sea to the southwest of the West Denmark coastline. Additionally, an increase in $H_{m0,50yr}$ can be seen from the depth dependent method to the west of Bornholm in the southern Baltic Sea. In the inner Danish waters of Kattegat, little difference between the two methods can be seen in the 50-year return period, $H_{m0,50yr}$.

Table 12: Details on the sample locations around the Danish waters used to assess the extreme analysis.

Element number	Longitude °E	Latitude °N	Water depth (m)	location
31629	11.79	56.28	9.4	Kattegat, Inner Danish Waters
73197	8.10	56.34	12.8	North Sea, West coast of Denmark
87929	12.54	56.75	18.3	Kattegat, Swedish Coastline
10723	9.19	57.61	30.2	Skagerrak, North Denmark
10096	5.52	58.44	291.444	North Sea, Southwest Norway
26683	9.53	58.27	626.675	Skagerrak Deep Shelf

Table 13: Summary of the EVA method used based on water depth.

Water depth (m)	Distribution	Peak events	Number of peak events
$d < 15$	Truncated Weibull	AAP	3
$15 \leq d < 300$	2-parameter Weibull	AAP	3
$d \geq 300$	Gumbel	AAP	3

Table 14: Summary of $H_{m0,50yr}$ (m) at 6 locations shown in Table 12.

Element number	Distribution dependent on water depth	Gumbel
31629	3.8	4.3
73197	5.6	6.3
87929	5.4	4.8
10723	9.6	8.6
10096	13.6	12.5
26683	8.1	8.2

10 Summary

With the background of the social relevance, scientific and technological challenges and the project impact have been introduced in section 1 "Preface" and section 3 "Background and Objectives", here we summarize the main findings from the project, including main achievements and remaining tasks and challenges, which are used to define our future efforts. We first address the "wind" part and then the "wave" part.

For the modeling of offshore wind, first of all, through the availability of some measurements as well as the successful numerical tool of coupling the atmospheric model and wave model, we show that the many parametrization schemes provide similar values for the roughness length for light to moderate winds, which explains the insignificant coupling effect on the wind modeling in many studies; however, these parametrization schemes provide diverse estimates of the roughness length, more diverse at stronger winds, leading to inconsistent calculation of winds from coupling when the winds are strong as well as the wave state becomes complicated, such as in the coastal zones. The diverse values of roughness lengths provided by different schemes result in uncertainties in the calculation of strong winds. This part of the study clarifies the role of the parametrization and the role of coupling.

For the modeling of offshore wind, secondly, a wave boundary layer model (WBLM) was developed and implemented in the wave model SWAN. WBLM calculates stress and kinetic energy budgets in the lowest atmospheric layer where the wave-induced stress is introduced to the atmospheric modeling. WBLM ensures consistent calculation of stress for both the atmospheric and wave modeling, which is considered as a major improvement compared with previous attempts in the literature. Through case studies, the coupled modeling system WRF-WBLM-SWAN has shown its ability in describing the drag relations with wave effect considered, showing better agreement with measurements in comparison with the many parametrization schemes for coastal and strong wind conditions.

23 years of storms that are defined to having contributed to the extreme wind

climate around Denmark have been modeled using the coupled modeling system WRF-WBLM-SWAN as well as a not-coupled WRF model. An improvement of 10% or more is present by using WRF-WBLM-SWAN at strong winds, which can affect the choice of the offshore wind turbine type.

For the modeling of waves, X-WiWa examined various methodologies. The offline coupling system using atmospheric data such as WRF or global reanalysis wind field to the MIKE 21 SW model has been improved with considerations of stability, air density, currents and new wind drag relations. X-WiWa suggests that, implementation of an online coupling technology does not necessarily provide better estimation of the waves, if the physics have not been properly described. This is supported by the comparisons of the modeled wave data between offline MIKE 21 SW modeling and the WRF-WBLM-SWAN modeling. The two provide comparably good wave calculations for coastal areas but the latter underestimates the wave height for far offshore areas, which is speculated to be related to the dissipation description in the wave source functions, where further improvement is seen necessary.

21 years of storms that are defined to having contributed to the extreme wave climate around Denmark have been modeled using the offline coupling system WRF-MIKE 21 SW and online coupling system WRF-WBLM-SWAN. The 50-year significant wave height for the Danish waters and surrounding North Sea and Baltic Sea are presented.

We see the following need to be considered for the future efforts:

- Further data analysis and validation of the output with many more measurements.
- Further investigation of the effect of heat exchange in the modeling system.
- Examination the model systems' applicability for other areas such as the tropical cyclone affected areas.
- Improvement of the source function in WBLM-SWAN for storm conditions.
- Make linkage of the modeling systems to other offshore calculation functions.

11 List of project deliverables

The project has delivered all planned deliverables in time. Though some of the planed deliverables have been merged into one due to the overlapping content and relevance between them. All deliverables have been presented to energinet.dk in Interim report format. The following is an overview of them with the references (www.xwiwa.dk/publications/projectreports/) in case people want to find the documents.

- D1.1: The offline coupling system and the online coupling system (Interim report I [14])
- D1.2: Implementation of wave stress in the atmospheric model WRF (Interim report V)
- D1.3: MIKE 3 coupling added value (Interim report VI)
- D1.4+D1.9: Database of simulated storms. (on the website, see www.xwiwa.dk/data)
- D1.5: Atlas of the 50-year return wind at hub height for the Danish coastal zone. (on the website, see www.xwiwa.dk/data)
- D1.6: Journal paper about the improved atmospheric modeling of storm cases (see section 12)
- D1.7: Journal paper about the sensitivity of the modeling on the resolution (Interim report VII, part of other publications)
- D1.8+D1.10+D1.12: Report describing the tests performed and the model efficiency and sensitivities (Interim report VI)
- D1.11+D1.12: Report on the strategy and efficiency of the methodology (Interim report V)
- D1.13+D1.14: Journal papers (see section 12)
- D1.15: Implementation od MIKE 3 (Interim report IV)
- D1.16: Sensitivity of the heat transfer during extreme events - Sea surface temperature experiments (Interim report IV)
- M1.4: Subroutines in MIKE SW to estimate the parameters to be transferred to the atmosphere model (Interim report II)
- M1.5: Implementation of a coupler (Interim report V)
- M1.7: Subroutines for the estimation of the sea spray heat fluxes and 2D fields of sea spray heat fluxes effect on the roughness (Interim report IV and VI (updated))
- D2.1: Report of X-WiWa Database (Interim report II)
- D1.6+D1.7+D3.1+D3.2: Validation of storm modeling (Interim report VII)
- D3.3: Reports on validation results of the improved extreme wind and description of strong wind statistics (This final report, section 8).
- D3.4: Reports on validation of wave modeling (This final report, section 9).
- D3.5: Final report (This final report)

[14] Only the technical reports in the original Interim report are provided. The description of the work progress and financial budget as in the original report can be found with energinet.dk

- M4.1: Mid-term assessment of the X-WiWa project (Interim report IV)
- D4.1: Periodic management reports (Interim reports)
- D4.2: Dissemination plan (Interim reports, see also this report)
- D4.3: Final management report (see this report)

There are a few other technical notes that can be found in the Interim report:
Du J.: An overview of the model couplers for X-WiWa (Interim report II)
Du. J., Larsén X. G. and Bolaños R.S.: Nested offline coupling experiments (Interim report II)
Bolaños R.: Small fetch and extreme winds wave growth in MIKE 21 SW (Interim report III) Imberger M. and Du J.: Impact of Sea Surface Roughness Parametrization on North Sea Storm Simulation (Interim report VI)

12 Publications

The publication includes journal articles (published and manuscripts), conference papers and presentations, Ph.D and master theses, database and model codes. The titles of the articles and theses are listed here. Information about the data and model codes are provided on the web *www.xwiwa.dk/data* and *http : //www.xwiwa.dk/publications/the − modeling − system*.

Published journal articles:

- Du J., Bolaños R. and Larsén X. (2017): The use of a wave boundary layer model in SWAN, Journal of Geophysical Research − Ocean, DOI:10.1002/2016JC012104. Vol. 122, No. 1, p. 42-62.
- Larsén X., Du J., Bolaños R. and Larsen S (2017): On the impact of wind on the development of wave field during storm Britta. Ocean Dynamics, 67:1407 - 1427, DOI:10.1007/s10236-017-1100-1.
- Mehrens A., Hahmann A., Larsén X., von Bremen L. (2016): Correlation and coherence of mesoscale wind speeds over the sea. Quarterly Journal of the Royal Meteorological Society, Vol 142, issue 701, 3186 − 3194.
- Ren D., Du J., Hua F., Yang Y. and Han L. (2016): Analysis of different atmospheric physical parameterizations in COAWST modeling system for the Tropical Storm Nock-ten application. Natural Hazards, vol 82, no. 2, pp. 903-920. DOI: 10.1007/s11069-016-2225-0
- Larsén X., C. Kalogeri, G. Galanis and G. Kalos, (2015): A statistical methodology for the estimation of extreme wave conditions for offshore renewable application. Renewable Energy, 80, 205 - 218.

Manuscripts of journal articles:

- Du J., Larsén X.G., Bolaños R., Kelly M. and Larsen S. (2017): A revised dissipation source function for the wave boundary layer model and its impact on wave simulations. Manuscript to be submitted to Ocean Science.
- Du. J., Larsén X.G., Bolaños R., Kelly M., Badger M. and Larsen S. (2017): The impact of wind-wave coupling on the coastal wind and wave simulations during storms. Manuscript to be submitted to Tellus A.
- Larsén et al. (2017): The impact of wind-wave coupled modeling on the estimation of offshore extreme wind. Manuscript in preparation, to be submitted to Journal of Applied Meteorology.

Ph.D. thesis and Master thesis:

- Du J. 2017: Coupling atmospheric and ocean wave models for storm simulation, Ph.D. thesis, Technical University of Denmark (DTU), Kgs. Lyngby. DTU Wind Energy PhD, DOI: 10.11581/DTU:00000020
- Imberger M. 2017: Modeling rough weather over the North Sea using COAWST for offshore wind energy application. DTU Wind Energy-M-0149, Master thesis.

Conference papers:

- Bolaños, R., Larsen, X.G., Petersen, O.S., Nielsen, J.R., Kelly, M., Kofoed-Hansen, H., Du, J., Søren-sen, O.R., Larsen, S.E., Hahmann, A., Badger, M., (2014). Coupling atmosphere and waves for coastal wind turbine

design, in: Lynett, P.J. (Ed.), 34th International Conference On Coastal Engineering. Coastal Engineering Research Council, Seoul, Korea, p. 11.

- Larsén X.G. and Kruger A. (2014): Extreme gust wind estimation using mesoscale modeling, in proceedings, EWEA 2014, paper and PPT.
- Du J., Larsén X.G. and Bolaños R. (2015) A coupled atmospheric and wave modeling system for storm simulations. Abstract and poster at EWEA Offshore conference March 2015, Copenhagen
- Karagali I., Høyer J., Du J. and Larsén X (2015): Implications of diurnal warming events on atmos-pheric modelling. In proceedings of the 16th Science Team Meeting, ESA/ESTEC.
- Larsén X.G., Du J. and Bolaños R. (2015) Wind structure during mid-latitude storms and its appli-cation in Wind Energy, conference abstract in proceedings, The 4th Hydrology-Atmosphere-Ocean conference, 19 − 21 July, 2015, Shanghai, China.
- Kelly M. and Volker P. (2016): WRF idealized-roughness response: PBL scheme and resolution dependence. EMS Annual Meeting Abstracts, Vol 13, EMS2016-389, 2016, 16th EMS/11th ECAC.
- Du J., Larsén X. and Bolaños R. (2016): Roughness length for coastal waters from wave boundary layer model. EMS Annual Meeting Abstracts, Vol 13, EMS2016-28, 2016, 16th EMS/11th ECAC.
- Larsén X. and Du J. (2016): Storm Britta. In Scientific Proceedings of WindEurope 2016, Hamburg, 27 − 29 Sep. 2016
- Larsén X., Du J., Badger M., Bolaños R., Kelly M. and Larsen S. (2017): Impact of the interfaces for wind and wave modeling interpretation using COAWST, SAR and point measurements. Oral presentation at European Geo. Union, Vienna, Austria, 2017.
- Larsén X., Bolaños R., Du J., Kelly M., Badger J., Badger M., Hahmann A., Karagali I., Kofoed-Hansen H., Petersen O., Sørensen J., Imberger M., Volker P. and Larsen S. (2017): Coastal extreme winds and waves from COAWST-WBLM modeling system. Presentation at Offshore Wind Energy − WindEurope, June 2017, London, UK.
- Rodolfo Bolaños, Palle Jensen, Henrik Kofoed-Hansen, Jacob Tornfeldt Sørensen (2017): Bottom friction. A practical approach to modelling coastal oceanography, Poster presentation at European Geo. Union, Vienna, Austria, 2017
- Bolaños, R., J. V. Tornfeld Sorensen, N. A. Beg, O. S. Petersen, M. Rugbjerg and H. R. Jensen (2013). Oceanographic downscaling with unstructured modelling: Towards ocean-wave-atmosphere coupling. The Future of Operational Oceanography (Futoore), Hamburg

Acknowledgement X-WiWa has received tremendous support from many finished as well as ongoing projects, including INNWIND, IRPWIND, RUNE, CEASELESS and MARINA. We also acknowledge the support from DONG Energy, Vattenfall and SMHI for the measurements from Horns Rev and Anholt. CFSR data are obtained from *http : //rda.ucar.edu/datasets*. We acknowledge DONG Energy and Vattenfall as end-users of this project. We acknowledge eKlima for the measurements in the North Sea (Ekofisk and Sleipner). Fachhochschule Kiel University of Applied Sciences GmbH is acknowledge for the data from the FINO platforms in the North Sea. We thank Kystdirektoratet for providing measurements around Denmark (Fjaltring, Nymindegab, Hirtshals West). We thank DONG for Nysted data and SMHI for Läsö Ost, Trubaduren and Väderöarna measurements.

References

[1] X. G. Larsén, S. Ott, J. Badger, A. H. Hahmann, and J. Mann. Recipes for correcting the impact of effective mesoscale resolution on the estimation of extreme winds. *J. Appl. Meteorol. Climat.*, 51(3):521–533, 2012.

[2] B. O. Hansen, X. G. Larsén, M. Kelly, O. S. Rathmann, J. Berg, A. Bechmann, A. M. Sempreviva, and H. E. Jørgensen. Extreme wind calculation applying spectral correction method - test and validation. Technical report, Wind Enery Department, Technical University of Denmark, DTU Wind Energy E-0098, 2016.

[3] X. G. Larsén, J. Badger, A. N. Hahmann, and N. G. Mortensen. The selective dynamical downscaling method for extreme-wind atlases. *Wind Energy*, 16:1167–1182, 2013.

[4] X.G. Larsén and Badger J. Final Report for Project PSO-10240: Calculation of extreme wind atlases using mesoscale modeling. Technical Report Wind Energy Report-E-0125, Wind Energy Department, DTU, Roskilde, Denmark, 2012.

[5] O. J. Aarnes, O. Breivik, and M. Reistad. Wave extremes in the northeast atlantic. *Journal of Climate*, pages 1529–1543, 2012.

[6] B. Cañellas, A. Orfila, F.J. Méndez, L. Gómez-Pujol M. Menéndez, and J. Tintoré. Application of a POT model to estimate the extreme significant wave height levels around the balearic sea (western mediterranean). *Journal of Coastal Research*, (SI 50):329–333, 2007.

[7] S. Caires and A. Sterl. 100-year return value estimates for ocean wind speed and significant wave height from the ERA-40 data. *Journal of Climate*, 18:1032–1048, 2005.

[8] W. Cieslikiewicz and B. Paplinska-Swerpel. A 44-year hindcast of wind wave fields over the Baltic Sea. *Coastal Engineering*, 55:894–905, 2008.

[9] P. Pilar, C. G. Soares, and J.C. Carretero. 44-year wave hindcast for the North East Atlantic European coast. *Coastal Engineering*, 55:861–871, 2008.

[10] A.W. Ratsimandresy, M.G. Sotillo, J.C. Carretero Albiach, E. Álvarez Fanjul, and H. Hajji. A 44-year high-resolution ocean and atmospheric hindcast for the Mediterranean Basin developed within the HIPOCAS Project. *Coastal Engineering*, 55:827–842, 2008.

[11] A. Sterl and S. Caires. Climatology, variability and extrema of ocean waves: the web-based KNMI/ERA-40 wave atlas. *International journal of climatology*, 25:963–977, 2005.

[12] X. G. Larsén, C. Kalogeri, G. Galanis, and G. Kallos. A statistical methodology for the estimation of extreme wave conditions for offshore renewable applications. *Renewable Energy*, 80:205–218, 2015.

[13] W. Wimmer, P. Challenor, and C. Retzler. Extreme wave heights in the North Atlantic from Altimeter Data. *Renewable Energy*, 31:241–248, 2006.

[14] H. Charnock. Wind stress on a water surface. *Q. J. R. Meteorol. Soc.*, 81:639–640, 1955.

[15] L. Mahrt, D. Vickers, J. Howell, J. Højstrup, J. Wilczak, J. Edson, and J. Hare. Sea surface drag coefficients in the Risø air sea experiment. *Journal of Geophysical Research*, 101:14327 – 14335, 1996.

[16] M. Zijlema, G. Ph Van Vledder, and L. H. Holthuijsen. Bottom friction and wind drag for wave models. *Coastal Engineering*, 65:19–26, 2012.

[17] W. Drennan, J. A. Zhang, J. F. French, C. McCormick, and P. G. Black. Turbulent fluxes in the hurricane boundary layer. Part II: latent heat flux. *Journal of Atmospheric Sciences*, 64:1103–1115, 2007.

[18] Y. Fan, S. Lin, I. M. Held, Z. Yu, and H. L. Tolman. Global ocean surface wave simulation using a coupled atmosphere-wave model. *Journal of Climate*, 25:6233–6252, 2012.

[19] B. Liu, H. Liu, L. Xie, C. Guan, and D. Zhao. A coupled atmosphere-wave-ocean modeling system: simulation of the intensity of an idealized tropical cyclone. *Monthly Weather Review*, 139:132–152, 2011.

[20] W.A. Oost, G. J. Komen, C. Jacobs, and C. Van Oort. New evidence for a relation between wind stress and wave age from measurements during ASGAMAGE. *Boundary-layer Meteorol.*, 102:409–438, 2002.

[21] P. Taylor and M. J. Yelland. The dependence of sea surface roughness on the height and steepness of the waves. *Journal of Physical Oceanography*, 31:572–590, 2001.

[22] Andreas E.L., Mahrt L., and Vickers D. An improved bulk air-sea surface flux algorithm, including spray-mediated transfer. *Q.J.R. Meteorol. Soc.*, 141:642–654, 2015.

[23] L. Mahrt, E.L. Andreas, J. B. Edson, D. Vickers, J. Sun, and E. G. Patton. Coastal zone surface stress with stable stratification. *Journal of Physical Oceanography*, 46:95 – 105, 2016.

[24] Marcel Zijlema and André J. van der Westhuysen. On convergence behaviour and numerical accuracy in stationary SWAN simulations of nearshore wind wave spectra. *Coastal Engineering*, 52(3):237–256, 2005.

[25] J. Du. Coupling atmospheric and ocean wave models for storm simulation. *DTU Wind Energy PhD-0074(EN)*, 2017.

[26] P.A.E.M. Janssen. Quansi-linear theory of wind generation applied to wave forecasting. *Journal of Physical Oceanography*, 21:1631–1642, 1991.

[27] P. a. E. M. Janssen, P. Lionello, and L. Zambresky. On the Interaction of Wind and Waves. *Philosophical Transactions of the Royal Society A: Mathematical, Physical and Engineering Sciences*, 329(1604):289–301, oct 1989.

[28] D. V. Chalikov and V. K. Makin. Introduction. *Vegetatio*, 97(2):97–98, 1991.

[29] V. K. Makin, V. N. Kudryavtsev, and C. Mastenbroek. Drag of the sea surface, 1995.

[30] Tetsu Hara and Stephen E Belcher. Wind forcing in the equilibrium range of wind-wave spectra. *Journal of Fluid Mechanics*, 470:223–245, oct 2002.

[31] T Hara and S E Belcher. Wind profile and drag coefficient over mature ocean surface wave spectra. *Journal of Physical Oceanography*, 34(11):2345–2358, 2004.

[32] Il J. Moon, Isaac Ginis, and Tetsu Hara. Effect of surface waves on Charnock coefficient under tropical cyclones. *Geophysical Research Letters*, 31(20):1–4, 2004.

[33] G. J. Komen, L. Cavareli, M. Donelan, K. Hasselmann, S. Hasselmann, and P. A. E. M. Janssen. *Dynamics and modelling of ocean waves.* Cambridge University Press, 1994.

[34] N. Booij, R.C. Ris, and L. H. Holthuijsen. A third-generation wave model for coastal regions: 1. model description and validation. *J. Geophys. Res. doi:10.1029/98JC02622*, 104(C4):7649, 1999.

[35] Ole R Sørensen, Henrik Kofoed-Hansen, Morten Rugbjerg, and Lars S Sørensen. A third-generation spectral wave model using an unstructured finite volume technique. *Proceedings of the 29th Intern. Conf. on Coastal Eng.*, pages 894–906, 2004.

[36] R E Jensen and V J Cardone. Performance of third generation wave models in extreme hurricanes. *9th International Workshop on Wave ...*, 54:258, 2006.

[37] Il-Ju Moon, Jae-Il Kwon, Jong-Chan Lee, Jae-Seol Shim, Sok Kuh Kang, Im Sang Oh, and Seok Jae Kwon. Effect of the surface wind stress parameterization on the storm surge modeling. *Ocean Modelling*, 29(2):115–127, 2009.

[38] Fabrice Ardhuin, Erick Rogers, Alexander V. Babanin, Jean-François Filipot, Rudy Magne, Aaron Roland, Andre van der Westhuysen, Pierre Queffeulou, Jean-Michel Lefevre, Lotfi Aouf, and Fabrice Collard. Semiempirical Dissipation Source Functions for Ocean Waves. Part I: Definition, Calibration, and Validation. *Journal of Physical Oceanography*, 40(9):1917–1941, 2010.

[39] Gang Chen and Stephen E. Belcher. Effects of Long Waves on Wind-Generated Waves. *Journal of Physical Oceanography*, 30(9):2246–2256, 2000.

[40] V. N. Kudryavtsev, V. K. Makin, and B. Chapron. Coupled sea surface-atmosphere model: 2. Spectrum of short wind waves. *Journal of Geophysical Research*, 104(C4):7625, 1999.

[41] V. K. Makin, H. Branger, W. L. Peirson, and J. P. Giovanangeli. Stress above Wind-Plus-Paddle Waves: Modeling of a Laboratory Experiment. *Journal of Physical Oceanography*, 37:2824–2837, 2007.

[42] Michael L Banner. Refined Source Terms in WAVEWATCH III with Wave Breaking and Sea Spray Forecasts. (2003):1–6, 2010.

[43] X. G. Larsén, J. Du, R. Bolaños, and S. Larsen. On the impact of wind on the development of wave field during storm Britta. *Ocean Dynamics, https://doi.org/10.1007/s10236-017-1100-1*, 67(11):1407–1427, 2017.

[44] S. F. Barstow, A. K. Magnusson, D. Peters, and H. E. Krigstad. Observations of extreme waves in the long-term measurements at ekofisk. *Rogue waves workshop, Brest, October 13-15, http://www.ifremer.fr/web-com/stw2008/rw/full/Krogstad.pdf*, 2008.

[45] E. M. Bitner-Gregersen and A. K. Magnusson. Effect of intrinsic and sampling variability on wave parameters and wave statistics. *Ocean Dynamics*, 64:1643–1655, 2014.

[46] A. J. Kettle. Review Article: Storm Britta in 2006: offshore damage and large waves in North Sea. *Nat. Hazards Earth Syst. Sci Discuss.*, 3:5493–5510, 2015.

[47] R. Floors, G. Lea, A. Peña, I. Karagali, and T. Ahsbahs. Report on rune's coastal experiment and first inter-comparisons between measurements systems. Technical Report DTU Wind Energy-E-Report-0115 (EN), Wind Energy Department, Roskilde, Denmark, *http://orbit.dtu.dk/files/127277148/final.pdf*, 2016.

[48] T. T. Ahsbahs, M. Badger, I. Karagali, and X. G. Larsén. Valiation of sentinel-1a sar coastal wind speeds against scanning lidar. *Remote Sensing*, 9:552, 2017.

[49] Rodolfo Bolaños. D3 . 3 Metocean Conditions and Wave Modelling. Technical Report November, 2016.

[50] Rodolfo Bolaños and Kim Rørbæk. D3 . 1 Metocean Buoy Deployment. Technical Report November, 2016.

[51] C. L. Vincent, X. G. Larsén, S. E. Larsen, and P. Sørensen. Cross-spectra over the sea from observations and mesoscale modelling. *Boundary-Layer Meteorol*, 146:297–318, 2013.

[52] X. G. Larsén, C. L. Vincent, and S. Larsen. Spectral structure of the mesoscale winds over the water. *Q. J. R. Meteorol. Soc.*, 139:685–700, 2013.

[53] C.B. Hasager, M. Badger, A. Peña, X.G. Larsén, and F. Bingöl. SAR-based Wind Resource Statistics in the Baltic Sea. *Remote Sens.*, 3:117–144, 2011.

[54] A. Peña, S. Gryning, and R. Floors. Lidar observations of marine boundary-layer winds and heights: a preliminary study. *Meteorol. Z.*, 24:581–589, 2015.

[55] A. Peña, R. Floors, R. Wagner, M. Courtney, S.-E. Gryning, A. Salthe, X. G. Larsén, A. N. Hahmann, and C.B. Hasager. Ten years of boundary-layer and wind-power meteorology at Høvsøre, Denmark. *Boundary-Layer Meteorol. in Revision*, 2015.

[56] X. G. Larsén, J. Du, R. Bolaños, M. Badger, S. Larsen, and M. Kelly. Impact of interfaces for wind and wave modeling - via coupled atmospheric and ocean wave models, with sar and mast measurements. In: EGU proceedings, April 2017, Vienna, Austria. 2017.

[57] H. Hersbach, A. Stoffelen, and S. de Haan. An improved c-band scatterometer ocean geographical model function: Cmod5. *J. Geophys. Res.*, 112:doi:10.1029/2006JC003743, 2007.

[58] I. Karagali, M. Badger, A. Peña, A. Hahmann, C.B. Hasager, and A.M. Sempreviva. Spatial and temporal variability of winds in the Northern European Seas. *Renewable Energy*, 57:200–210, 2013.

[59] I. Karagali, A. Peña, M. Badger, and C.B. Hasager. Wind characteristics in the North and Baltic Seas from the QuikSCAT satellite. *Wind Energy*, 17:123–140, 2014.

[60] J. Du, X. G. Larsén, and R. Bolaños. A coupled atmospheric and wave modeling system for storm simulations. *Proceedings of EWEA Offshore Conference, Copenhagen*, 2015.

[61] C.B. Hasager, A. Mouche, M. Badger, F. Bingöl, I. Karagali, T. Driesenaar, A. Stoffelen, A. Peña, and N. Longépé. Offshore wind climatology based on synergetic use of Envisat ASAR, ASCAT and QuikSCAT. *Remote Sensing of Environment*, 156:247–263, 2015.

[62] J. Du, R. Bolaños, and X. G. Larsén. The use of a wave boundray layer model in SWAN. *Journal of Geophysical Research - Ocean, in press*, 2016.

[63] Peter a. E. M. Janssen. Quasi-linear Theory of Wind-Wave Generation Applied to Wave Forecasting. *Journal of Physical Oceanography*, 21(11):1631–1642, 1991.

[64] Mikio Nakanishi and Hiroshi Niino. An improved Mellor-Yamada Level-3 model with condensation physics: Its design and verification. *Boundary-Layer Meteorology*, 112(1):1–31, 2004.

[65] Mikio Nakanishi and Hiroshi Niino. An improved Mellor-Yamada Level-3 model: Its numerical stability and application to a regional prediction of advection fog. *Boundary-Layer Meteorology*, 119(2):397–407, mar 2006.

[66] Zaviša I. Janjić. The Step-Mountain Eta Coordinate Model: Further Developments of the Convection, Viscous Sublayer, and Turbulence Closure Schemes. *Monthly Weather Review*, 122(5):927–945, may 1994.

[67] William M. Drennan. On the wave age dependence of wind stress over pure wind seas. *Journal of Geophysical Research*, 108(C3):1–13, 2003.

[68] S. Saha and Co-authors. The NCEP climate forecast system reanalysis. *American Meteorological Society, BAMS*, pages ES9–ES25, 2010.

[69] S. Saha and Co-authors. Supplement to the NCEP climate forecast system reanalysis. *American Meteorological Society, BAMS*, pages 1015–1057, 2010.

[70] Golestani M., Janssen P.M., and Kofoed-Hansen H. On the influence of atmospheric stablity on the wave climate in a warm and saline water body. Technical report, St. Jones, Newfoundland, Canada:OMAE, 2015.

[71] M. D. Powell, P. J. Vickery, and T. A. Reinhold. Reduced drag coefficient for high wind speeds in tropical cyclones. *Nature*, 422:279–283, 2003.

[72] Y.Y. Chao, J. H. Alves, and H. L. Tolman. An operational system for predicting hurricane-generated wind waves in the north atlantic ocean. *Weather Forecasting*, 20:652–671, 2005.

[73] Y.C. Chang, G.Y. Cheo, R.S. Tseng, L.R. Centurioni, and P.C. Chu. Observed near surface currents under high wind speeds. *Journal of Geophysical Research*, 117:1–6, 2012.

[74] R. Bolaños and P.H. A practical approach to modeling coastal oceanography. European Geophysical Union, Vienna. 2017.

[75] Battjes J. and JPFM. Energy loss and set-up due to breaking of random waves. Technical Report 16th Int. Conf. on Coastal Eng., p569-587, NY: ASCE, 1978.

[76] J. Bidlot, P. Jansen, and S. Abdalla. A revised formulation of ocean wave dissipation and its model impact. Technical Report ECMWF Technical Momorandum No 509, ECMWF, 2007.

[77] Imberger M. Modeling rough weather over the north sea - using coawst for offshore wind energy applications. Technical Report DTU Wind Energy-M-0149, Technical University of Denmark, 2017.

[78] M. Nakanishi and H. Niino. Development of an improved turbulence closure model for the atmospheric boundary layer. *J. Meteorol. Soc. Jpn*, 87:895–912, 2009.

[79] G. Thompson, R. M. Rasmussen, and K. Manning. Explicit forecasts of winter precipitation using an improved bulk microphysics scheme. Part-I: Description and sensitivity analysis. *Mon. Weather Rev.*, 132:519–542, 2004.

[80] M. J. Iacono, J. S. Delamere, E. J. Mlawer, M. W. Shephard, S. A. Clough, and W. D. Collins. Radiative forcing by long-lived greenhouse gases: Calculations with the AER radiative transfer models. *Journal of Geophysical Research*, 113:13013, 2008.

[81] J. S. Kain and J. M. Fritsch. Convective parameterization for mesoscale models: The Kain-Fritsch scheme. The representation of cumulus convection in numerical models, Meteor. Monogr. *Ameri. Meteor. Soc.*, 24:165–170, 1993.

[82] X. G. Larsén, J. Mann, O. Rathmann, and H. E. Jørgensen. Uncertainties of the 50-year wind from short time series using generalized extreme value distribution and generalized Pareto distribution. *Wind Energy*, 18:59–74, 2015.

[83] J. Abild. Application of the wind atlas method to extremes of wind climatology. Technical Report Risoe-R-722(EN), Risø National Laboratory, Roskilde, Denmark, 1994.

[84] E. J. Gumbel. *Statistics of Extremes*. Columbia University Press, 1958.

[85] X. G. Larsén and J. Mann. Extreme winds from the NCEP/NCAR reanalysis data. *Wind Energy*, 12:556–573, 2009.

[86] J.R.M. Hosking. Estimation of the generalized extreme value distribution by the method of probability-weighted moments. *Technometrics*, 27:251–261, 1985.

[87] J. Mann, L. Kristensen, and N. O. Jensen. Uncertainties of extreme winds, spectra and coherences. In Larsen and Esdahl, editors, *Bridge Aerodynamics, ISBN 9054109610*. Rotterdam, Balkema, 1998.

[88] G. W. Kite. Confidence limits for design events. *Water Resources Research*, 11:48–53, 1975.

[89] X. G. Larsén, S. Larsen, and A. Hahmann. Origin of the waves in "a case study of mesoscale spectra of wind and temperature, observed and simulated': Lee waves from the norwegian mountains'. *Q. J. R. Meteorol. Soc.*, 138:274–279, 2012.

[90] X. G. Larsén, S. Larsen, and M. Badger. A case study of mesoscale spectra of wind and temperature, observed and simulated. *Q. J. R. Meteorol. Soc.*, 137:264–274, 2011.

[91] A.-S. Smedman. Occurrence of roll circulation in a shallow boundary layer. *Boundary-Layer Meteorol*, 51:343–358, 1991.

[92] A. J. Kettle. Britta storm in the North Sea and damage to the FINO 1 platform, Nov. 1, 2006. *RAVE Research at Alpha Ventus, ID:2827, http://folk.uib.no/ake043/Presentations/kettle2015_rave_bremerhaven.pdf*, 68, 2015.

[93] S. Emeis and M. Türk. Wind-driven wave heights in the German Bight. *Ocean Dynamics*, 59:463–475, 2009.

[94] S. Brusch, S. Lehner, and J. Schulz-Stellenfleth. Synergetic use of radar and optial satellite images to support severe storm prediction for offshore wind farming. *IEEE Journal of selected topics in applied earth observations and remote sensing*, 1:57 –66, 2008.

[95] A. Pleskachevsky, S. Lehner, and W. Rosenthal. Storm observations by remote sensing and influences of gustiness on ocean waves and on generation of rogue waves. *Ocean Dynamics*, 62:1335–1351, 2012.

[96] C. Schneggenburger, H. Günther, and W. Rosenthal. Spectral wave modeling with non-linear dissipation: validation and applications in a coastal tidal enviroment. *Coast Eng.*, 41:201–235, 2002.

[97] B. W. Atkinson and J. W. Zhang. Mesoscale shallow convection in the atmosphere. *Reviews of Geophysics*, 4:403–431, 1996.

[98] B. Brümmer, B. Rump, and G. Kruspe. A cold air outbreak near spitsbergen in spring time: Boundary layer modification and cloud development. *Boundary-Layer Meteorol.*, 61:13 –46, 1992.

[99] S. Bakan and E. Schwarz. Cellular convection over the north-eastern atlantic. *International journal of climatology*, 12:353–367, 1992.

[100] X. G. Larsén, S. E. Larsen, and E. L. Petersen. Full-scale spectrum of boundary-layer winds. *Boundary-Layer Meteorol*, 159:349–371, 2016.

[101] R. Bolaños and S. Jackson. DHI report for ForskEL X-WiWa. Technical Report 11812962, DHI, Hørsholm, Denmark, 2017.